ISSN

GMSARN INTERNATIONAL JOURNAL

Vol. 1 No. 1
June 2007

Published by the

GREATER MEKONG SUBREGION ACADEMIC AND RESEARCH NETWORK
c/o Asian Institute of Technology
P.O. Box 4, Klong Luang, Pathumthani 12120, Thailand

GMSARN INTERNATIONAL JOURNAL

ADVISORY AND EDITORIAL BOARD

GMSARN MEMBERS

Asian Institute of Technology (AIT)	P.O. Box 4, Klong Luang, Pathumthani 12120, Thailand. www.ait.ac.th
Hanoi University of Technology (HUT)	No. 1, Daicoviet Street, Hanoi, Vietnam S.R. www.hut.edu.vn
Ho Chi Minh City University of Technology (HCMUT)	268 Ly Thuong Kiet Street, District 10, Ho Chi Minh City, Vietnam. www.hcmut.edu.vn
Institute of Technology of Cambodia (ITC)	BP 86 Blvd. Pochentong, Phnom Penh, Cambodia. www.itc.edu.kh
Khon Kaen University (KKU)	123 Mittraparb Road, Amphur Muang, Khon Kaen, Thailand. www.kku.ac.th
Kunming University of Science and Technology (KUST)	121 Street, Kunming P.O. 650093, Yunnan, China. www.kmust.edu.cn
National University of Laos (NUOL)	P.O. Box 3166, Vientiane Perfecture, Lao PDR. www.nuol.edu.la
Royal University of Phnom Penh (RUPP)	Russian Federation Blvd, PO Box 2640 Phnom Penh, Cambodia. www.rupp.edu.kh
Thammasat University (TU)	P.O. Box 22, Thamamasat Rangsit Post Office, Bangkok 12121, Thailand. www.tu.ac.th
Yangon Technological University (YTU)	Gyogone, Insein P.O. Yangon, Myanmar
Yunnan University	2 Cuihu Bei Road Kunming, 650091, Yunnan Province, China. www.ynu.edu.cn

GMSARN
INTERNATIONAL JOURNAL

GREATER MEKONG SUBREGION ACADEMIC AND RESEARCH NETWORK (http://www.gmsarn.org)

The Greater Mekong Subregion (GMS) consists of Cambodia, China (Yunnan & Guanxi Provinces), Laos, Myanmar, Thailand and Vietnam.

The Greater Mekong Subregion Academic and Research Network (GMSARN) was founded followed an agreement among the founding GMS country institutions signed on 26 January 2001, based on resolutions reached at the Greater Mekong Subregional Development Workshop held in Bangkok, Thailand, on 10 - 11 November 1999. GMSARN is composed of eleven of the region's top-ranking academic and research institutions. GMSARN carries out activities in the following areas: human resources development, joint research, and dissemination of information and intellectual assets generated in the GMS. GMSARN seeks to ensure that the holistic intellectual knowledge and assets generated, developed and maintained are shared by organizations within the region. Primary emphasis is placed on complementary linkages between technological and socio-economic development issues. Currently, GMSARN is sponsored by Royal Thai Government.

The GMSARN member institutions are the Asian Institute of Technology; the Institute of Technology of Cambodia; Kunming University of Science and Technology, Yunnan Province, China; National University of Laos; Yangon Technological University, Myanmar; Khon Kaen University, Thailand; Thammasat University, Thailand; Hanoi University of Technology, Vietnam; Ho Chi Minh City University of Technology, Vietnam; the Royal University of Phnom Penh in Cambodia, and Yunnan University in Yunnan Province, China.

GMSARN International Journal

Volume 1, Number 1, June 2007

CONTENTS

Stepwise Restoration of DG-integrated Distribution Network under Cold Load Pickup

Vishal Kumar*, Rohith Kumar. H.C., I. Gupta and H.O. Gupta

Abstract— *A scheme for step-by-step restoration of a power distribution network under Cold Load Pickup condition has been presented in this paper. The proposed scheme uses the optimal load shedding at each step of restoration process while taking into account the effects of dispersed generation (DG). The load diversity conserved by DG has been effectively utilized for quicker restoration of the network. The optimization is performed to achieve multiple objectives of minimum load curtailment and minimum switching operations while satisfying all the network constraints. Genetic Algorithm has been utilized to search the optimal solution. A considerable amount of improvement in the reliability has been observed in case of DG incorporation. The proposed scheme has been illustrated on a 33-bus radial distribution network.*

Keywords— **Cold load pickup, Distributed generation, Optimal load shedding, Power distribution network restoration.**

1. INTRODUCTION

Loss of diversity among electrical loads during the restoration following an extended outage can lead to heavy loading on system during post-outage period. This loss of diversity is mainly due to thermostatically controlled loads connected in the system being switched ON simultaneously at the instant of supply restoration, causing post-outage load-demand to reach 2 to 5 times the diversified load, such a high load condition is known as 'Cold Load Pickup' (CLPU) [1]. The proportion of thermostatically controlled loads is increasing at a high rate and these loads constitute the major portion of the load on the system today. Such a raise has made the CLPU problem a prevalent feature of distribution system restoration, especially in the power deficient countries where scheduled and forced power outages are frequent.

CLPU has more than sixty years old history, however low percentage of thermostatically controlled loads at that time did not make the problem so severe. It was first recognized as inrush phenomenon in 1952, and change of relays settings were proposed [2]-[4]. In the recent past, researchers started paying attention towards CLPU problem, and several efforts have been made to model the connected loads and also the interconnecting elements under this condition [5]. During last few years much of research in this area has been oriented towards optimal designing of the distribution network and development of better restoration techniques under CLPU [3], [6]-[9]. A critical survey has been conducted recently to highlight various aspects of CLPU problem [2].

The CLPU condition mainly depends on several factors such as the duration of outage, type of connected load, weather condition, living habits of the user, and thermal characteristics of the building. Researchers have divided CLPU condition in to four phases: Inrush, motor starting current, motor accelerating current, and enduring current phase [10]-[12]. Initial three phases are transient in nature and die out within few seconds, whereas the enduring phase can last for long duration thereby causing significantly high loading on the distribution network elements, thereby violating voltage and current limits of the feeder [2]. Hence, all the connected loads can not be switched ON simultaneously during the initiation of restoration. However, the aggregated load decreases with time, and allows more loads to be switched ON as the network regains diversity gradually.

As evident from the literature, extensive research in the area of CLPU has been carried out to restore network in minimum duration. Several heuristic and non-heuristic approaches have been used to obtain the optimal sequence of restoration. Ucak and Pahwa [6] aimed at minimizing the total restoration time and customer interruption duration by making use of derived function between restoration time and restoration order. Further, the authors determined the optimal switching order to minimize customer average interruption duration index (CAIDI) by using adjacent pair wise interchange method [7]. Walkilesh and Pahwa [8] performed a cost optimization to determine the size of substation transformer and number of sectionalizing switches that minimize the total annual cost. The same authors also applied Genetic Algorithm (GA) for optimal restoration of an actual feeder. The capacitor banks were used for

*Vishal Kumar (corresponding author) is with Electrical Engineering Department (EED), Indian Institute of Technology Roorkee (IITR), Roorkee-247667, India. (Telephone: 91-1332-286294, e-mail: vishal_saxena72@hotmail.com)

Rohith Kumar H.C. is with EED, IITR, Roorkee-247667, India (Telephone: 91-1332-286294, e-mail: hc_rohi@yahoo.com)

Indra Gupta is Assistant Professor in EED, IITR, Roorkee-247667 India. (Telephone: 91-1332-285395, e-mail: indrafee@iitr.ernet.in)

H.O.Gupta is Professor in EED, IITR, Roorkee-247667 India. (Telephone:91-1332-285576 e-mail: harifee@iitr.ernet.in)

boosting the voltage to meet the under-voltage permissible limit [9]. As the restoration time is based on the order in which sections are restored, for sequencing the switches, GA [10] and Ant Colony algorithm [13] have also been exploited. The issues like voltage and current constraints of buses and branches, and location for placement of sectionalizing switches have been addressed in a recent paper by Gupta and Pahwa [14], they have taken the base of voltage drop to find the location of sectionalizing switches and optimal size of transformer and feeder, while minimizing the restoration time. Therefore, it is evident from the above references that rigorous work has been carried out on transformer overloading and cost minimization for cold load pickup condition.

The main reason for occurrence of CLPU condition is the loss of diversity among the loads. However, in the modern days of integrated power system, most of the high priority loads such as hospitals, and commercial complexes etc. prefer to have their own DG plants to meet their demand during outages. These non-utility-owned generators (NUGs) are operated in rollover mode and they conserve load-diversity during CLPU condition, thereby reducing the total load requirement during restoration. This paper studies the effect of presence of such NUGs in distribution network during restoration under CLPU condition, and proposes a scheme to restore the network quickly by making use of the diversity conserved by NUGs. The scheme is demonstrated on a 33 bus, 12.66kV radial distribution system. The results obtained for the network with and without incorporation of NUG are compared, and quicker restoration of the network was achieved.

CLPU Model

Variety of models for CLPU condition with various approaches is available in the literature [15]-[21]. However, in the present work, the delayed exponent model has been considered [21]. The model characterizes CLPU condition as an exponential function with delay.

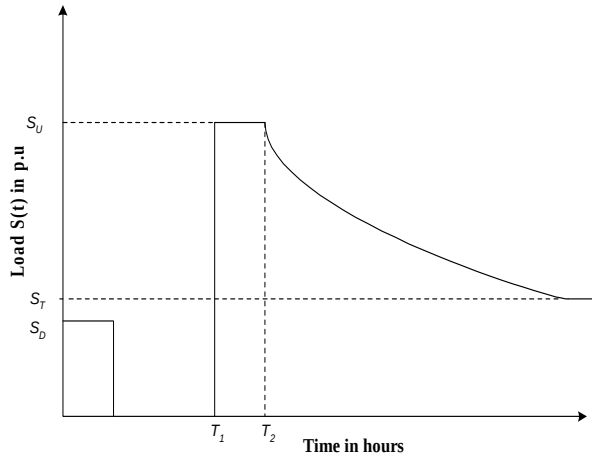

Fig.1. CLPU model represented as a delayed exponent

In the delayed exponential model, un-diversified load S_U remains constant from restoration time T_1 to T_2, showing delay, and after T_2 it decreases exponentially to diversified level S_D as shown in the above Fig 1. Mathematically, this model can be expressed as (1) [14].

$$S(t) = \left\{ \begin{array}{r} [S_D + (S_U - S_D) e^{-\alpha (t-T_2)}] u(t-T_2) \\ + S_U [1-u(t-T_2)] u(t-T_1) \end{array} \right\} \quad (1)$$

2. AIM AND APPROACH

The aim of the present work is to study the effect of presence of NUGs on the restoration of network under CLPU in a DG-integrated distribution system.

The approach adopted in the proposed scheme for restoration of a network under CLPU is based on load curtailment. The loads are curtailed to restart the network and then are restored in step-by-step manner as the loading of the network elements decays with time. It is assumed that all the loads follow the delayed exponent model of CLPU [21] except the loads with NUG, which are supplied during outage and maintain their diversity. Some predetermined step-points are considered on the load profile, and corresponding locations for optimal load shedding/restoring at each step are determined with the help of GA. Main objective is to determine the optimal locations for load curtailment, and the sequence of restoration of loads as to achieve maximum utilization of the existing network capacity.

Methodology

The enduring phase of CLPU condition persists for much longer period and causes excessive loading on substation transformer, current violation in the feeders, and voltage violation at the buses. Hence, loads are picked up in an optimal sequence so that all the operational constraints could be satisfied [3]. However, loads connected to NUG are being supplied during the outage, and they maintain their diversity, hence contribution of such loads to the total load demand remains constant during pre and post outage period. Here, the methodology is to determine the optimal load shedding locations and restore the network in steps, besides the inclusion of effects of NUG.

Consider load at bus *i*, switched ON at time step T_j, if this load is not connected with NUG during outage period, then it follows CLPU profile given by (2.a) on restoration, else the load diversity is conserved (2.b), and this aids the process of network restoration.

$$S_i(t) = [S_{D_i} + (S_{U_i} - S_{D_i}) e^{-\alpha (T_j - \Delta T)}] u(t - \Delta T) \quad \forall j = 1...m \quad (2.a)$$

$$S_i(t) = S_{D_i} \quad \forall j = 1...m \quad (2.b)$$

Here, *m* is the total number of distinct discrete step-

points considered on the CLPU load profile, and the corresponding timing instants can be evaluated from (3).

$$T_j = -\frac{1}{\alpha}\ln\left[\left(\frac{S^j - S_D}{S_U - S_D}\right)\right] + \Delta T, \quad \forall j = 1...m \quad (3)$$

The S^j is loading corresponding to predetermined step point j considered on CLPU model as shown in Fig. 1.

Here, in the case study presented in next section these are considered as given in Table 1.

Problem Formulation

The main objective here is to minimize the load curtailed at each step while restoring the network along with minimum switches being operated. This is a case of nonlinear combinatorial problem with multiple objectives. This multi-objective optimization problem is converted to a single objective problem with the help of suitable weights, and the mathematical formulation of the problem is expressed as (5).

$$Min \quad f = W_{Load}\frac{\left[S_{Total} - S_{Supplied}\right]}{S_{Total}} + W_{IV}I_V + W_{VV}V_V + W_{TV}S_{TV} + W_{SW}SW \quad (5)$$

Objective function given by (5) is subjected to operational constraints as mentioned below.

- All the power flow equations of the network should be satisfied
- The utility voltage at each load bus should be within permissible limit (Utility's standard ANSI Std. C84.1-1989) (±5%).

$$V_{\min} \le V_i \le V_{\max}, \quad \forall i \in \{buses\ of\ the\ network\} \quad (6)$$

- In a feeder or conductor, current cannot be increased beyond a specified limit, which is decided by thermal capacity of the conductor.

$$I_i \le I_i^{Rated}, \quad \forall i \in \{branches\ of\ the\ network\} \quad (7)$$

Here, I_i^{Rated} is current permissible for branch *i* within safe limit of temperature.

- The total power supplied to the network must be within the substation transformer capacity limit. In the proposed scheme for network restoration, maximum loading of the transformer is considered as the loading limit of transformer for no additional loss of life.

$$S_{T_{Max}} < K_{TM} \times S_T \quad (8)$$

Loading limit of the forced air-cooled transformer for a delayed exponential CLPU model has been explained for different outage-duration, and pre-outage and post-outage loading conditions. The maximum un-diversified load for different diversified loads and outage duration is also reported, and the maximum supplying limits for one-hour outage with different pre and post outage load conditions have also been determined [6], [22].

Weights considered in (5) reflect the relative priority of each term present in the objective function. The weights act as the penalty to be imposed in case of violation of constraints. However in the present work, the weight is also used to convert multi-objective optimization problem to a single objective problem. Since the main objective is to achieve a small quantity of loss of load, heavy penalty is imposed to the first term. The second and the third terms in the objective function are steady state security constraints, and heavy penalties are applied in case if these limits are violated. Fourth term is of slightly lesser significance in comparison with second and the third, as the distribution transformers are rated for a short period of overloading with no or a very nominal loss of life. Varying these weights can lead to alternative solutions.

Genetic Algorithm

Genetic algorithms are the computerized search and optimization algorithms based on the mechanism of natural genetics and selection [23], [24]. These algorithms work with a population of possible solutions, rather than a single point as in conventional optimization techniques. The population of possible solution continuously undergoes the process of natural changes such as selection, crossover and mutation finally to arrive with a global optimum solution. In the present research work, binary encoding system has been successfully adopted owing to its simplicity of representation and ease of understanding. The length of the encoded string is equal to the total number of buses in the system, and each bit of this string represents the status of the load connected at that bus. GA here uses roulette wheel selection, one-point crossover and bit-wise mutation along with elitism preserving mechanism [23], [24]. Maximum number of generations is used to terminate GA.

The algorithm designed for the determination of the optimal locations for load curtailment/restoration is explained as follows.

Algorithm

Some load-points are considered on the CLPU profile; these load points actually represent the steps of restoration. Following is the computational flow for designed algorithm using GA, applied for a load-point, which determines the load shedding locations corresponding to that load-point. The application of the algorithm for each restoration step enables to know the optimal sequence of restoration of the loads.

```
INPUT : P_SIZE , Ge_MAX , P_C , P_M , N
Generate random population P_0 of P_SIZE
for (i = 1 : i ≤ Ge_MAX )
      set: j=1;
       While( j ≤ P_SIZE )
        set: k=1;
          While(k ≤ N )
            Update P_i^k (j) by eq. (2.a); //if bus k
                        not connected to NUG//
            Update P_i^k (j) by eq. (2.b); //if bus k
                          connected to NUG//
            k++;
         end While
         Evaluate  P_i(j) from eq. (5)
         j++;
      end While
      /* Apply genetic operators as below */

    Select(P_i);   // Subroutine for Roulette wheel
                     selection //
    Xover(P_i);    // Subroutine for one-point
                     crossover //
    Mutate(P_i);   // Subroutine for bit-wise
                     mutation //
    Elite(P_i,P_i-1);   // Subroutine for elitism //
    i++; // Increment generation counter //
end for
OUTPUT : Optimal Switching locations
```

3. CASE STUDY

The proposed scheme is illustrated on a 33-bus, 12.66 kV radial distribution network [25] with a substation transformer capacity of 5MVA. Under CLPU condition, most of the system buses violate the lower voltage limit, and hence to effectively utilize the permissible range of the utility voltage, the substation voltage has been considered as 1.045 p.u.. It is considered that the network is initially compensated for reactive power through the optimal placement of capacitors at buses, and the corresponding values are given in Appendix-I [26]. In order to illustrate the effects of presence of NUGs, It is assumed that NUGs are present at buses 14, 17, 25 and 30.

Table 1. Values of time elapsed for the step-points

Step-point (j)	Time Elapsed in Minutes	Description of Step-point/(S^j)
-1	-120	Outage duration
0 (Restart)	0	Start of Restoration 2.50 x S_D
1	54.33	2.0 x S_D
2	95.92	1.50 x S_D
3	137.51	1.25 x S_D
4	192.48	1.10 x S_D
5	234.07	1.05 x S_D

The typical values of weights applied in the objective function for the present case-study are: 75.0 for the lost load, 500.0 for the current violation, 10000.0 for the voltage violation, 50.0 for the transformer violation, and 10.0 for number of switching operations.

The proposed scheme utilizes a delayed exponential model as explained in section-1. The associated parameters to the model are taken as α =1 hr^{-1}, $\Delta T = T_2 - T_1$=30 minutes, S_U= 2.5 p.u., and S_D=1.0 p.u., and K_{TM} =1.50. Time instances and loadings corresponding to each step of stepwise restoration of the network are illustrated in Table 1.

4. RESULTS AND DISCUSSION

The current restoration problem is a nonlinear combinatorial problem and GA has been used to obtain the optimal solution. GA is applied with different population size: 60, 80, 100 and 150, and the best result obtained has been reported here. The corresponding GA convergence curve for step-point-0 is shown in Fig.2. The following are the considered GA parameters

Population size:	100
Crossover rate:	0.8
Mutation rate:	0.05
Maximum no of generations:	50

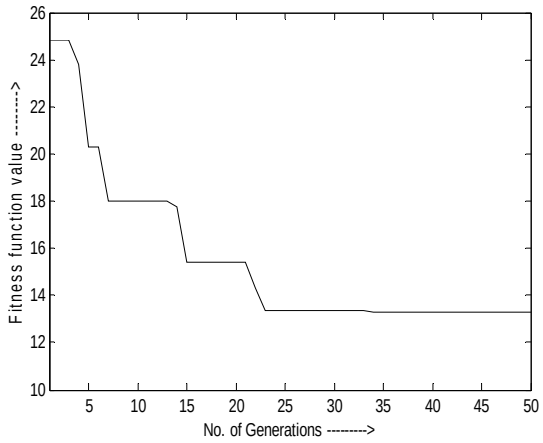

Fig.2. Convergence curve of GA for step-point-0 of case-2

Table 2 shows the results obtained for stepwise restoration of the network in both the cases, without NUGs (Case-1) and with NUGs (Case-2). It is clear that during step-wise restoration of Case-2, restoration of network takes place in step-point 3 against step-point-4 for Case-1. Also, the number of loads being disconnected is lesser in all the steps in Case-2. This is mainly because of the reduction in the total load demand owing to conservation of diversity of loads connected with NUG during outage period. The graphical view of step-wise restoration under both the cases has been presented in Fig.3 and 4; the load supplied by NUG during the outage is also shown in the figure. The expected load represents the required load to be restored for the complete restoration of the network corresponding to the load-points. The analysis was conducted by self developed codes written in MATLAB-R2006a package, on PC with Intel P-IV processor of 2.0 GHz clock frequency, and the average CPU execution time pertaining to Case-1 and

Case-2 has been reported in Table 3.

Table 2. Results of step-wise restoration of network

	Case 1 With out NUGs	**Case 2** With NUGs
Step-point: 0		
Total load served in MVA	7.1292	7.0541
Load at the buses to be disconnected	7,8,12,13,17,18,31,32,33	14,16,18,29,32
Total number of switching operation	9	5
Step-point: 1		
Total load served in MVA	6.6940	6.2166
Load at the buses to be disconnected	12,13,17,18,31,32,33	14,18,32
Total number of switching operation	7	3
Step-point: 2		
Total load served in MVA	5.7207	5.2726
Load at the buses to be disconnected	17,18,32	14,18
Total number of switching operation	3	2
Step-point: 3		
Total load served in MVA	4.8092	4.7846
Load at the buses to be disconnected	17,32	Nil
Total number of switching operation	2	Nil
Step-point: 4		
Total load served in MVA	4.6994	3.7631

Table 3. Average CPU Time per Step-point

	Case-1	**Case-2**
CPU Time (in sec./step)	231.03	217.43

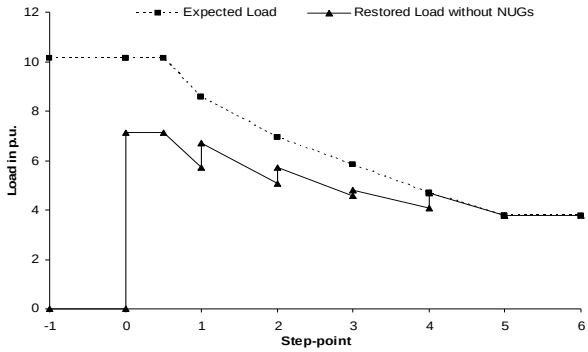

Fig.3. Step-wise restoration of network in case-1

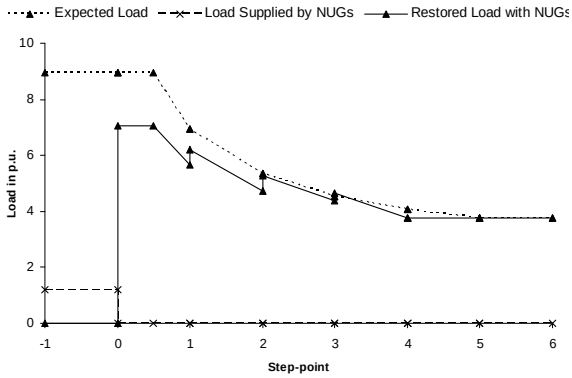

Fig.4. Step-wise restoration of network in case-2

The presence of DG in distribution network also improves the reliability indices of supply. For the purpose of illustration, a case has been considered where the total connected load is equal to substation transformer capacity. An average load per customer of 2kW is assumed and reliability indices are evaluated. The number of customers restored under both the cases is presented in Fig.5, it is evident that more number of customers are restored in Case-2.

A considerable improvement in the reliability indices has been observed in Case-2. To support the previous statement, few of the basic customer oriented reliability indices such as System Average Interruption Duration Index (SAIDI), System Average Interruption Frequency Index (SAIFI) are evaluated and given in Table 4.

Table 4. Evaluated Reliability Indices

Index	**Case-1**	**Case-2**
SAIDI (min/customer)	181.07	147.39
SAIFI (int/customer)	1.649	1.331

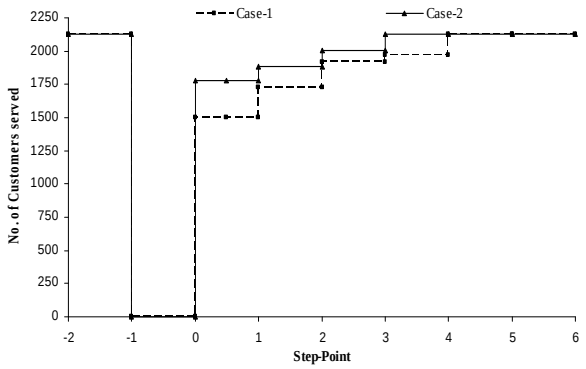

Fig.5. Number of customers served in both cases

5. CONCLUSION

In the present work, the effect of presence of NUGs on network restoration during CLPU condition has been investigated. A scheme has been proposed, to restore the network under CLPU with the utilization of diversity conserved by the NUGs. The proposed scheme for incorporation of NUGs restored the network quicker than the one without considering the NUG, moreover minimized the total number of switching operations required with maximum utilization of existing capacity of the system. It is concluded that the presence of NUGs also improves the reliability indices. The scheme is illustrated on a 33-bus 12.66kV distribution system. The subject matter discussed in this paper is of high relevance, as the amount of DG integrated network is rising, as to meet the customers supply requirement during outages, and the utilities seem to benefit under such scenario by being able to restore the network at a faster rate.

NOMENCLATURE

α	Rate of decay of load under CLPU
Ge_{MAX}	Maximum number of generations
I_V	Sum of the ratios of line-current violations to its thermal limit
K_{TM}	Transformer maximum loading factor
N	Total no of buses in the system
NUG	Non Utility-owned Generator
$NUGs$	Non Utility-owned Generator units
P_C	Probability of crossover
P_M	Probability of mutation
P_{SIZE}	Population size
$P_i^k(j)$	k^{th} bus of j^{th} chromosome during i^{th} generation
$S(t)$	Load Demand with respect to time for $t \geq T_1$
S_D	Diversified Load in p.u.
$S_{Supplied}$	Load supplied during CLPU
S_T	Substation transformer rating
$S_{T\,Max}$	Maximum transformer loading
S_{Total}	Total connected load in the network
S_{TV}	Transformer loading-limit violation
S_U	Un-diversified load in p.u.
SW	Number of switching operations
T_1	Initiation of restoration
T_2	Initiation of decay towards S_D
$u(t)$	Unit step function
V_V	Sum of the ratios of bus-voltage violations to the limiting value
W_{IV}	Weight for I_V
W_{Load}	Weight for ratio of lost load over total load
W_{SW}	Weight for SW
W_{TV}	Weight for S_{TV}
W_{VV}	Weight for V_V

REFERENCES

[1] Mcdonald, J.E.; Bruning, A.M.; and Mahieu, W.R. 1979. Cold Load Pickup. *IEEE Transaction on Power Apparatus and Systems*, vol. 98, pp. 1384-1386.

[2] Kumar, V.; Gupta, I.; and Gupta, H.O. 2006. An Overview of Cold Load Pickup Issues in Power Distribution Systems. *Electric Power Components & Systems.* Vol. 34, No.6, pp. 639-651.

[3] Pahwa, A. 2001. Role of distribution automation in restoration of distribution systems after emergencies. In *Proceedings of the Transmission and Distribution Conference and Exposition, IEEE/PES*, vol. 2, pp. 1204–1205.

[4] Ramsaur, O. 1952. A new approach to cold load restoration. *Electrical World*, vol. 138, pp. 101–103.

[5] Agneholm, E.; and Daalder, J. 2000. Cold load pickup of residential load. *IEE Pro. Gener. Transm. Distrib.*, vol. 147, no. 1, pp. 44–50.

[6] Ucak, C.; and Pahwa, A. 1994. An analytical approach for step-by-step restoration of distribution systems following extended outages. *IEEE Transactions on Power Delivery*, vol. 9, no. 3, pp. 1717–1723.

[7] Ucak, C.; and Pahwa, A. 1995. Optimal step-by-step restoration of distribution systems during excessive loads due to cold load pickup," *Electric Power Systems Research*, vol. 32, no. 2, pp. 121–128.

[8] Wakileh, J. J.; and Pahwa, A. 1996. Distribution system design optimization for cold load pickup. *IEEE Transactions on Power Systems*, vol. 11, no. 4, pp. 1879–1884.

[9] Wakileh, J. J.; and Pahwa, A. 1997. Optimization of distribution system design to accommodate cold load pickup," *IEEE Transactions on Power Delivery*, vol. 12, no. 1, pp. 339–345, January 1997.

[10] Chavali, S.; Pahwa, A.; Das, S. 2002. A Genetic algorithm Approach for Optimal Distribution Feeder Restoration during Cold Load Pickup. In *Proceedings, World Congress 011 Computational Intelligence*, Honolulu, Hawaii.

[11] Agneholm, E. 1995. *Cold Load Pick-Up*, PhD thesis, Department of Electric Power Engineering, Chalmers University of Technology, Goteborg, Sweden.

[12] Mirza, O. H. 1997. Usage of CLPU curve to deal with cold load pickup problem. *IEEE Transactions on Power Delivery*, vol. 12, no. 2, pp. 660–667.

[13] Mohanty, I.; Kalita, J.; Das, S.; Pahwa, A.; and Buehler, E. 2003. Ant algorithms for the optimal restoration of distribution feeders during cold load

pickup. In *Proceedings of the Swarm Intelligence Symposium 2003, SIS'03*, pp. 132–137, 24–26 April 2003.

[14] Gupta, V.; and Pahwa, A. 2004. A voltage drop-based approach to include cold load pickup in design of distribution systems. IEEE *Transactions on Power Systems*, vol.19, no.2, pp. 957-963.

[15] Law, J.; Minford, D.; Elliott, L.; and Storms, M.; 1995. Measured and predicted cold load pick up and feeder parameter determination using the harmonic model algorithm. *IEEE Transactions on Power Systems*, vol. 10, Issue 4, pp. 1756 – 1764.

[16] Nehrir, M. H.; Dolan, P. S.; Gerez, V.; and Jameson, W. J. 1995. Development and validation of a physically-based computer model for predicting winter electric heating loads. *IEEE Transactions on Power Systems*, Vol. 10, Issue: 1, pp. 266 – 272.

[17] Laurent J. C.; and Malhame, R. P. 1994. A physically-based computer model of aggregate electric water heating loads. *IEEE Transactions on Power Systems*, Vol. 9, Issue: 3, pp. 1209 – 1217.

[18] Athow D.; and Law, J. 1994. Development and applications of a random variable model for cold load pickup. *IEEE Transactions on Power Delivery*, Vol. 9, Issue: 3, pp. 1647 – 1653.

[19] Aubin, J.; Bergeron, R.; and Morin, R. 1990. Distribution transformer overloading capability under cold-load pickup conditions. *IEEE Transactions on Power Delivery*, Vol. 5, Issue: 4, pp. 1883 – 1891.

[20] Leou, R.C.; Gaing, Z. L.; Lu, C. N.; Chang, B. S.; and Cheng, C. L. 1996. Distribution system feeder cold load pickup model. *Electric Power Systems Research*, Vol. 36, Issue 3, pp. 163-168.

[21] Lang, W.W.; Anderson M. D.; and Fannin, D.R. 1982. An Analytical method for quantifying the electrical space heating component of cold load pickup. *IEEE Transactions on Power Apparatus and Systems*, vol. PAS-101, no. 4, pp. 924-932.

[22] ANSI/IEEE C57.92-1981, Guide for loading mineral-oil-immersed power transformer up to and including 100 MVA with 55°C or 65°C winding rise, The Institute of Electrical and Electronics Engineers, Inc.,1981 from the World Wide Web: http://ieeexplore.ieee.org/xpl/standardstoc.jsp?isnumber=1103&isYear=1981.

[23] Deb, K. 2004. *Multi-Objective optimization using evolutionary algorithms*. Singapore: John Wiley & Sons.

[24] Goldberg, D.E. 1989. *Genetic algorithm in search, optimization and machine learning*.-: Addison-Wesley.

[25] Mesut, E.B.; and Felix, F.Wu. 1989. Network Reconfiguration in Distribution System for Loss Reduction and Load Balancing. *IEEE Transaction on Power Delivery*, Vol.4, No.2.

[26] Kumar, V.; Gupta, I.; Gupta, H.O.; and Jhanwar, N. 2005. Optimal Location and Sizing of Capacitor Banks for Power Distribution Systems. *Journal of International Association on Electricity Generation Transmission & Distribution (Afro-Asian Region)*, Vol. 17-18, No. 1.

APPENDIX-I

Listing of the bus numbers and the amount of reactive power compensation provided [26].

Bus No.	Capacitor Values in kVar
9	100
14	300
19	100
21	100
23	100
24	100
25	100
29	200
30	500
31	100

Measurement and RTU Placement for State Estimation by Loop Decomposition

Thawatch Kerdchuen* and Weerakorn Ongsakul

Abstract*— *This paper proposes a novel loop decomposition technique for optimal measurement and RTU placement for power system state estimation. Loop decomposition is based on the loops of system topology, which does not require the reduced measurement graph. The power injection and power flow measurement are properly installed at buses and branches which make the system observable considering single measurement loss and critical measurement pair free. The optimal number of measurement pairs is equal to minimum number. The minimum number of RTUs is equal to the number of power injection measurement pairs. The observability and critical measurement on the 10-bus, IEEE 14, 30, 57 and 118-bus systems are checked by $P\delta$ observability analysis and residual analysis respectively.

***Keywords*— Critical Measurement Pair, Loop Decomposition, Observability, Single Measurement Pair Loss.**

1. INTRODUCTION

Power system state estimation is used to estimate the steady state system conditions using the online measurements. Measurement placement is to provide the sufficient system data for state estimator. The inaccurate measured system conditions may lead to insecure state operation.

Measurement placement should be sufficient to make the system observable for running state estimation [1-4]. Moreover, the number of measurements should be minimized for investment cost savings. The heuristic approach presented the measurement placement in measurement graph [5]. It considers a single measurement pair loss while the system is still observable. This single measurement pair loss requires an additional measurement pair. Bad data or gross error in any single measurement pair of a system without the critical measurement pair can be detected [6-8]. The critical measurement pair is identified by residual analysis. However, the measurement graph is too complicated to construct. In [8], although the measurement placement without critical measurement is considered, the genetic algorithm for optimization is required. Decomposition technique [9] has been used for measurement and phase measurement unit (PMU) placements in multi-area system. This decomposition is used to make subsystem areas observable before data from each area is synchronized by the global positioning system (GPS) satellite trans-mission.

In this paper, loop decomposition technique is used to minimize measurement and RTU placement on the 10-bus, IEEE 14, 30, 57 and 118-bus systems considering single measurement pair loss. The system is decomposed according to system topology. Then, the injection and flow measurement pairs are installed to handle any single measurement pair loss. The absence of critical measurement is verified by the residual analysis.

2. MEASUREMENT PLACEMENT FUNDAMENTAL

The weight least squares (WLS) state estimation equations relating to the measurements and the state vector are

$$\mathbf{J}(\mathbf{x}) = (\mathbf{z} - \mathbf{H}\mathbf{x})^T \mathbf{R}^{-1} (\mathbf{z} - \mathbf{H}\mathbf{x}) \quad (1)$$

where $\mathbf{z} = \mathbf{H}\mathbf{x} + \mathbf{e}$ is the measurement vector, $\mathbf{H}$ is the $(m \times N)$ Jacobian matrix $\mathbf{H} = \partial \mathbf{h}(\mathbf{x}) / \partial \mathbf{x}$, $\mathbf{x}$ is the $(N \times 1)$ system state vector, $\mathbf{R}$ is the diagonal covariance matrix, $\mathbf{h}(\bullet)$ is the $(m \times 1)$ nonlinear function vector, $\mathbf{e}$ is the $(m \times 1)$ measurement error vector, m is the number of measurements, and N is the number of buses.

In case measurement pair PQ is used in power system and $\mathbf{H}$ matrix is block diagonal, the observability problem can be decoupled into $P\delta$ observability and QV observability. A power system is defined to be $P\delta$ (QV) observable with respect to a measurement set if the $\mathbf{H}_{P\delta}$ ($\mathbf{H}_{QV}$) matrix is of rank $N-1$ (N) [1, 5]. Therefore, the critical number of real and reactive measurement pairs is $(N-1)$ [5] and additional one of bus voltage magnitude measurement at any bus.

Single Measurement Loss Contingency

For single measurement pair loss contingency, any single injection or flow of real and reactive measurement pair

* T. Kerdchuen (corresponding author) is with the Energy Field of Study, Asian Institute of Technology (AIT), P.O. Box 4, Klong Luang, Pathumthani 12120, Thailand (e-mail: st101454@ait.ac.th), and also is with Rajamangala University of Technology Isan, Nakhonratchasima, Thailand.

W. Ongsakul is with the Energy Field of Study, AIT, Thailand (e-mail: ongsakul@ait.ac.th).

can be lost from the power system. This loss is due to either communication failure or measurement failure. When a single measurement pair is lost, the entire row of measurement observability matrix is deleted. Then, the reduced measurement matrix is used to determine observability.

Critical Measurement Identification

If a single measurement pair can be lost from the power system, the system is considered as critical measurement free. In the absence of critical measurement in the power system, the bad data in any single measurement pair can be detected. The residual vector **r** is defined as the difference between **z** and the corresponding filtered quantities $\hat{\mathbf{z}} = \mathbf{H}\hat{\mathbf{x}}$. The residuals in terms of the elements of matrix **E** as follows

$$\begin{aligned}\mathbf{r} &= \mathbf{z} - \hat{\mathbf{z}} = \mathbf{z} - \mathbf{H}\hat{\mathbf{x}} = \mathbf{z} - \mathbf{H}(\mathbf{G}^{-1}\mathbf{H}^T\mathbf{z}) \\ &= (\mathbf{I} - \mathbf{H}\mathbf{G}^{-1}\mathbf{H}^T)\mathbf{z} = \mathbf{E}\mathbf{z}\end{aligned} \quad (2)$$

where $\mathbf{E} = \mathbf{I} - \mathbf{H}\mathbf{G}^{-1}\mathbf{H}^T$, $\mathbf{z}$ is a unity vector [6] (This simplification is based on the fact that critical measurement is independently of the measurement values) and $\mathbf{G} = \mathbf{H}^T\mathbf{H}$ is a gain matrix. Therefore, the ith component of the residual vector is calculated by

$$r(i) = \sum_{k=1}^{m} E(i,k) \quad (3)$$

For each $z(i)$ of the measurement set, if $r(i)$ and $E(i,i)$ are zero, $z(i)$ is defined as a critical measurement [6-8].

3. LOOP DECOMPOSITION AND MEASUREMENT PAIR PLACEMENT

The rationale behind loop decomposition is that the power flow measurement pair loss can be handled by injection measurement pair. Also the power injection measurement pair loss can also be handled by power flow measurement pair and the adjacent power injection measurement pair. The decomposition loop is a strategic trial and error method used to properly place those measurement pairs. To make the system observable considering single measurement pair loss, the measurement and RTU placement in the loop decomposition procedures are as follows.

***Measurement pair placement*:**

This procedure is to optimally place the measurement pairs for making the number of measurement pairs equal to number of system buses so that the system is observable with single measurement pair loss. The procedure starts with the system loop decomposition.

Step 1: Decompose a power system topology into either a single or multiple loops of subsystems, each loop does not overlap with each other.

Step 2: Power injection measurement pairs are placed at the boundary buses of the loop. The boundary bus is the bus whose branch is incident to other buses outside the loop.

Step 3: Power flow measurement pairs are placed at the internal branches near injection measurement bus which are incident to other buses without power injection measurement pairs. There should be only single power flow measurement pair connected to the same internal bus.

Step 4: At the radial bus outside the loop, power injection measurement pair is placed at all buses next to the end bus and power flow measurement pair is placed on the branch near injection measurement bus incident to the end bus.

Step 5: Place the injection measurement pairs at all buses of the line with intermediate buses inside or outside the loop.

Step 6: Power flow measurement pairs are placed at the branches near injection measurement bus incident to the external buses which are not associated with other loops. There should be only single power flow measurement pair connected to the same external bus.

Step 7: Check observability with single measurement pair loss and critical measurement pair identification. Remove single measurement pair one by one for single measurement loss consideration to check $P\delta$ observability. Also the critical measurement pair is identified by residual analysis. If unobservable or critical measurement pair exists, find the bus without injection measurement pair and replace the incident flow measurement pair with the injection measurement pair. Repeat this step until the system is observable or the system is critical measurement pair free.

***RTU placement*:**

This procedure is to reduce the number of required RTUs.

Step 8: For the line with intermediate buses inside each loop, an injection measurement pair is replaced by a flow measurement pair near to the adjacent injection measurement pair bus to minimize the number of power injection measurement pairs inside the observable loop considering single measurement pair loss. Keep repeating this step until every buses with injection measurement pair inside observable loop is considered.

Step 9: For the line with intermediate buses between the loops, an injection measurement pair is replaced by a flow measurement pair near to the adjacent injection measurement pair to minimize the number of power injection measurement pairs considering single measurement pair loss. Keep repeating this step until every buses with injection measurement pair is considered.

Step 10: For the bus with injection measurement pair and without flow measurement pair on the incident

branches, the injection measurement pair is replaced by a flow measurement pair near to the adjacent bus with injection measurement pair to minimize the number of power injection measurement pairs if observable. Keep repeating this step until every buses with injection measurement pair and without flow measurement pair on the incident branches is considered.

4. LOOP DECOMPOSITION RESULTS

The final measurement pair placement for the 10-bus system [5] is illustrated in Fig. 1. The optimal number of measurement pairs and installed RTUs at buses B2, B5, B6 and B9 considering single measurement pair loss is shown in Fig. 2 (a). One loop decomposition on the IEEE 14-bus system with optimal number of measurement pairs and RTUs considering single measurement pair loss is also shown in Fig. 2 (b). The results of loop decomposition method are shown in Table 1. For the IEEE 14, 30, 57 and 118-bus systems, they are observable with minimum number of measurement pairs and reasonable small number of RTUs considering single measurement pair loss.

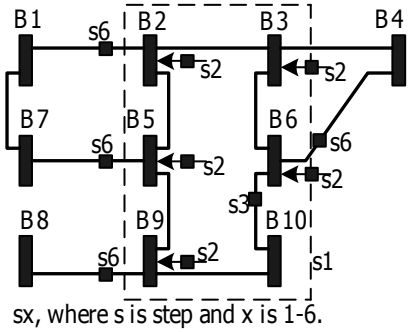

(a)

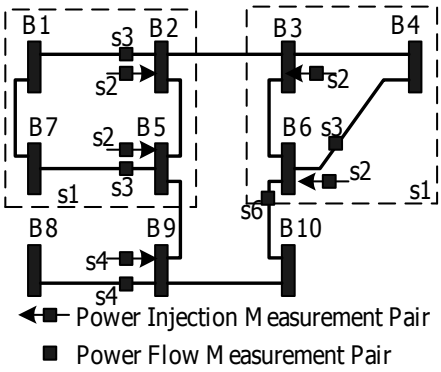

(b)

Fig. 1. Measurement pair placement for 10-bus system (a) one loop decomposition (b) two loops decomposition.

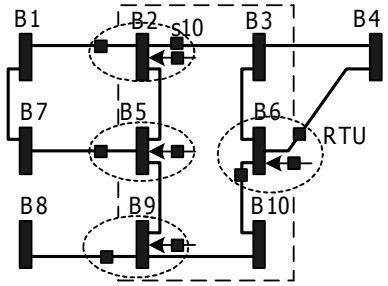

(a)

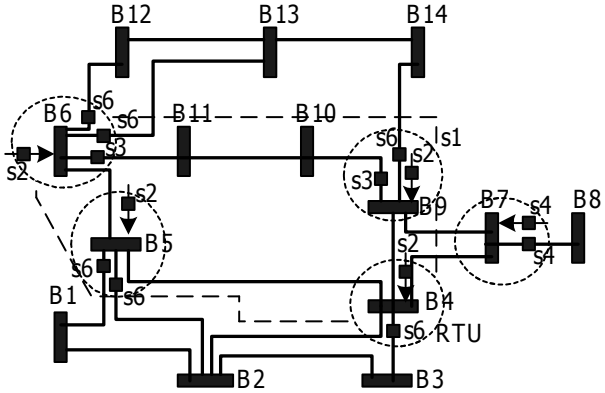

(b)

Fig. 2. Measurement pair and RTU placement results (a) 10-bus system (b) IEEE 14-bus system

Table 1. Measurement Placement Results of Loop Decomposition Method

System	No. of Loops	No. of Power Injection Meas. Pairs	No. of Power Flow Meas. Pairs	No. of RTUs
10-bus	1	4	6	4
10-bus	2	4	6	4
10-bus [5]	-	4	6	4
IEEE 14-bus	1	5	9	5
IEEE 14-bus [8]	-	5	9	5
IEEE 30-bus	3	11	19	11
IEEE 57-bus	5	30	27	30
IEEE 118-bus	12	45	73	45

In Table 1, even thought the number of measurement pairs and RTUs are the same as [5] and [8], the loop decomposition technique is fast and easy to implement.

5. CONCLUSION

The loop decomposition is fast in placing the measurement pairs and RTUs in the system considering single measurement pair loss. The measurement pair placement contains no critical measurement. Test results on the systems indicate that loop decomposition could result in the minimum number of measurement pairs and reasonable small number of RTUs, leading to investment cost savings.

REFERENCES

[1] G.R. Krumpholz, K.A. Clements and P.W. Davis, (1980). Power System Observability: A Practical Algorithm Using Network Topology. *IEEE Trans. Power App. Syst.*, vol. PAS-99, no. 4, pp. 1534-1542.

[2] A. Monticelli and F. F. Wu, (1985). Network Observability: Theory. *IEEE Trans. Power App. Syst.*, vol. PAS-104, no. 5, pp. 1042-1048.

[3] A. Monticelli and F. F. Wu, (1985) Network Observability: Identification of Observable Islands and Measurement Placement. *IEEE Trans. Power App. Syst.*, vol. PAS-104, no. 5, pp. 1035-1041.

[4] G. N. Korres, P. J. Katsikas, K. A. Clements and P. W. Davis, (2003). Numerical Observability Analysis Based on Network Graph Theory. *IEEE Trans. Power Syst.*, vol. 18, no. 3, pp. 1035-1045.

[5] G. M. Huang, J. Lei and A. Abur, (2003). A Heuristic Approach for Power System Measurement Placement Design. In *Proc. IEEE ISCAS*, vol. 3, pp. 407-410.

[6] M. B. Do Coutto Filho, J. C. S. Souza, F. M. F. Oliveira and M. Th. Schilling, (2001). Identifying Critical Measurements & Sets for Power System State Estimation. Present at *IEEE Porto Power Conference*, Porto, Portugal.

[7] A. S. Costa, T. S. Piazza and A. Mandel, (1990). Qualitative Methods to Solve Qualitative Problems in Power System State Estimation. *IEEE Trans. Power Syst.*, vol. 5, no. 3, pp. 941-949.

[8] J. C. S. Souza, M. B. Do Coutto Filho, M. Th. Schilling and C. Capdeville, (2005). Optimal Metering Systems for Monitoring Power Networks Under Multiple Topological Scenarios. *IEEE Trans. Power Syst.*, vol. 20, no. 4, pp. 1700-1708.

[9] C. Rakpenthai, S. Premrudeepreechacharn, S. Uatrongjit and N. R. Watson, (2005). Measurement placement for power system state estimation using decomposition technique. *Electric Power Systems Research*, vol. 75, pp. 41-49.

Reliability Evaluation of Micro Hydro-Photo-Voltaic Hybrid Power Generation Using Municipal Waste Water

R.K. Saket*, R.C. Bansal, and K.S. Anand Kumar

Abstract— *This paper describes a technology based on municipal waste water for electric power generation and evaluates the reliability of the micro-hydro-photo-voltaic (MHPV) hybrid power system using Gaussian distribution approach and flow duration curve (FDC). Reuse of municipal waste water of the city can be a stable, inflation proof, economical, reliable and renewable source of electricity. The hydro potential of waste water from community flowing through sewage system has been determined to produce a FDC by ordering the recorded water flows. Several factors such as design pressure, the roughness of the pipe's interior surface, method of joining, weight, ease of installation, accessibility to the sewage system, design life, maintenance, weather conditions, availability of material, related cost and likelihood of structural damage have been considered for a particular penstock. A MHPV has been proposed to provide reliable electric energy to Banaras Hindu University (BHU), Varanasi (India).*

***Keywords*— Flow duration curve, micro-hydro-photo-voltaic hybrid power system, municipal waste water, reliability evaluation.**

1. INTRODUCTION

Small-hydro power (SHP) systems are relatively small power sources that are appropriate in many cases for individual users or groups of users who are independent of the electricity supply grid. Although this technology is not new, its wide application to small waterfalls and other potential sites is new. It is best suited to high falls with low volume, which occur in high valleys in the mountains. SHP is the application of hydroelectric power on a commercial scale serving a small community and are classified by power and size of waterfall. A generating capacity up to 10 MW is generally accepted as the upper limit of small hydro, although this may be stretched upto 30 MW in some countries. Small hydro can be further subdivided into mini hydro, usually defined as less than 1.0 MW, and micro-hydro which is less than 100 kW [1], [2]. Hydroelectric power is the technology of generating electric power from the movement of water through rivers, streams, and tides. Water is fed via a channel to a turbine where it strikes the turbine blades and causes the shaft to rotate to which generator is connected which converts the motion of the shaft into electrical energy. Small hydro is often developed using existing dams or through development of new dams whose primary purpose is river and lake water-level control, or irrigation. A small-scale hydroelectric facility requires a sizeable flow of water and a reasonable height of fall of water, called the head. Another advantage of using water resources is that hydraulic works can be made simple and large constructions, such as dams, are not usually required [1]-[5]. When dams are necessary, they affect less area than in lower zones because of the steepness of the terrain. Dams, which exploit the kinetic energy of water by raising small quantities of water to heights through the use of regulated pressure valves, can provide water for domestic uses and for agriculture in areas that are moderately higher than adjacent water courses.

Generally, in an autonomous hybrid power system, the wind/small-hydro power generators are the main constituents of the system and are designed to operate in parallel with local diesel grids. The main reasons are to obtain economic benefit of no fuel consumption by wind/hydro turbines, enhancement of power capacity to meet the increasing demand, to maintain the continuity of supply in the system, etc. Wind/small-hydro system is highly fluctuating in nature [6]-[8] and may affect the quality of supply considerably and even may damage the system in the absence of proper control mechanism. Main parameters to be controlled are the system frequency and voltage, which determine the stability and quality of the supply.

In a power system, frequency deviations are mainly due to real power mismatch between generation and demand, whereas voltage mismatch is the sole indicator of reactive power unbalance in the system [9], [10]. In a power system active power balance can be achieved by controlling the generation i.e. by controlling the fuel input to the diesel electric unit and this method is called automatic generation control (AGC) or load frequency control (LFC). Another method of controlling the frequency of hybrid system is by means of controlling the output power which includes dump load control, priority load control, battery energy storage (BES), flywheel storage, pump storage, hydraulic/pneumatic accumulators, superconducting magnetic energy storage

*R.K. Saket (corresponding author) is with the Electrical Engineering Department, Institute of Technology, Banaras Hindu University, Varanasi (India). E-mail: saketrk@yahoo.com.

R.C. Bansal is with the Electrical and Electronics Engineering Division, School of Engineering and Physics, The University of the South Pacific, Suva, Fiji, email: rcbansal@hotmail.com

K.S. Anand Kumar is with the University Works Department, Banaras Hindu University, Varanasi (India), E-mail: anand_kumarks@yahoo.com

(SMES), etc. [11]. Reactive power balance in the hybrid system can be obtained by making use of variable reactive power device e.g. static var compensator (SVC) [12]-[15].

Micro-hydro power system using waste water from community neither requires a large dam nor is land flooded. Only waste water from different parts of the city is collected to generate power which has minimum environmental impact. After proper treatment water can be provided to farmers for irrigation purpose. Micro-hydro power using waste water of sewage plant can offer a stable, inflation-proof, reliable, economical and renewable source of electricity. This technology has been designed and implemented at Institute of Technology, BHU, Varanasi (India). This paper presents a new renewable resource of hydroelectric power generation using waste water from community of the city.

2. SELECTION OF BASIC COMPONENTS OF SYSTEM

The principal components of the micro-hydro power system using sewage system are shown in Fig. 1. Interconnection of the micro hydro and PV system for reliable operation of the hybrid plant is shown in Fig. 2. A tailrace and solar pump through which the water is released back of the sewage storage plant to maintain head of the water according to flow rate v/s duration curves is shown in Fig. 3. The basic components of typical hybrid micro-hydro power plant using waste water from community are as follows:

- An intake or weir to divert stream flow from different parts of the city.
- A sewage line to carry water flow to the forebay from the intake of the system.
- A forebay tank and trash rack to filter debris and prevent it from being drawn into the turbine at the penstock pipe intake.
- A penstock pipe to convey the waste water to the power source.
- Civil work components viz. head work, intake, headrace canal/sewage lines, forebay/sewage reservoir tank, penstock pipe, power house and tailrace with back up system.
- Power house components (turbines, generators, drive system and controllers). A water turbine converts the hydro energy into mechanical energy that drives a generator (induction, synchronous or permanent magnet AC generator. which generates electrical power and an automatic control mechanism provides stable electrical power using municipal waste water of the city.
- Transmission and distribution network from generating plant to load centre.

(a) Selection of penstock pipe

The penstock is often the most expensive item in the project which may cost upto 40% of total project cost. Several factors should be considered when deciding which material to use for a particular penstock design pressure i.e. the roughness of the pipe's interior surface, method of joining, weight, ease of installation, accessibility to the site, design life, maintenance, weather conditions, availability, relative cost and likelihood of structural damage [3]. The pressure rating of the penstock is critical because the pipe wall must be thick enough to withstand the maximum water pressure otherwise there may be a risk of bursting. The pressure of the water in the penstock depends on the head, the higher the head, the higher the pressure. The most commonly used materials for a penstock are mild steel, high density poly ethylene (HDPE) and unplastified polyvinyl chloride (uPVC). The uPVC exhibits excellent performance over mild steel and HPDE in terms of least friction losses, weight, corrosion, and cost, etc.

(b) Selection of turbines

Turbine is connected either directly to the generator or via gears or belts and pulleys, depending on the speed required for the generator. The choice of turbine depends mainly on the head and the design flow for the proposed micro-hydro power installation. The selection also depends on the desired running speed of the generator. To adjust for variations in stream flow, water flow to these turbines can be controlled by changing nozzle sizes or by using adjustable nozzles. Turbines used in the hydro system can be classified as Impulse (Pelton, Turgo and Cross flow), Reaction (Frencis, Propeller, and Kaplan) and Waterwheels (undershort, breastshot and overshot). Typical efficiency of Impulse and Reaction turbines range 80-95% and for Waterwheels it ranges 25-75% [3].

(c) Selection of generator

Induction and synchronous generators are used in power plants and both are available in three phase or single phase systems. Induction generators are generally appropriate for micro hydro power generation [1]. Induction generator offers many advantages over a conventional synchronous generator as a source of isolated power supply. Reduced unit cost, ruggedness, brush less (in squirrel cage construction), reduced size, absence of separate DC source and ease of maintenance, self-protection against severe overloads and short circuits, are the main advantages [16]-[21]. Capacitors are used for excitation and are popular for smaller systems that generate less than 10 to 15 kW. All generators must be driven at a constant speed to generate steady power at the frequency of 50 Hz. The two pole generator with a speed of 3000 RPM is too high for practical use with micro hydro power system. The 1500 RPM, four pole genitor commonly used. Generator operating at less than 1000 RPM becomes costly and bulky and to match the speed of the generator to low speed of the turbine, a speed increasing mechanism such as belt and /or gear box is required.

Fig. 1. Principal components of micro-hydro power systems

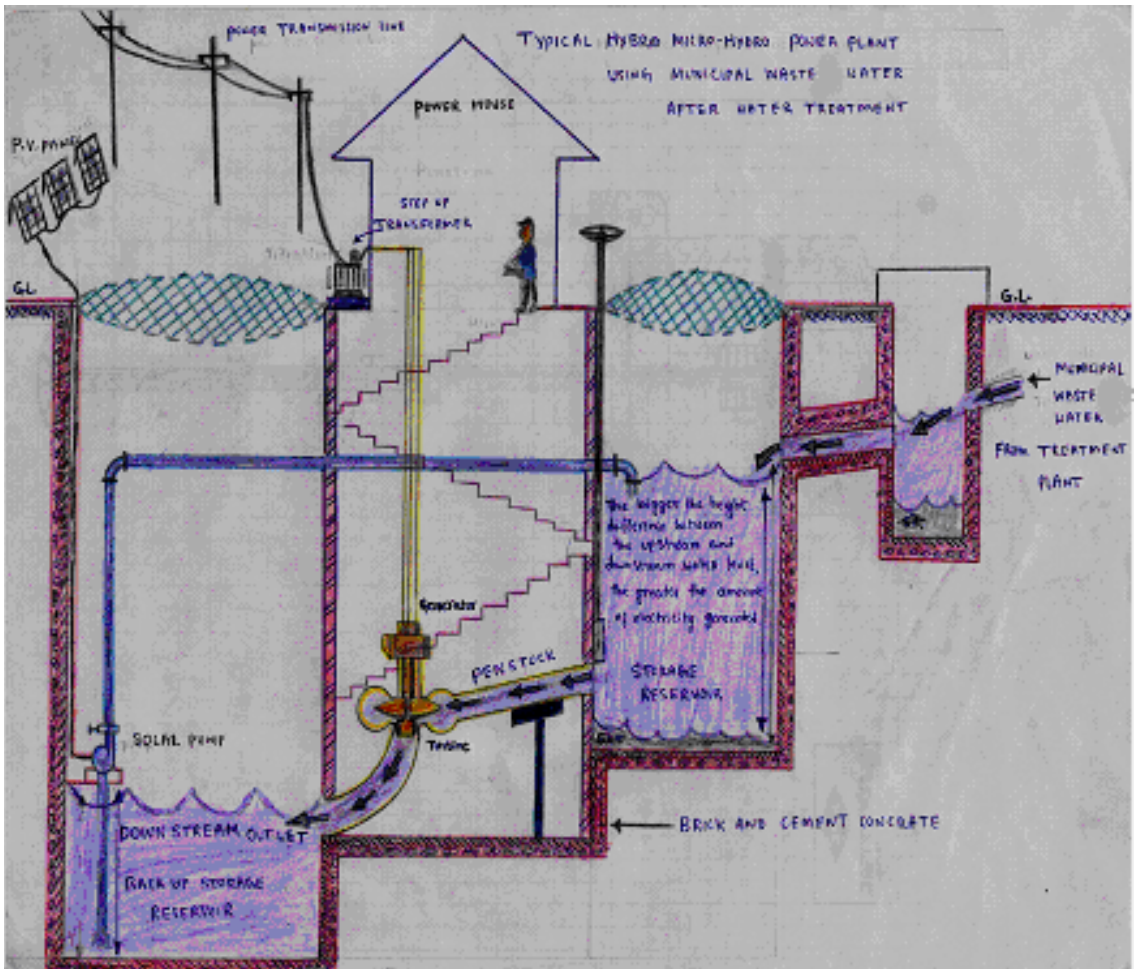

Fig. 2. Interconnection of the Micro Hydro and PV system for reliable operation of the hybrid power system

Fig. 3. Solar pump for recycle waste water from the down stream to upstream storage reservoir

3. MEASUREMENT OF POTENTIAL POWER WITH VARIOUS HEAD AND WATER FLOW RATES

The theoretical amount of power available from a micro-hydro power system is directly related to the flow rate (Q), head (H) and the force of gravity (g) as given below,

$$P_{th} = Q \times H \times g \quad (1)$$

To calculate the actual power output (P_{act}) from micro-hydro power plant, it is required to consider friction losses in the penstock pipes and the efficiency of the turbine and generator. Typically overall efficiencies for electrical generating systems can vary from 50 to 70 % with higher overall efficiencies occurring in high head systems. Therefore, to determine a realistic power output as shown in Table 1, the theoretical power must be multiplied by an efficiency factor of 0.5 to 0.7 depending on the capacity and type of system as given below.

Table 1. Typical power output with various head and water flow rates

Head (m)	Flow rates (lps)					
	10	20	40	60	80	100
	Power output (W)					
1	49	98	196	294	392	490
2	98	196	392	588	784	980
4	196	392	784	1176	1568	1960
8	392	784	1568	2352	3136	3920
10	490	980	1960	2940	3920	4900
15	735	1470	2940	4410	5880	7350
20	980	1960	3920	5880	7840	9800
30	1470	2940	5880	8820	14112	17640
40	1960	3920	7840	14112	18816	23520
60	2940	5880	14112	21168	28224	35280
80	3920	7840	18810	28224	37632	47040
90	4410	8820	21168	31752	42336	52920
100	4900	9800	23520	35280	47040	58800

$$P_{act} = Q \times H \times g \times e \quad (2)$$

where e = efficiency factor (0.5 to 0.7).

4. FLOW DURATION CURVE AND ENERGY CALCULATION

In the paper annual as well as monthly/daily flow duration curve (FDC) has been obtained for municipal waste water from community of the city by recording water flows as shown in Fig. 4 (a). The load duration curve (LDC) of the hybrid system has also been obtained according to reliability evaluation of the plant as shown in Fig. 4 (b). The FDC and LDC are used to asses the expected availability of water flow, load variations and power capability to select the type of the turbine and generator. From Fig. 4 (a) it is seen that, there is a difference in waste water flow between summer and winter and this can affect the power output produced by a micro hydro power system.

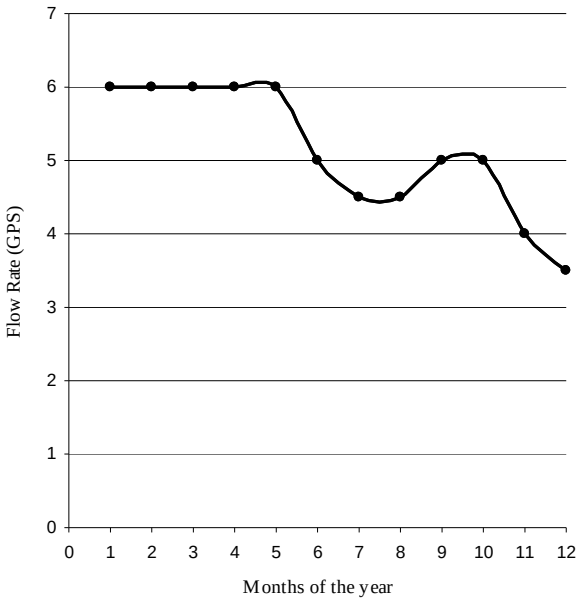

Fig. 4(a) Typical Annual Duration Cureve of System

These variations have been considered in the estimation of total energy generation expected from the site with recycle of the water using solar pumping system as shown in Fig. 3. Peak demand as shown in Table 2 has been calculated to evaluate the reliability [22]-[26] of the hybrid power system.

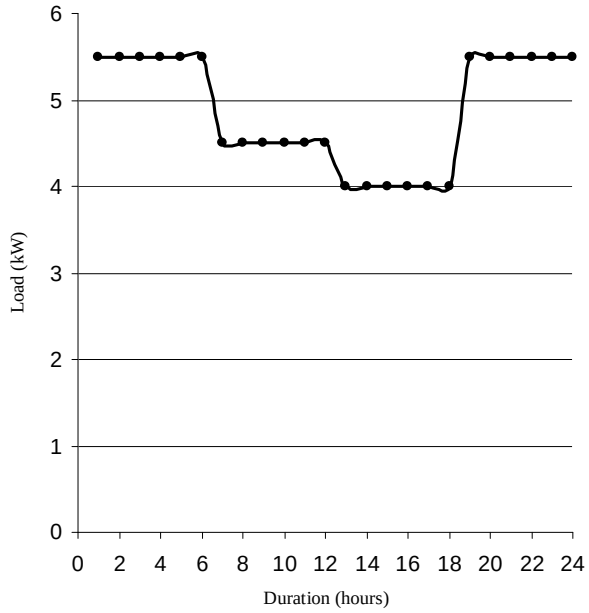

Fig. 4(b). Typical Load Duration Curve of the System

Table 2. Sample load analysis

Appliances	Power rating (W)	Hours /day	Monthly consumption (kWh)	Annual consumption (kWh)
Fluorescent Lamps (4 No.)	160	8	38.4	460.8
Colour Television (1 No.)	140	3	12.6	151.2
Refrigera--tor (1 No.)	500	8	120	1440
Water pump (1 No.)	800	1.5	36	432
Computer (1 No.)	200	10	60	720
Total energy consumption			267	3204

5. RELIABILITY EVALUATION OF SYSTEM

The load on the MHPV hybrid generating station according to load duration curve of the sewage system to have a Gaussian distribution for a specified time interval is given as follows.

$$f(P_d) = \frac{1}{\sigma_d \sqrt{2\pi}} e^{-0.5\left(\frac{P_d - \bar{P}_d}{\sigma_d}\right)^2} \quad (3)$$

The aggregate generation capacity model is approximated as Gaussian [22]-[23].

$$f(C) = \frac{1}{\sigma_c \sqrt{2\pi}} e^{-0.5\left[\frac{C - \bar{C}}{\sigma_c}\right]^2} \quad (4)$$

P_s is known as probability of success and can be expressed as follows

$$P_s = \int_{-\infty}^{\infty} \int_{-\infty}^{C} \frac{1}{2\pi\sigma_c\sigma_d} e^{-0.5\left[\frac{C-\bar{C}}{\sigma_c}\right]^2} e^{-0.5\left(\frac{P_d - \bar{P}_d}{\sigma_d}\right)^2} dc dP_d \quad (5)$$

Equation (5) can be written as follows [24].

$$P_s = \int_{-\infty}^{\infty} \left[\int_{-\infty}^{z} e^{-0.5\left(x^2+y^2\right)} dy \right] dx \quad (6)$$

where β is given as follows.

$$\beta = \frac{\bar{C} - \bar{P}_d}{\sqrt{\sigma_d^2 + \sigma_C^2}}$$

Equation (6) is simplified as follows.

$$P_s = \int_{-\infty}^{\beta} \left[\int_{-\infty}^{\infty} \frac{1}{\sqrt{2\pi}} e^{-0.5\left(x'^2\right)} dx' \right] e^{-0.5\left(y'^2\right)} dy'$$

$$= \int_{-\infty}^{+\beta} \frac{1}{\sqrt{2\pi}} e^{-0.5\left(y'^2\right)} dy' = \varphi(\beta) \quad (7)$$

Where, φ [β] is the area under the normal distribution curve having 0 mean and standard deviation [N (0, 1)] 1 from - ∞ to β and this value can be conveniently obtained from standard normal distribution table.

6. RESULTS AND DISCUSSIONS

A MHPV hybrid power system can be reliable and provide stable electric power. The reliability of MHPV hybrid power system has been evaluated at different conditions of the LDC and FDC using a methodology based on Gaussian distribution approach. The mean load has been assumed 1.0 kVA. The mean capacity and standard deviation data are given in Table 3.

The standard deviations for both generating capacity and mean load have been assumed 10% of the generating capacity and mean load respectively. Using the relation (7), the failure probability has been evaluated assuming generating capacity $\bar{C}$ = 1.2 kVA as P_F = 0.1013.

Now the generating capacity is increased in step of 50 VA at the fixed value of the mean load at 1.0 kVA and

the probability of failure has been calculated. Various plots of failure probability v/s generating capacity are shown in Fig. 5, selecting the following values of the standard deviations.

Table 3. Mean capacity and standard deviation

$\bar{C}$	1.2 kVA	1.25 kVA	1.3 kVA	1.35 kVA	1.4 kVA
σ_C = 10%	120	125	130	135	140
σ_C = 20%	240	250	260	270	280
σ_C =15%	180	187	195	202	210

(a) [σ_1 =10% of $\bar{L}$ and σ_C =10% of $\bar{C}$] = σ_1

(b) [σ_1 =10% of $\bar{L}$ and σ_C =20% of $\bar{C}$] = σ_2

(c) [σ_1 =20% of $\bar{L}$ and σ_C =10% of $\bar{C}$] = σ_3

(d) [σ_1 =20% of $\bar{L}$ and σ_C =20% of $\bar{C}$] = σ_4

The various curves are drawn for various combinations of σ_C and σ_1 as shown in the Fig. 5. It is observed from curve A and B that for the same generating capacity of the system, the probability of failure with σ_2 is more than σ_1. This is due to fact that large uncertainty involved in generating capacity distribution function.

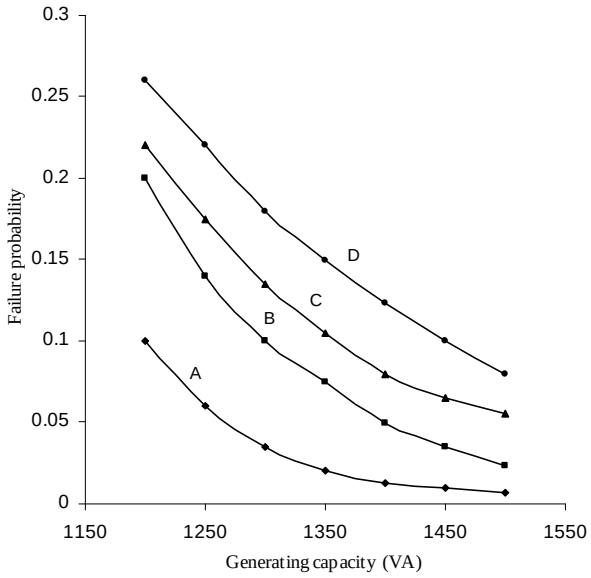

Fig. 5. Failure probability v/s generating capacity of power system

Similarly by observing the curve A and C for the same generating capacity the probability of failure for σ_2 is more than σ_3 and so on. From the curve D, the failure probability for any generating capacity is more than from other curves. In summary, the probability of failure increases with either increase of σ_1 or increase of σ_c or both σ_1 and σ_c.

7. CONCLUSIONS

A MHPV hybrid power system is stable, cheap and capable of producing reliable power because the head/pressure of the sewage reservoir has been maintained at constant using back up service by PV pump in summer and winter cycles of the country. A new methodology has been introduced in this paper for hybrid generating system reliability evaluation using different load and generation models. The evaluation of loss of load probability has been based on load generation models as peak load of the MHPV hybrid power plant is less than generating capacity, failure probability is negligible; and normal distribution is assumed as generation capacity model and load duration curve as load models and normal distribution model as generating capacity. Further in all cases it is confirmed that the failure probability of the system increases with an increase in variance of load or generation capacity.

ACKNOWLEDGMENT

Authors are grateful to BHU, Varanasi (India) for the encouragement and financial support for carrying out the research work.

NOMENCLATURE

P_d = Demand at the generating stations

$\overline{P}_d$ = Average or mean load of plant

σ_d = Standard deviation of demand

C = Capacity of the generating station

$\overline{C}$ = Mean capacity of the plant

σ_c = Standard deviation of capacity

P_F = Probability of failure of generating station

P_S = Probability of success of generating station

P_{th}= Theoretical power output in kW

Q = Usable flow rate in m^3/s

H = Gross head in m

g = Gravitational constant ($9.81 m/s^2$)

LOLP = Loss of load probability

f (L) = Normal distribution

L = Total load in VA

Φ = Rotational angle

Φ(β) = Area under normal distribution curve

S = Safety factor

n = Total duration of the study

P_{fi} = Failure probability for L_i th load level

REFERENCES

[1] Bhatti, T.S.; Bansal, R.C.; and Kothari D.P. (Ed.). 2004. *Small Hydro Power Systems*. Delhi, India: Dhanpat Rai and Sons.

[2] Jiandong, T.; Naibo, Z.; Xianhuan, W.; Jing, H.; and Huishen D. (Ed.). 1995. *Mini Hydropower*. Chichester, England: John Wiley and Sons.

[3] Fraenkel, P.; Paish, O.; Harvey, A.; Brown, A.; Edwards, R.; and Bokalders, V. 1991. Micro-Hydro Power: A guide for Development Workers. London, UK: Intermediate Technology.

[4] Tripathy, S.C. and Bhardwaj, V. 1996. Automatic Generation control of a small hydro-turbine driven generator. *Energy Conversion and Management*, 37(11): 1635-1645.

[5] Roy, S. 2005. Optimal planning of generating units over micro-hydro resources within a catchment area. *IEEE Trans. Energy Conversion* 20(1): 231-236.

[6] Bhatti, T.S.; Bansal, R.C.; and Kothari D.P. 2002. On some of the design aspects of wind energy conversion systems. *Energy Conversion and Management* 43(16): 2175-2187.

[7] Bansal, R.C.; Zobaa, A.; and Saket, R.K. 2005. Some issues related to power generation using wind energy conversion systems: an overview. *Int. Journal of Emerging Electric Power systems* 3(2): 1-19.

[8] Bhatti, T.S.; Bansal, R.C.; and Kothari D.P., 2001. Some aspects of grid connected wind electric energy conversion systems. *Interdisciplinary Journal of Institution of Engineers (India)* 82(1): 25-28.

[9] Bhatti, T.S.; Al-Ademi, A. A. F.; and Bansal, N. K. 1997. Load frequency control of isolated wind diesel hybrid power systems. *Energy Conversion and Management* 38(9): 829-837.

[10] Bhatti, T.S.; Al-Ademi, A. A. F.; and Bansal, N. K. 1997. Load-frequency control of isolated wind-diesel-micro hydro hybrid power systems (WDMHPS). *Energy* 22(5): 461-470.

[11] Hunter, R. and Elliot, G. 2004. Wind-diesel systems: a guide to the technology and its implementation. New York, USA: *Cambridge University Press*.Bansal.

[12] R.C. 2006. Automatic reactive power control of isolated wind-diesel hybrid power systems. *IEEE Trans. of Industrial Electronics* 53(4): 1116-1126.

[13] Bansal, R.C. 2005. Reactive power compensation of wind-diesel hybrid power systems using matlab/simulink. *Int. Journal of Energy Technology and Policy* 3(3): 237-252.

[14] Bhatti, T.S.; Bansal, R.C.; Kothari D.P.; and Bhat, S. 2005. Reactive power control of isolated wind-diesel-micro-hydro hybrid power systems using matlab/simulink. *Int. Journal of Global Energy Issues* 24(1/2), 86-99.

[15] Bhatti, T.S.; Bansal, R.C.; and Kothari D.P. 2004. Automatic reactive power control of isolated wind-diesel hybrid power systems for variable wind speed/slip. *Int. Journal of Electric Power Components and Systems* 32(9): 901-912.

[16] Bhatti, T.S.; Bansal, R.C.; and Kothari, D.P. 2003. A bibliographical survey on induction generators for application of non-conventional energy systems. *IEEE Trans. Energy Conversion* 18(3): 433-439.

[17] Nacfaire, H. (Editor). 1989. *Wind-diesel and wind autonomous energy systems*. London, UK: Elsevier Applied Science.

[18] Twidel, J.W. and Weir, A.D. 2006. *Renewable Energy Sources*, 2nd Edition, New York, USA: Taylor and Francis.

[19] Sandhu Khan, P.K. and Chatterjee, J.K. 1999. Three-phase induction generators: a discussion on performance. *Electric Machines and Power Systems* 27(8): 813-832.

[20] Bansal, R.C. 2005. Three-phase self-excited induction generators (SEIG): an overview. *IEEE Trans. Energy Conversion* 20(2): 292-299.

[21] Simoes, M.G. and Farret, F.A. 2004. *Renewable Energy Systems: Design and Analysis with Induction Generators*. New York, USA: CRC Press.

[22] Arya, L.D.; Choube, S.C.; and Saket, R.K. 2000. Composite system Reliability Evaluation based on voltage stability limit. *Journal of The Institution of Engineers (India)* EL-80(1): 133-137.

[23] Arya, L.D.; Choube, S.C.; and Saket, R.K. 2001. Generation system adequacy evaluation using probability theory. *Journal of The Institution of Engineers (India)* EL-81(1): 170-174.

[24] Saket, R.K. and Bansal, R.C. 2005. Generating capacity reliability evaluation using gaussian distribution approach, *Proc. of the Int. Conf. on Reliability and Safety Engineering*, Kharagpur, India. 21-23 December. *Reliability Engineering Centre*, Indian Institute of Technology.

[25] Saket, R.K. and Bansal, R.C. 2006. Reliability evaluation of interconnected composite electrical power system considering voltage stability at continuation power flow, *Proc. of the Int. Conf. on Power System Operation in Deregulated Regime (ICPSODR-2006)*, New Delhi, India. 6-7 March. Institute of Technology, Banaras Hindu University, Varanasi Allied publishers Pvt. Ltd.

[26] Saket, R.K. and Kaushik, S.P. 2005. Use of gaussian distribution method for biorhythmic analysis to prevent aviation accident, *Pro. of the 14th ISME Int. Conf. on Mechanical Engineering in Knowledge age*, Delhi, India. December. Delhi Collage of Engineering.

Five Level Diode-Clamped Voltage Source Converter for Custom Power Device Applications

N. Mithulananthan and P. Boonchiam*

Abstract—*Custom power devices are the importance to secure the sensitive loads from power quality problems. Especially in medium-voltage grids, the demand for securing larger loads has increased significantly. Installing of higher power levels leads to consider the multilevel converters with an increased number of levels and different topologies. Therefore, the five-level diode-clamped converter could be the interesting solution. This paper presents a method to allow a short-time stable operation of this topology without oversizing the DC-link capacitor and shows the drawback of this topology that its voltage levels are not stable for active power transmission and therefore the usage of this converter for custom power device applications. The voltage source converter is simulated in the power system using MATLAB program.*

Keywords—**Custom Power Devices, Power Quality Problem, Voltage Sag/Swell, Multilevel Converter, Distribution of Electrical Energy.**

1. INTRODUCTION

Concerns on power quality problem have come into attention to many utilities and researchers for a decade. Many literatures devoted to obtain the methodology to find the way to prevent and relieve the power quality problem. The custom power had been proposed which concept of custom power and power electronic control in distribution areas by using the forced-commutation switches. It introduced the custom power solutions of power reliability rely on such novel components and systems as Solid State Circuit Breaker (SSCB) and distribution static compensator (D-STATCOM), Dynamic Voltage Restorer (DVR) and Unified Power Quality Conditioner (UPQC) [1-2].

Presently new systems for medium voltage grids with a compensation power of several MW are developed [3]. Even though several inverter topologies were already presented for custom power devices, the H-Bridge inverter is used in nearly all applications [4]. Going to higher power levels for compensating voltage disturbances in medium-voltage grids leads to the need of a series or parallel connection of devices or converters. One solution is a multilevel inverter with a high number of levels, especially the five-level diode-clamped inverter could be an interesting solution for this application. The main drawback of a five-level diode-clamped inverter is that it is not feasible for an active power transmission [5], because the capacitor voltage cannot be balanced for all four capacitors within the DC-link. Since delivering active power is essential in the custom power devices, a five-level diode-clamped converter seems not a suitable topology. However, the operation time of custom power device systems is quite short, therefore it may be possible to use different capacitances to make this inverter work properly. In this paper the derived equations will be explained and the needed capacitances will be calculated. Finally, these calculations will be verified with simulations of the designed system.

Fig. 1 shows the basic concept of custom power devices. For a successful compensation, the custom power devices must be able to detect voltage disturbances and control the converter to prevent against sags, swells, flicker, harmonic, etc.

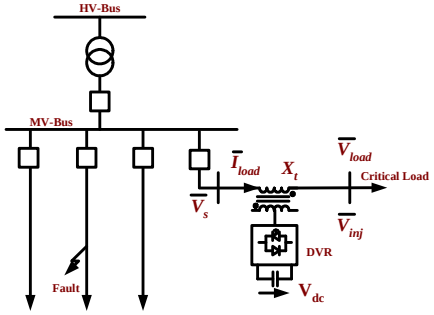

(a) Dynamic Voltage Restorer

2. FIVE-LEVEL DIODE-CLAMPED VOLTAGE SOURCE CONVERTER

Main Circuit and Component

During the last 10 years, there has been steady growth multilevel converter topology as they can suit for the high voltage and high power applications. Multilevel VSC are the attractive technology for the medium voltage application, which includes power quality and power conditioning applications in the distribution system. The most well-known multilevel topologies

Nadarajah Mithulananthan and *Paisan Boonchiam (corresponding author) are with the Energy Field of Study, Asian Institute of Technology, P.O. Box 4, Klong Luang, Pathumthani 12120, Thailand (corresponding author to provide phone: 66-2-524-5398; Fax:66-2-524-6589; e-mail: st101633@ait.ac.th and mithulan@ait.ac.th

developed so far are shown in Fig. 2. There is diode-clamped multilevel voltage source converter.

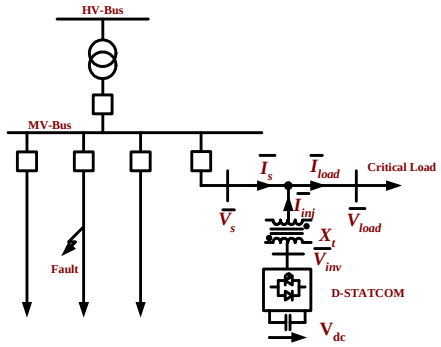

(b) Distribution Static Compensator

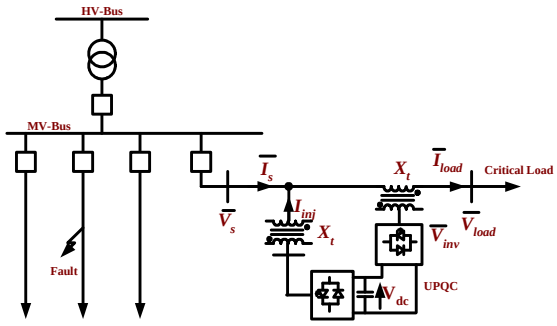

(c) Unified Power Quality Conditioner

Fig.1 Simplified diagram of custom power devices connected between supply network and a critical plant

This multilevel topology can generate multilevel output voltages with low harmonics and reduce voltage stress on the power electronic devices. In order to compare the different multilevel topologies, a quantity called N_{index} is defined as given in Equation (1).

$$N_{index} = \frac{V_{dc,\max}}{V_{D,\max}} \quad (1)$$

where $V_{dc,\max}$ is the maximum dc bus voltage and $V_{D,\max}$ maximum nominal voltage requirement of the devices.

Fig. 2 depicts one leg circuit diagram of a five-level diode-clamped voltage source converter. This topology uses clamping diodes to limit dynamic and static overvoltages for switching devices. The clamping diodes are connected to taps of dc bus capacitor. In medium voltage grids, dc bus voltage is so high therefore capacitors are connected in series. Diode-clamped voltage source converter generates different voltage levels for output voltage in the ranging between positive and negative of $V_{dc}/2$. The number of levels N_{level} is

$$N_{level} = ceil(N_{index}) + 1 \quad (2)$$

The symbol *ceil*(x) represents the ceiling number of *x*. N_{index} is the number battery cell. The number of single capacitors N_C is

$$N_C = ceil(N_{index}) \quad (3)$$

and number of main switching devices is

$$N_{SW} = 2 \times ceil(N_{index}) \quad (4)$$

In contrast to main devices, the nominal voltage of the clamping diodes is higher than the voltage of one level. Therefore, it becomes necessary to place several diodes in series to achieve the required voltage. If rated voltage of a clamping diode equals rate voltage of the main switching devices, a N_{level}-level inverter leg needs the following number of clamping diodes.

$$N_{D,Clamp} = (N_{level} - 1)(N_{level} - 2) \quad (5)$$

For example, the five-level DC-VSC needs 4 capacitors, 6 diodes and 8 power switches. However, in practice, more diodes are needed due to the voltage derating of the series connection of up to (N_{level}-2) diodes. This fact introduces practical problems such as parasitic inductances or package difficulties.

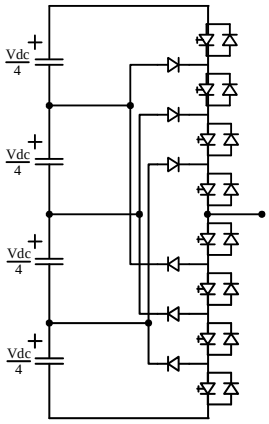

Fig. 2 One Phase Leg of a five-level topology

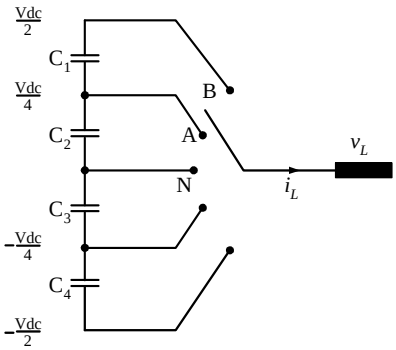

Fig. 3 Principle of a 5–level NPC

Switching Strategy

The most popular and simple switching schemes for the diode voltage source converter are step modulation and sine pulse width modulation (SPWM). Assume the magnitude of the reference sinusoid is 1.0. Comparing between triangular carrier waves and the references signal, this method calculates at switching states directly.

Each device is only switched twice per period Fig. 4 shows the switching principle for a five-level converter.

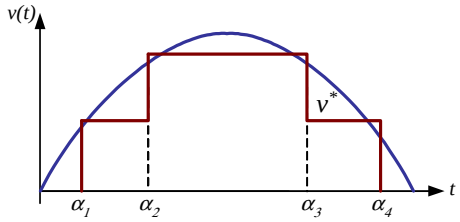

Fig. 4 Five-level step modulation switching strategy

The first level is turned-on at α_1 and the second level at α_2. To achieve a completely symmetrical switching scheme, the switch-off instances has to be

$$\alpha_3 = \frac{T}{2} - \alpha_2 \qquad \alpha_4 = \frac{T}{2} - \alpha_1 \tag{6}$$

And the switching times for the seconded half-period have to be delayed on T/2. The amplitudes of the fundamental sine-wave and the harmonics can be determined by a Fourier analysis. The decomposition of the function will be in the form

$$f(x) = \frac{a_0}{2} + \sum_{n=1}^{\infty} \left(a_n \cos(nx) + b_n \sin(nx) \right) \tag{7}$$

where

$$a_n = \frac{1}{\pi} \int_{-\pi}^{\pi} f(x) \cos(nx)\, dx \tag{8}$$

$$a_n = \frac{1}{\pi} \int_{-\pi}^{\pi} f(x) \sin(nx)\, dx \tag{9}$$

Because of the symmetry of the output signal, no a_n-coefficient exist and all even harmonics $b_{2k}, k \in N_0$ disappear. The fundamental amplitude b_1 can be found as:

$$b_1 = \frac{2}{\pi} \int_{\alpha_1}^{\pi - \alpha_1} f(x) \sin(x)\, dx = \frac{4}{\pi} \left(\cos(\alpha_1) + \cos(\alpha_2) \right) \times V_{DC} \tag{10}$$

Assuming V_{DC} the voltage of one level. B1 is depended on two variables α_1 and α_2 and has one degree of freedom. For example α_1 and α_2 can be chosen to minimize one specific harmonic. Depending on the demands of the electrical structure at the output of the converter, the 3rd or the 5th harmonics is chosen. The related Fourier-coefficients are

$$b_3 = \frac{1}{\pi} \int_{-\pi}^{\pi} f(x) \sin(3x)\, dx = \frac{4}{3\pi} \left(\cos(3\alpha_1) + \cos(3\alpha_2) \right) \times V_{DC} \tag{11}$$

In order to obtain the desired output magnitude and to minimize the desired harmonics, the following equation set has to be solved:

$$b_1(m_a) = m_a \times 2 \times V_{DC} \tag{12}$$

$$\frac{d}{d(\alpha_1, \alpha_2)} \times b_3 = 0 \tag{13}$$

The analytical solution of this nonlinear problem leads to piecewise linear functions over the entire modulation range. For minimizing the third harmonic, they will be

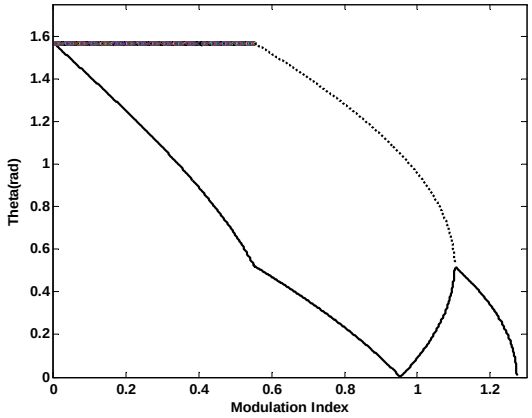

Fig. 5 Switching angles with minimizing the 3rd harmonics

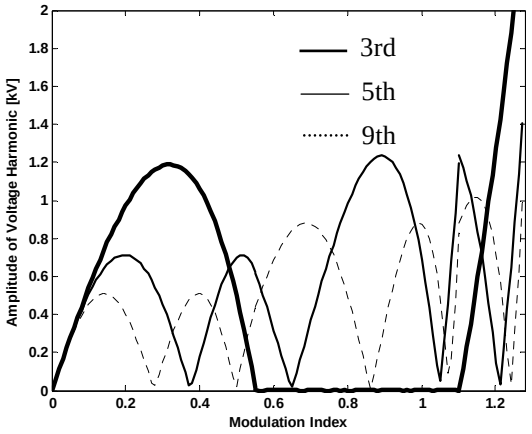

Fig. 6 Harmonic content of the output voltage

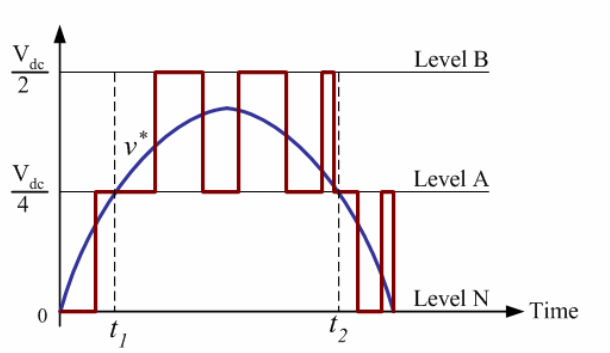

Fig. 7 Voltage Waveform of a 5-level NPC.

Fig. 5 illustrates these switching angle α_1 and α_2 and Fig. 6 depicts the amplitude of the first harmonics. Concerning the harmonic content this method seems to be the most suitable so far. With an increasing as well because this introduces new degree of freedom and more harmonics can be eliminated.

$$\alpha_1(m_a)=\begin{cases}\arccos\left(m_a\dfrac{\pi}{2}\right) & 0\le m_a\le\dfrac{\sqrt{3}}{\pi}\\ \arccos\left(\dfrac{m_a\pi}{4}+\dfrac{1}{12}\sqrt{36-3m_a^2\pi^2}\right) & \dfrac{\sqrt{3}}{\pi}\le m_a\le\dfrac{2\sqrt{3}}{\pi}\\ \arccos\left(m_a\dfrac{\pi}{4}\right) & \dfrac{2\sqrt{3}}{\pi}\le m_a\le\dfrac{4}{\pi}\end{cases} \quad (14)$$

$$\alpha_2(m_a)=\begin{cases}\dfrac{\pi}{2} & 0\le m_a\le\dfrac{\sqrt{3}}{\pi}\\ \arccos\left(\dfrac{m_a\pi}{4}+\dfrac{1}{12}\sqrt{36-3m_a^2\pi^2}\right) & \dfrac{\sqrt{3}}{\pi}\le m_a\le\dfrac{2\sqrt{3}}{\pi}\\ \arccos\left(m_a\dfrac{\pi}{4}\right) & \dfrac{2\sqrt{3}}{\pi}\le m_a\le\dfrac{4}{\pi}\end{cases} \quad (15)$$

Characteristic of DC-link Capacitors

In Fig.3, the equivalent circuit of a 5-level NPC inverter is depicted. The DC-link voltage is divided into four different capacitors, which all have the same capacitance and voltage. Due to the modulation of a sinusoidal output voltage the load will be connected to the upper three voltages (B, A, N) during the positive semi-cycle and to the lower voltages for the negative half-wave. For the subsequent analysis only the positive half-wave is used, therefore only the three switching states B, A and N have to be considered.

First, the voltage stability problem of a five-level diode-clamped converter will be briefly described. Fig. 7 shows one half period of the output voltage of the inverter. As long as the reference voltage (v^*) has a magnitude which is below the voltage of level A, the output is switched between the two potentials A and N. therefore, only the inner capacitor is discharged. If the reference voltage exceeds the value of Level A the modulation charges and the output is switched between the potentials A and B. It becomes obvious that the two capacitors are not discharges equally.

The reason for the different discharge is, that the inner capacitor is constantly discharged during the first semi-cycle whereas the outer one is only discharged between t_1 and t_2. Hence, the voltage distribution in the DC-link cannot be kept constant for active power transmission. Consequently, a five-level diode-clamped converter can only be used for active power transmission if a Back-to-Back solution is used.

Although it is not possible to achieve stable DC levels with a five-level diode-clamped converter for a standard drive application it could be possible to use this circuit for the short operation times of custom power devices. One solution could be a different size of the inner and the outer capacitor. The disadvantage of different capacitors is, that the DC-link cannot be recharge by one source. Hence, each capacitor has to be charged separately. Since the recharge must not be very fast for custom power devices, relatively small sources can be used and therefore this is no real disadvantage for such a system.

3. FIGURES AND TABLES SIZING OF CAPACITORS AND ENERGY

Ratio of Capacitances

The positive and negative half-waves lead to the same discharge of the two upper and two lower capacitors. As a result, the calculation effort can be reduced to one half cycle. The calculate the charge Q_1 drawn from each capacitor, the half cycle between 0 and T/2 is divided in two parts. During the first part, the output is only switched between the levels N and A (t = [0, t_1] & [t_2, T/2]). For the duration of the second interval (t = [t_1, t_2]) the voltage level is switched between the levels A and B. The first step is to calculate the borders of the interval, therefore t_1 and t_2 must be calculated. These times can be calculated by considering the fact that, as soon as the reference voltage elapses the voltage of level A, the second starts ($v^*(t) = V_m sin(\omega t) = V_{dc}/4$). Using these fact two equations can be derived.

$$t_1=\frac{T}{2\pi}\arcsin\left(\frac{V_{dc}}{4V_m}\right)=\frac{T}{2\pi}\cdot x \quad (16)$$

$$t_2=\frac{T}{2\pi}-t_1=\frac{T}{2\pi}\cdot(\pi-x) \quad (17)$$

where $x=\arcsin\left(\dfrac{V_{dc}}{4V_m}\right)$

Based on these two equations and by comparing the voltage-sec area of the reference voltage and the output voltage, the complete time interval during which the output voltage is connected to level A(t_A) and to level B(t_B) can be calculated. Within the first section, the inverter is switched between the neutral point and level A. By comparing the voltage-sec areas of the reference voltage and the output voltage the time t_{A1} can be calculated. This is the interval where the output is connected to level A, as long as the reference voltage is below the magnitude of level A. This leads to the following equations (18).

$$\frac{V_{dc}}{4}\cdot t_{A1}=\int_0^{t_1}V_m\sin(\omega_0\cdot t)\cdot dt+\int_{t_2}^{T/2}V_m\sin(\omega_0\cdot t)\cdot dt \quad (18)$$

$$t_{A1}=\frac{8\cdot V_m\cdot T}{2\cdot\pi\cdot V_{dc}}\cdot(1-\cos x)$$

Analog to these considerations the other needed time intervals can be calculated. In this case the voltage-sec area for the section where the reference voltage is above level A has to be considered. The time t_{A2} is equal to the interval during which level A is connected to the output and during t_B the output voltage is equal to level B. Thus, the equations (19) and (20) can be derived.

$$t_{A2}=T\cdot\left(1-\frac{2}{\pi}\cdot x-\frac{4\cdot V_m}{\pi\cdot V_{dc}}\cdot\cos x\right) \quad (19)$$

$$t_B=T\cdot\left(\frac{4\cdot V_m}{\pi\cdot V_{dc}}\cdot\cos x+\frac{x}{\pi}-\frac{1}{2}\right) \quad (20)$$

Finally, the time intervals for level A and B connected to the output can be derived. This leads to the total time t_A during which level A is connected to the output.

$$t_A = t_{A1} + t_{A2} = T \cdot \left[1 - \frac{2 \cdot x}{\pi} + \frac{4 \cdot V_m}{\pi \cdot V_{dc}} \cdot (1 - 2 \cdot \cos x) \right] \quad (21)$$

To determine the change drawn from the capacitors the load current must be assumed next. To get a worst case estimation a pure ohmic load is considered. Therefore, a constant current is drawn from each capacitor during the time intervals. Whereas during t_A charge is only drawn from the inner capacitor, during t_B both capacitors are discharged. Using the current (I_{LA}, I_{LB}) during the two time intervals the charge drawing from the capacitors can be derived, with Q_1 draw from the outer capacitor and Q_2 from the inner one.

$$Q_1 = \frac{V_{dc}}{2R} t_B \qquad \text{with } I_{LB} = \frac{V_{dc}}{2R} \quad (22)$$

$$Q_2 = \frac{V_{dc}}{2R} t_B + \frac{V_{dc}}{2R} t_A = \frac{V_{dc}}{2R} \left(t_B + \frac{t_A}{2} \right) \text{ with } I_{LA} = \frac{V_{dc}}{4R} \quad (23)$$

via the amplitude modulation index ($m=V_m/(V_{dc}/2)$) the needed quotient of the charges draw from the capacitors can be calculated with the following expression.

$$\begin{aligned} q &= \frac{Q_1}{Q_2} = 2\cos x + \frac{1}{2m}(2x - \pi) \\ &= 2\cos\left(\arcsin\left(\frac{1}{2m} \right) \right) + \frac{1}{2m} \left[2\left(\arcsin\left(\frac{1}{2m} \right) \right) - \pi \right] \end{aligned} \quad (24)$$

Since both capacitors will be charged to the same voltage, equation 13 expresses also the needed capacitor ratio for a constant discharge of the outer and the inner capacitor. It becomes obvious that this quotient depends on the modulation index, therefore it is not possible to achieve equal discharge for all modulation indexes. If the modulation index is below 0.5 the outer capacitance will not be discharged, because only the level A and N will be connected to the output.

In Fig. 8 the derived equation is depicted for a modulation index from 0.5 to 1.2. As expected, a low modulation index leads to a very large capacitor C_2, because for a modulation index below 0.5 the energy will only be drawn from the inner capacitor. Therefore, a low index leads to large discharge of the inner capacitor and a lower for the outer capacitor. On the contrary, a large modulation index corresponds to a long time interval in which the output is switched between level A and B. Consequently, both capacitors are discharged during most of the period and the needed ratio is approaching unity.

In view of the fact the custom power devices needs different modulation indexes – depending on the sag depth and the needed compensation time – it is also not possible to achieve an equal discharging. One advantage f a custom power devices is that the minimum modulation index is above 0.5, because shallow sags can be compensated up to the maximum voltage of 10% above the nominal value. Therefore, a higher modulation index can be chosen to assume a proper functionality of the custom power devices. As a consequence, an average value of the modulation index should be used to assure compensation with the five-level diode-clamped converter topology. In most custom power devices applications the amount of energy needed for the application can easily be calculated. Therefore, it is important to calculate the different capacitances from this value by considering the needed ratio derived in equation (24). The stored energy and the needed capacitors can be calculated with the following equation (25).

$$E_{dc} = 2 \cdot \frac{1}{2} \cdot (C_1 + C_2) \cdot \left(\frac{V_{dc}}{4} \right)^2 \quad (25)$$

$$C_1 = \frac{16 E_{dc}}{V_{dc}^2 \left(1 + \frac{1}{q} \right)} \qquad C_2 = \frac{16 E_{dc}}{V_{dc}^2 (1 + q)}$$

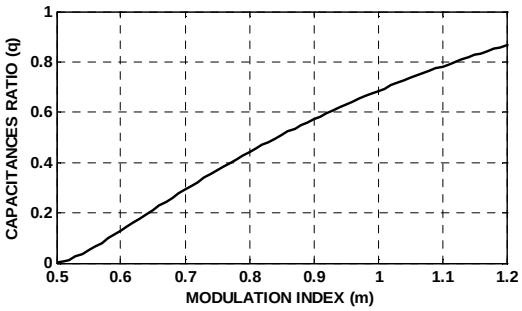

Fig. 8 Needed ratio of capacitances depending on modulation index

Reduced Amount of Energy Needed

The main advantage of different capacitance is the reduced amount of energy needed for the compensation process. In general, the minimum amount of energy is determined by the value needed for a successful compensation, therefore it can be calculated by considering the worst case failure and the minimum compensation time. If a standard design is chosen all capacitors will be equal, leading to a similar amount of energy within each capacitor.

Due to the unsymmetrical discharge of the capacitors a larger portion of energy is drawn from the inner capacitors. Consequently, these capacitors will be discharged quit fast and the semiconductors needed to block higher voltages. Hence, the amount of energy must be increased to avoid these problems. By varying the capacitances this oversizing can be reduced significantly, because the capacitors are designed according to the needed energy during compensation.

Considering the needed size of the inner capacitor (C_2) the needed amount of energy can be calculated. For the standard solution all capacitors will be design equally, whereas for the presented solution the outer capacitor will be reduced according to the calculated ratio (equation (26)).

$$E_{S\tan dard} = 4 \cdot \frac{1}{2} \cdot C_2 \cdot V_{dc}^2 = 2 \cdot C_2 \cdot V_{dc}^2 \quad (26)$$

$$E = 2 \cdot \frac{1}{2} \cdot C_2 \cdot V_{dc}^2 + q \cdot \frac{1}{2} \cdot C_2 \cdot V_{dc}^2$$

This leads to the following equation:

$$\frac{E}{E_{S\tan dard}} = \frac{1+q}{2} \quad (27)$$

It should be kept in mind that the ratio between the capacitors cannot be reduced too much, because the voltage of the outer capacitor is needed to assure a correct compensation of the load voltage and therefore the energy storage in these devices has to be sufficient. Various simulations were accomplished to find the minimal value for the capacitor ratio for worst case scenarios. In the presented application the lowest ratio realized was 0.4, leading to 30% less energy needed for the custom power devices application. As a consequence, the enormous cost for the large DC-link capacitors can be reduced considerably compared to a standard 5-level design.

4. SIMULATION RESULTS

To prove the calculation from the previous section, simulations were done with a DVR based on a five-level diode-clamped converter. Fig.9 shows the DC-link voltage during a three-phase sag under full load conditions. In this case, the remaining voltage is 75% of the nominal voltage with a total compensation power of 10 MW.

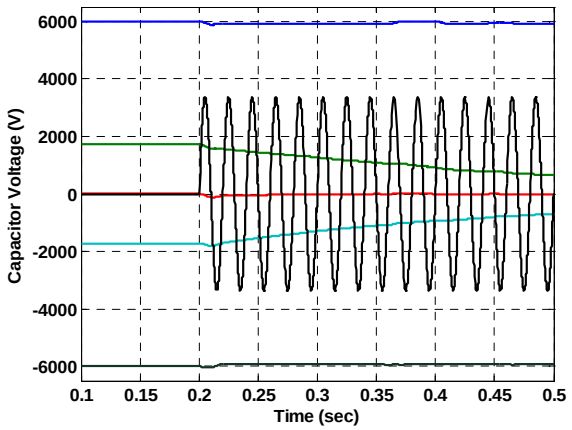

Fig.9 DC-link voltage during the compensation of a three-phase sag with ohmic load.

At approximately 200 ms, the sag is detected and the custom power devices starts to compensate the voltage. From that point on the DC-link constantly discharged. The ratio of the outer and the inner capacitor is 0.4, which corresponds to a modulation ratio of 0.75. It becomes obvious that the capacitors are not discharged equally, because the modulation ratio changes during the compensation. Due to the needed large energy storage device, a custom power devices is only used for short compensations of 300 ms under full load conditions [6]. During the 300 ms the voltage difference is still quite low, so that the inverter is still operational. Therefore, it was proven that the five-level diode-clamped converter can be used for an active power compensation with different capacitances. As already mentioned, the load was assumed to be ohmic to calculate the needed capacitor ratio for a worst-case scenario. This calculated ratio can also be used for different displacement factors, to prove this the same capacitors were used for a similar load and voltage sag. The power factor of 0.8. In Fig.10 the different DC-link voltages are depicted. By comparing these results to the previous pure ohmic load it becomes obvious that the voltage difference between the outer and the inner capacitors has decreased. Thus, the previously described assumption leads to a worst-case scenario and can be used for the design of a custom power devices based on a five-level diode-clamped converter topology.

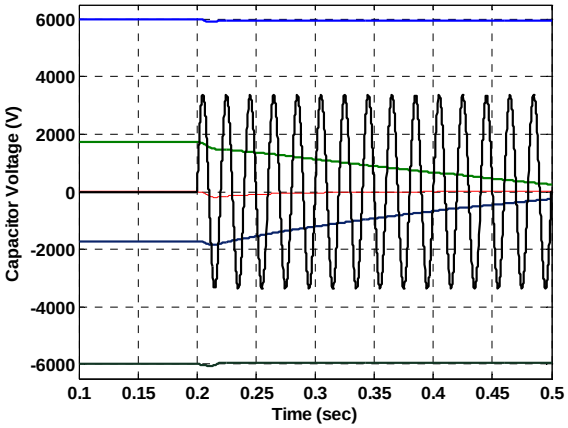

Fig.10 DC-link voltage during the compensation of a three-phase sag.

5. CONCLUSION

One major power quality problem in distribution grids are voltage sags, which lead to production losses in sensible processes. For medium voltage and high power loads custom power devices are one solution. Since the power of the protected loads is constantly increasing, new inverter concepts should be examined, i.e. higher number of levels. Therefore, a five-level diode-clamped converter was examined for this application. The main disadvantage of the five-level diode-clamped converter topology is that it can only be used in a back-to-back configuration if active power is needed. Otherwise, the capacitor voltages will deviate from each other and a steady-state operation is not possible. However, for custom power devices applications active power is needed, but only for a short time interval.

REFERENCES

[1] M. Bollen, “Understanding Power Quality Problems, voltage sag and interruptions” IEEE press 1999.

[2] Kara, D. Amhof, P. Daehler, H. Gruening, “Power Supply Quality Improvement with a Dynamic

Voltage Restorer (DVR)", Applied Power Electronics Conference Proceedings, 1998, No. 2, pp.986-993.

[3] R. Affolter, B. Connell, "Experience with Dynamic Voltage Restorer for a critical manufacturing facility", IEEE/PES Transmission and Distribution Conference Dallas, 2003.

[4] J. G. Nielsen, F. Blaabjerg, "Comparison of System topologies for Dynamic Voltage Restorer", Industry Application Conference, 2001, No. 4, pp. 2397-2403.

[5] F.Z. Peng, P. Zhiguo, K. Corzine, V. Stefanovic and M. Leuthen, "Voltage balancing control of diode-clamped multilevel rectifier/inverter systems", Industry Applications Conference, 2003. 38th IAS Annual Meeting Conference Record of the, Volume: 1, 12-16 Oct. 2003 pages: 182-189.

[6] P. Boonchiam and N. Mithulananthan, "Custom Power technology: Concept and Definition", Conference on Advances in Engineering between Thai and Japan universities, Supalai Resort Hotel, Saraburi, Thailand, (2005).

[7] P. Boonchiam and N. Mithulananthan, "Diode-clamed multilevel voltage source converter for medium voltage dynamic voltage restorer," ESD2006 conf., Phuket, Thailand, (2006).

[8] N.G. Hingorani, "Introducing custom power," presented at Spectrum, IEEE , (1995)

[9] N.G. Hingorani, "Flexible AC transmission", IEEE Spectrum, 3 (1993) 40-45.

[10] T.Bernet, S.Recent, "Development of High Power Converters for Industry and Traction Application," IEEE Trans. on Power Electronics, 15 (2000).

[11] R. De Doncker, "Recent Power Electronic Developments for FACTS and Costumed Power," Japan, (2000)

BIOGRAPHY

Paisan Boonchiam was born in Surin province, Thailand. He received his B.Eng. and M.Eng. degrees in Electrical Engineering from Rajamangala University of Technology Thanyaburi (RMUTT), and Chulalongkorn University, Thailand, in April 1997 and April 2000, respectively. In November 2001- December 2003, he worked as research associate at Institut fuer Stromrichtertechnik und Elektrische Antriebe, Rheinisch-Westfaelische Technische Hochschule Aachen, Germany. He is currently a doctoral student at the Asian Institute of Technology, Thailand. His main research interests are applications of FACTS Controllers, Power Quality Monitoring, Power Electronic System and Optimization Techniques.

Nadarajah Mithulananthan received his Ph.D. from University of Waterloo in Electrical and Computer Engineering in 2002. He has worked as an electrical engineer at the Generation Planning Branch of the Ceylon electricity Board, and as a researcher at Chulalongkorn University, Bangkok, Thailand. Dr. Mithulananthan is currently an Assistant Professor at the Asian Institute of Technology and his research interests are voltage stability and oscillation studies on practical power systems and applications of FACTS controllers in transmission and distribution systems.

A Calculation of Neutral Current for Two Step Type Pole in Distribution Line

K. W. Park*, O. S. Kwon, H. C. Seo, C. H. Kim

Abstract— *The one step type pole and two step type poles are used in KEPCO's distribution system. An unbalanced current may flow through neutral wire in three-phase four-wire distribution system due to unbalanced load. Generally, power line and communication line are installed at contiguity by effect of topography in Korea. To this end, the damaged such as electrostatic induction, electromagnetic induction, and harmonic induction will generated by induced voltage and current are occurred in power line and communication line. This paper calculates the neutral current in KEPCO's distribution system using EMTP by composing various simulated condition. Also, that result is verified by vector analysis.*

Keywords— **One Step Type Pole, Two Step Type Pole, KEPCO's distribution system, EMTP.**

1. INTRODUCTION

Korea Electric Power Corporation (KEPCO) distribution system is using 22.9[kV] Y-connected three-phase four-wire at high-tension line for voltage improvement and power damage reduction and low-tension wire boosts the voltage by 220/380[V] three-phase four-wire system and supplies to customer. KEPCO's distribution system using combination of one step type pole and two step type pole. Then, neutral current can generate by unbalanced current in three-phase. The neutral currents on the overhead distribution line produce a harmful induced voltage to a communication line. So, the KEPCO restricts within 20% of neutral current compare with normal phase current in overhead distribution line.

Due to topography factors in Korea, there are many areas where the power lines are installed at proximity to the communication lines. In such cases of proximity, both voltage and currents are induced by communication lines and may lead to damages such as electrostatic induction, electromagnetic induction, and harmonics induction.

In this paper, neutral current of KEPCO's distribution system of 'X S/S Y D/L' section and 'X S/S Z D/L' section, which is composed of one step type pole and two step type pole, was calculated using EMTP. Neutral current of two step type pole have calculated more exactly through 12,000 samplings per one cycle according to change of time using EMTP/MODELS. In addition, to identify an increase and decrease of the neutral current in the system composed of two step type pole has used vector analysis.

2. EMTP / MODELS

The EMTP (Electromagnetic transient program) is the simulation tool used to simulate the electromagnetic transient phenomenon, and it is one of the most widely used programs throughout electric utilities.

MODELS is a symbolic language interpreter for the EMTP that has recently gained popularity for the electromagnetic transients phenomenon modeling. The MODELS provides the monitoring and controllability of power system as well as some other algebraic and relational operations for programming MODELS is able to change dynamically states of power system in response to the simulated results of EMTP based power system[1-2].

In this paper, the EMTP program is used for calculation the neutral current. A system model had been drawn using EMTP/ATPDraw. Then defined the MODELS for calculation the neutral current of distribution system and connected it with the system model. We obtained the result of neutral current calculation after ran the simulation using EMTP. The parameters of system models are base on the real data of distribution system which are belong to the KEPCO.

3. DISTRIBUTION SYSTEM MODEL

In this paper, KEPCO's distribution system of 'X S/S Y D/L' section and 'X S/S Z D/L' section are targeted for calculation of neutral current for unbalanced load as shown in Fig. 1. In Fig. 1 'XZ 8~44' section is composed of two step type pole and the remaining sections is composed of one step type pole. The 'X S/S Y D/L' section on the upper portion is designated as PART 1 and the 'X S/S Z D/L' section on the lower portion is designated as PART 2. There are total of twenty-four

*K.W. Park (corresponding author) is with Sungkyunkwan University, Suwon, Kyeonggi-do, Korea (phone: +82-31-299-4630; Fax: +82-31-290-7955; e-mail: nsdapss@gmail.com)

O. S. Kwon is with Samsung Electronics CO., LTD., Kyeonggi-do, Korea

H.C. Seo is with Korea Electrical Engineering & Science Research Institute, Seoul, Korea

C.H. Kim is with Sungkyunkwan University, Suwon, Kyeonggi-do, Korea

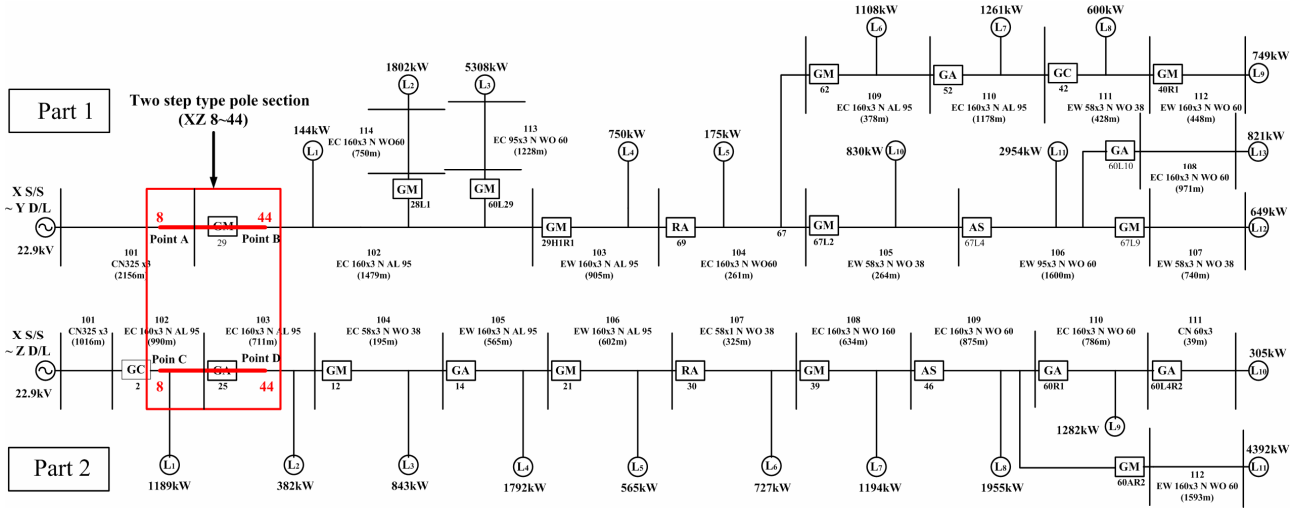

Fig. 1. Distribution System Model

There are total of twenty-four loads connected to PART 1 and PART2, and all loads are three-phase load. In here, X, Y and Z express place name of the Seoul city in Korea. S/S means substations and D/L means distribution line. So, X S/S Y D/L expresses the transmission line from substation of place X to the distribution line of place Y, and X S/S Z D/L expresses the transmission line from substation of place X to the distribution line of place Z.

Fig. 2. shows that the structure of one step type pole and two step type pole which are being used in KEPCO.

The left diagram is a one step type pole. The transmission lines are connected with a neutral wire. And right diagram is a two step type pole. The transmission lines of upper side and lower side are connected with the common neutral wire.

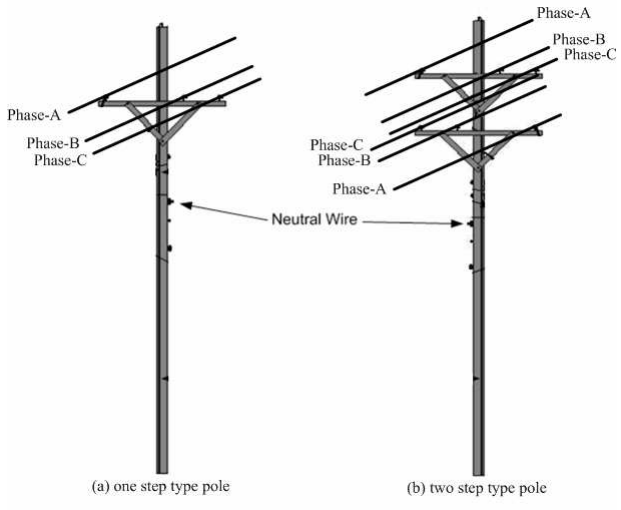

Fig. 2. Structure diagram of pole type

4. MODEL SYSTEM USING EMTP

To identify the effects and the variations of the neutral current each of the distribution pole of the model system shown in Fig. 1, four different types of models were formed. CASE-1 is a model which combined entire sections of both 'X S/S Y D/L' and 'X S/S Z D/L'. CASE-2 and CASE-3 was a model that is expressed only 'X S/S Y D/L' and 'X S/S Z D/L' section respectively from the CASE-1 model. In other words, CASE-2 and CASE-3 were made to examine the changes of neutral currents between the one step type pole and two step type pole 'XZ 8~44'sections, which is the main purpose in this paper. In CASE-4, even though the model system is the same as in CASE-1, the difference is that the CASE-1 is a model system that does not common the upper and lower neutral grounding points of the two step type pole, where as the CASE-4 is a model system that common the upper and lower neutral grounding points of the two step type pole.

4.1 Load modeling

In order to maintain balance on the three phases, the value of the load must be same and the load impedance can be calculated as follows in (1), the power consumption during Autumn Season was assumed to be 30% of the maximum consumption amount of the Summer Season and power factor was assumed at 0.9. The load impedance was calculated as (2)[3-5].

$$Z_{load} = (\frac{V_{LL}^2}{P}) \times \cos\theta \quad (1)$$

$$Z_{load} = (\frac{V_{LL}^2}{P \times 0.3}) \times 0.9 \quad (2)$$

4.2 Line modeling

Depending on the length of the line, there are number of different line models including Lumped series line

model, T-equivalent model, π-equivalent model, and Distribution line model in EMTP. The model distribution system is applicable to short distance line; therefore, the Lumped series line model was applied.

4.3 Calculation of neutral current

The calculation of neutral current on CASE-1~3 was used method that is presented to the reference [3]. The calculation of neutral current on CASE-4 was conducted with the assumption that the upper and lower side are common the neutral grounding points. The neutral current in 'ZX 8~44'section were composed of EMTP/MODELS and their method of calculation are given in (3) ~ (6).

$$I_{N1} = I_{A1} + I_{B1} + I_{C1} \quad (3)$$

$$I_{N2} = I_{A2} + I_{B2} + I_{C2} \quad (4)$$

$$I_{NEU} = I_{N1} + I_{N2} \quad (5)$$

$$I_{NEU\_RMS} = \sqrt{\frac{1}{T}\int_0^T I_{NEU}^2 dt} \quad (6)$$

where

$I_{A1,A2}$: Phase-A current in upper and lower side

$I_{B1,B2}$: Phase-B current in upper and lower side

$I_{C1,C2}$: Phase-C current in upper and lower side

$I_{N1,N2}$: Phase-N current in upper and lower side

I_{NEU} : Total neutral current

I_{NEU_RMS} : RMS values of I_{NEU}

5. CALCULATION OF NEUTRAL CURRENT AND DISCUSSION OF THE RESULTS

5.1 In case of equal upper and lower unbalanced load ratio

In this paper, from the largest load downwards on each PART, four loads were selected for the simulation samples. Simulation was conducted with consideration to the states that the unbalanced ratio must not exceed 30[%], the ratio of unbalanced load impedance was assumed at '1.35:1.2:1.0'.

Therefore, the loads, L3, L11, L2, and L7 was simulated changing depend on the unbalanced load ratio in PART1.

In PART 2, selected loads L11, L8, L4, and L9 was adjusted and simulated.

The adjusted unbalance occurrence states of load impedance for simulation the unbalanced loads condition are as follows.

- Case in which unbalance has occurred in the largest load (PART 1-L3, PART 2-L11) in each PART
- Case in which unbalance has occurred in the two loads (PART 1-L3·L11, PART 2-L11·L8) in each PART
- Case in which unbalance has occurred in the three loads (PART 1-L3·L11·L2, PART 2-L11·L8·L4) in each PART
- Case in which unbalance has occurred in the four loads (PART 1-L3·L11·L2·L7, PART 2-L11·L8·L4·L9) in each PART

Above 4 cases were set as EXAMPLE 1, 2, 3 and 4, and with consideration to load unbalance state, neutral currents were calculated after conducting simulation using CASE-1, CASE-2, CASE-3, CASE-4 model system. The following Figre.3 is the graph showing the variation in neutral current per unbalanced load rates.

The results of analysis conducted per each points shows that the neutral current was the largest in EXAMPLE-4, followed by EXAMPLE-3, and then EXAMPLE-2. Therefore, the neutral current increases as the number of unbalanced load increase.

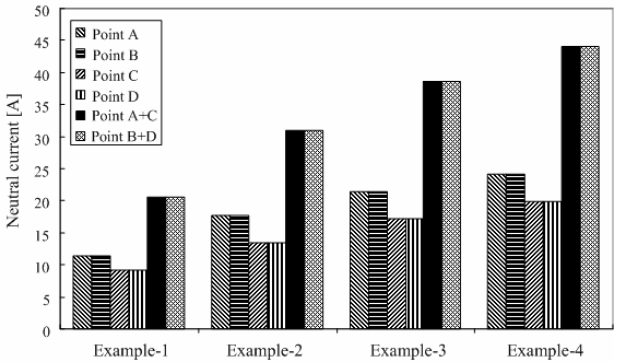

Fig. 3. Variation of neutral current by the number of unbalanced load

Each point in Fig. 3 are as follows,
Point A : XZ Point No. 8 in 'X S/S Y D/L'
Point B : XZ Point No. 44 in 'X S/S Y D/L'
Point C : XZ point No. 8 in 'X S/S Z D/L'
Point D : XZ point No. 44 in 'X S/S Z D/L'
Point A+C : Common neutral point of Point A and C
Point B+D : Common neutral point of Point B and D

5.2 In case of unequal upper and lower unbalanced load ratio

CASE-4 was tested in this simulation with various changes of unbalanced load ratio in each phase of the upper and lower side. This was set as EXAMPLE-5 and its neutral current was compared with EXAMPLE-1.

The unbalanced ratio of upper and lower load impedance in EXAMPLE-1~4 was made equal but in EXAMPLE-5, the upper and lower load impedance was simulated with different unbalanced ratio as shown in Table 1.

To compare the value of the neutral current of the

upper and lower load unbalanced ratio when neutral grounding point is common. The ratio of upper and lower side was based on EXAMPLE-1, which has the same ratio. With such basis, the value of the neutral current in point A+C and B+D of EXAMPLE-5-1~5 were compared and that is shown as a graph in Fig.4.

Table 1. Unbalanced load ratio of each phase at EXAMPLE-5

EXAMPLE -5	Section	Load	Ratio of each phase (A:B:C)
EXAMPLE -5-1	PART 1	L3	1.35:1.2:1.0
	PART 2	L11	1.35:1.0:1.2
EXAMPLE -5-2	PART 1	L3	1.35:1.2:1.0
	PART 2	L11	1.2:1.35:1.0
EXAMPLE -5-3	PART 1	L3	1.35:1.2:1.0
	PART 2	L11	1.2:1.0:1.35
EXAMPLE -5-4	PART 1	L3	1.35:1.2:1.0
	PART 2	L11	1.0:1.2:1.35
EXAMPLE -5-5	PART 1	L3	1.35:1.2:1.0
	PART 2	L11	1.0:1.35:1.2

Fig.4 is the case where the unbalanced load ratio of upper is fixed and variation was made only the loads of lower.

In Fig.4, EXAMPLE-1 can be noted as the largest. This case shows that the unbalanced load occurrence in upper and lower is extreme in specific phase. In other words, the unbalanced loads ratio in phase A, B, C was the upper at 1.35:1.2:.1.0, and the lower at 1.35:1:21.0. Therefore, in case where unbalanced load ratio is the largest in both upper and lower, and neutral current is also the largest.

It can provably that the next largest case is the EXAMPLE-5-2.

It can see that at specific phase in EXAMPLE-2, the synthetic of the unbalanced load ratio was 2.55 in two specific phases. In EXAMPLE-5-1, the unbalanced load ratio in specific phase was 2.7.

In addition, the next large value was EXAMPLE-5-3 and EXAMPLE-5-5. In these two cases, specific phases showed unbalanced load ratio of both 2.55 and 2.35 simultaneously. In smallest case is EXAMPLE-5-4. The synthetic of the unbalanced load ratio was 2.4. As a result, it can be confirmed that the neutral current will also become larger in specific phase of higher unbalanced load ratio.

In cases of same unbalanced load ratio only in the same phase, the value of the neutral current was resulted as the scalar sum of neutral current in upper and lower. However, in case of different upper and lower load unbalanced ratio, Fig.4 show that the value of the neutral current always is not the scalar sum of upper and lower neutral current, even though the two step type pole is common the neutral grounding point.

Results of the principal of superposition and vector analysis, that because each neutral current of each different phase is counterbalanced. In other words, regardless of common the neutral grounding point, changes of the neutral current becoming the scalar sum of the one step type pole is extremely unlikely.

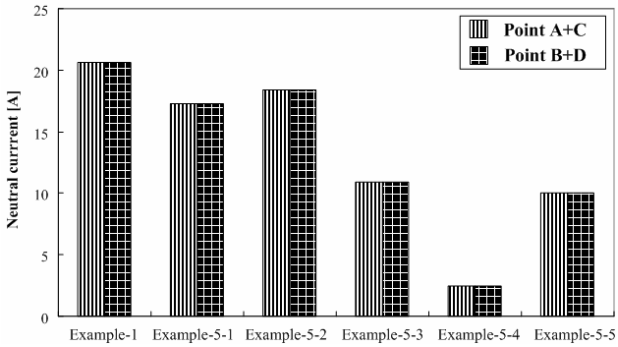

Fig 4. Neutral current of each phase by various unbalance factors

6. CALCULATION OF UNBALANCE FACTOR AND DISCUSSION OF THE RESULTS

Each of phase current and neutral current in various conditions were measured, unbalance factor was able to be obtained based on such that. The unbalance factor was based on Electric Facility Standards and its as shown in (7).

$$\text{Facility Unbalance Factor} = \frac{\text{The difference between maximum and minimum of total facility capacity of the single phase load connected to each line}}{\text{Facility value of all load / 3}} \times 100 \quad (7)$$

Prior to verification at each of the measuring point of the KEPCO's distribution system, total facility capacity of the single phase load connected to each line was unknown, but the phase current in each measuring points were identifiable. Since P=VI, and the load capacity is proportional to current, the equation (7) was able to be calculated as shown in (8).

$$\text{Unbalance Factor} = \frac{\text{The different between maximum and minimum of three-phase current}}{\text{Sum of three-phase current / 3}} \times 100 \quad (8)$$

6.1 Change in unbalance factor corresponding to the increase in the number of unbalance loads in upper and lower side

Using the results of the unbalance factor calculated with (8) with CASE-1 as the basis, it was confirmed that the unbalance factors were the same in all of CASE-2, CASE-3, and CASE-4. Therefore, with CASE-1 as the basis, the unbalance factor corresponding to increase the number of loads in upper and lower side is shown as Fig. 5.

The unbalance factor in cases of increased number of loads in unbalanced load was calculated and its results are as follows.

- In all cases, the unbalance factor was the same on the same measuring point. In case of unbalance factor the two step type pole, common or not of the neutral grounding point made no difference whether the upper and lower side are explicated separately. In other words, the unbalance factor in one step type pole and two step type pole are equal.
- As the number of unbalanced loads in upper and lower side increases, the unbalance factor also increases.

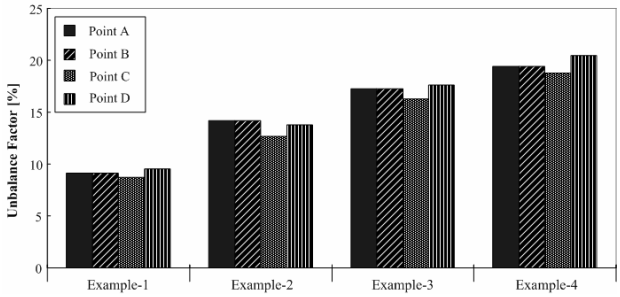

Fig. 5. Unbalance factor by increase o f the number of unbalanced load at upper and lower side

6.2 In case where the unbalanced load ratio in upper and lower side are unequal

In the same measuring point of CASE-1 and CASE-4, the unbalance factors are also equal. Through this, the unbalance factor in two step type pole is not effected whether the neutral grounding point is common or not and make no difference whether the upper and lower side are explicated separately. In other words, the unbalance factor is the same as in one step type pole.

In Fig. 6, it can be seen that unbalance factors in Point A and Point B are equal. That's there are no load existing between Point A and Point B. As a result, it can be seen that the circuit is connected in direct line and phase current in the same. Therefore, the unbalance factor is also equal. But, it can note that between Point C and D, the unbalance factor in Point D is larger. Because there exists load between the Point C and D, and since Point D is in close with the unbalanced load.

Since the unbalance factors in each measuring Point of CASE-1 and CASE-4 are equal, it is confirmed that the unbalance factor has no relationship with the common of the neutral grounding point.

7. VERIFICATION BY VECTOR ANALYSIS

In two step type pole distribution system, it was verified by EMTP, that the value of neutral current is shown to be largely different whether neutral grounding point in upper and lower side are common or not. Even though the neutral grounding point was common, if the unbalanced ratio of neutral current in upper and lower side are different, the neutral current does not become the scalar sum of the upper and lower neutral current, also may even be smaller than the neutral current of one step type pole.

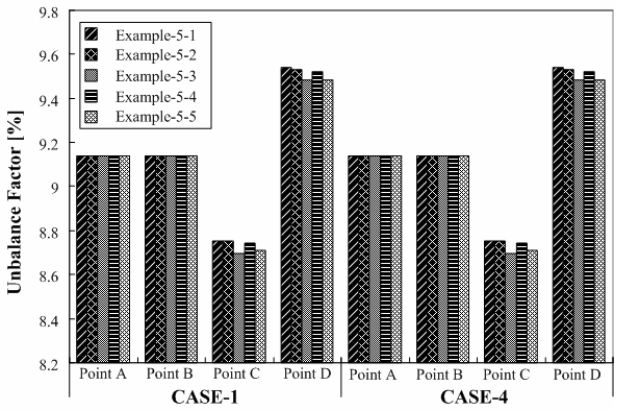

Fig. 6. Each point unbalance factor of CASE-1 and CASE-4

Table II. Resultant Vector of the Each Example

	Resultant Vector Point (A+C)	Resultant Vector Point (B+D)
EXAMPLE-1	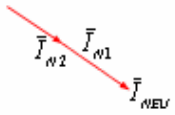	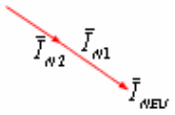
EXAMPLE -5-1	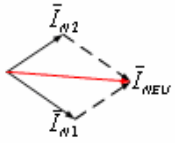	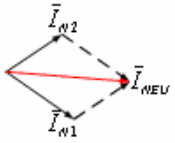
EXAMPLE -5-2	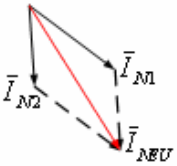	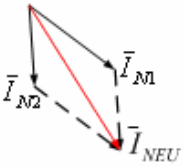
EXAMPLE -5-3	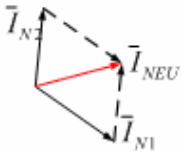	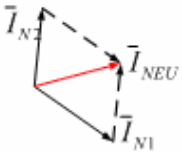
EXAMPLE -5-4	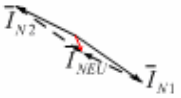	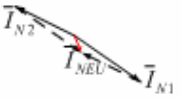
EXAMPLE -5-5		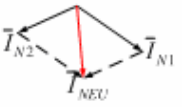

The neutral current of the three-phase power system composed of Y-Y circuit was shown to be the resultant vector by the phase current of three-phase[6][7].

Table 2 is the calculation result of the resultant vector. It shows the neutral current of point (A+C) and point (B+D) in EXAMPLE-1 and EXAMPLE-5 in accordance with the vector analysis.

As shown in the results of EXAMPLE-5-1~5, if the unbalanced loads of upper and lower side are different, the neutral current of two step type pole does not become the scalar sum of neutral current in upper and lower side. It is verified through that resultant vector both cancels out each other. In addition, in cases where both do not cancel out each other by resultant vector, but become the scalar sum, it's in the case as in EXAMPLE-1, where the value and direction of the neutral current in upper and lower side are equal (in other words, each phases of unbalanced loads in upper and lower are equal) but chances of such cases are extremely unlikely.

8. CONCLUSIONS

In this paper, analysis using EMTP was conducted to identify the superposition of the neutral current, which is the inductive current that causes the inductive disturbance when the neutral wire of extra high voltage power line was common. The results of the research are as follows.

(1) In the distribution system composed of two step type pole, the phase current in each level had no difference in common or not of the neutral grounding point. Only the current pertaining to the value of the load exists.
(2) In case each phase unbalance ratio is different in the upper and lower side, the current in the common neutral wire is decreased. However, if the combination of load unbalanced ratio in specific phase is increased, then the neutral current may also increase.
(3) The neutral current flow increases as the number of unbalanced load is increased.
(4) If each of the neutral grounding points on the two step type pole distribution system is no common, value of neutral current is the same as the individual interpretation of upper and lower side.
(5) In general, since the load unbalance in upper and lower neutral current are different in most cases, current value of the neutral grounding is resultant vector of the upper and lower individual current and it is smaller than the scalar sum of both currents. Composition value of the neutral current becomes smaller than the maximum current size of the upper and lower neutral current.

ACKNOWLEDGEMENTS

This paper was supported by Faculty Research Fund, Sungkyunkwan University, 2006

REFERENCES

[1] "Alternative Transients Program ATP Rule Book", EEUG, Canadian/American EMTP User Group
[2] Laurent Dube. MODELS RULE BOOK(New Version);Apr. 1996
[3] Korea Electric Power Corporation., "Correlation analysis of between neutral current in two step type pole and power induction using KEPCO's distribution system." 2005
[4] H. C. Sep, K. W. Park, C. H. Kim, C. S. Jung, Y. P. Yoo, Y. H. Lim, L. H. Seol, "Neutral Current Calculation of One Step Type Pole using KEPCO's Distribution System", *Trans. KIEE*, Vol. 56, No. 1, Jan. 2007
[5] H.C. Seo, O.S. Kwon, C.H. Kim, C.S. Jung, Y.P. Yoo, "Neutral Current Calculation of Pole-Top Overhead Distribution Line", *KIEE Trans*, Vol. 55A, No.7, pp.290-296, July. 2006.
[6] Thomas M. Gruzs, "A survey of neutral currents in three-phase computer power system", *IEEE Trans. on Industry Application*, Vol. 26, No.4, pp.719-725, 1990
[7] J. C. Balda, A. R. Oliva, D. W. McNabb, R. D. Richardson "Measurements of Neutral currents and Voltages on a distribution Feeder", *IEEE Trans. On Power Delivery*, Vol. 12, No. 4, Oct. 1997

Sustainable Energy Development in Urban Transportation System under TOD Pattern: a Case Study in China

Min He*, Mingwei He, Zhanqiong He, Zidong Zhang

Abstract— *Energy sustainable development faces tremendous challenge today. Transportation is one of the major sources of energy demand and its consumption of energy is rising continually around the world. How to build a sustainable energy development transportation system is an important research topic for transportation engineers, planners and policy makers. The paper pays attention to energy consumption under TOD (Transit-Oriented Development) strategy and gives a case study in china. Energy consumption and energy-related emission under TOD and AOD (Auto-Oriented Development) pattern are computed based on the transportation planning data of Dongguan, China. As a result, TOD is more efficient and environment friendly than AOD, the former pattern is a good choice for sustainable energy development in urban transportation system.*

***Keywords*— Energy consumption, Sustainable development, TOD.**

1. INTRODUCTION

In 1987, a report entitled *our common future*，which was published by the World Commission on Environment and Development (WCED) ，put forward the sustainable development strategy. Sustainable development is development that meets the needs of the present without compromising the ability of future generations to meet their own needs [1]. However, energy sustainable development faces tremendous challenge today. Energy supply security is a big concern to major industrialized countries like U.S.A., Europe and Japan, they depend increasingly on several unstable supplying regions with uncertain reservation of gas and oil, China follows soon.

With the rapid economic development, energy consumption in China goes up greatly. China has become the second largest energy consumer in the world after U.S.A. According to the data from National Bureau of Statistics of China [2], China's total primary energy consumption reached 2.22 billion tons of standard coal in 2005. From 1990 to 2004 china's oil consumption has kept a consistent upward trend, with an annual increase of 9.2%, far higher than that of other resource consumption during the same period (3.9%). By 2003, China, with its total oil consumption of 240 million tons, overtook Japan and became the second largest oil consumer in the world. According to the predictions by the National Development and Reform Commission (NDRC) of China [3], oil import will reach 150～220 million tons by 2020, and 50% of China's oil demand will rely on import. The growing oil import will influence the economic development of China.

Transportation is one of the major sources of energy demand and its consumption of energy is rising continually around the world. International Energy Agency (IEA) projects that over the next 20 years energy demand growth in transport will be greater than that in other end-use sectors. Transport's share of total energy usage will increase from 28% in 1997 to 31% in 2020[4]. Despite efforts to use alternative fuels, oil will continue to dominate this sector. In America, oil accounts for 97 % of the transportation sector's energy [5]. Transport will account for more than half of the world's oil demand in 2020[4]. In china, the share of energy consumption of transport sector has experienced a continuous increase, and has gradually become the dominant part. From the report of the IEA, 50% of crude oil consumption has been consumed by road transport in China. In 2003, road transport consumed 38.114 million tons of gasoline and 17.096 million tons of diesels, accounting for 87.9% of the national gasoline and 22.1% of the national diesel production respectively [3]. Due to the fossil fuel such as oil dominate this sector, the massive gas emission of transport such as CO_2 and NOx is harmful to environment. In China, 60% of air pollution comes from the emission of mobilized vehicles in many urban areas. Transportation becomes the biggest pollutant source for urban environment [6].

Energy consumption and the energy-related emission in transportation sector are closely related with the mode of urban transportation system. Over the past two decades, China has experienced an unprecedented rate of urbanization and motorization. Urban population now accounts for 41.8% of the total Chinese population, and it will reach 57% in 2020. At present, 10% of the world's population lives in China cities, and the

*Min He (corresponding author) is Prof. Dr., Faculty of Transportation Engineering, Bailong Campus, Kunming University of Science and Technology, Kunming, P.R.China; P.O. 650224; E-mail: kmhemin@gmail.com

Mingwei He is Graduate Student, Faculty of Transportation Engineering, Bailong Campus, Kunming University of Science and Technology, Kunming, P.R.China; P.O. 650224; E-mail: hmwei01@yahoo.com.cn

Zhanqiong He is Lecturer, Faculty of Management and Economics, Kunming University of Science and Technology, 121 Street, Kunming, P.R.China; P.O. 650093; E-mail: hezhanqiong@yahoo.com.cn.

Zidong Zhang is Transportation Engineer, Transport Institute of China Academy of Urban Planning and Design

proportion will rise to 15% by 2020[7]. The urbanization in china brings great mobility demand and huge energy consumption. How to build a sustainable development urban transportation system to improve energy efficiency and reduce energy-related pollution is an important research subject for transportation engineers, planners and policy makers.

In this paper, a model is formulated to analyze energy use and emissions in meeting the travel requirements of the residents of Dongguan city, China. Most variables of the model such as travel demand, modal split, vehicle ownership and vehicle miles traveled are obtained from an interactive planning of Light Rail Transit (LRT) system and land use. The model illustrates the effect of two strategies, namely TOD and AOD, on energy use and emissions. Under the TOD strategy, if both the LRT projects and corresponded land use plan can be implemented, 51.93% of energy, that is about 0.18 million tons of oil equivalent, could be saved in 2020. Compared with AOD, this strategy could also reduce the emissions of CO_2, NOx by 51.90% and 53.05% respectively.

In section 2, the paper discusses the reduction of energy consumption under TOD pattern by improving urban transport structure and land use pattern. A case study in Dongguan, china, is presented in section3. The last part provides some conclusions.

2. TOD PATTERN AND ENERGY

Put forward by American architect and planner Peter Calthorpe in 1980s, Transit-oriented development (TOD) is moderate to higher-density development, located within an easy walk of a major transit stop, generally with a mix of residential, employment and shopping opportunities designed for pedestrians without excluding the auto. TOD can be new construction or redevelopment of one or more buildings whose design and orientation facilitate transit use [8]. In recent years, many researches and case studies have discussed TOD strategy extensively. Some cities which carried out TOD such as Hongkong, Tokyo, and Curitiba, have achieved great success. Analysis of the reduction of energy consumption under TOD pattern mainly includes two dimensions, namely urban transport structure and land use.

2.1 Optimization of Urban Transport Structure under TOD Pattern

TOD pattern can optimize urban transport structure based on the travel mode change of people. TOD pattern gives preference to pedestrian and bicyclists, increase the use of mass-transit, reduce people's dependence on the automobile. Mixed land use and higher densities under TOD pattern mean that many destinations can be reached by transit, walking or by bicycle, thereby enable these methods to become more viable travel options. A study points out that, travel by automobile decease 20%-25% in the district based on TOD pattern, compared with that of conventional development pattern [9].

Compared with bus, rail transit can provide higher quality of service with comfort and less delay. So, it is a good choice in TOD design. Rail transit tends to leverage additional automobile travel reductions by providing a catalyst for more accessible land use patterns and reduced per capita vehicle ownership [10]. It reduces automobile travel both directly and indirectly. The former happens when a rail passenger-mile substitutes an automobile vehicle-mile, and the latter happens when it creates more accessible land use and reduces automobile ownership in that area. Although indirect effects are difficult to measure, some studies suggest that they are often larger than direct effects. Research indicates that each rail transit passenger-mile represents a reduction of 3 to 6 automobile vehicle-miles [11].

According to a report in 1999 by the Energy Foundation on energy consumption and energy-related emission of different travel modes (shown in table 1), transit modes, especially BRT (Bus Rapid Transit), Rail transit, is the most energy efficient and environmental friendly transportation mode.

It is very clear that TOD pattern can greatly reduce the energy consumption in urban transportation system. This energy savings is achieved not only by shifting riders to more energy efficient transportation modes, but also by reducing vehicle miles traveled (VMT).

Table 1. Emission and Energy Consumption of Different Modes (per million per kilometer)

Mode / Indexes	Private Car	Taxi	Conventional Bus	BRT	Rail Transit	Motorcycle
CO_2 (ton)	140.2	116.9	19.8	4.7	7.5	62.0
NO_x (kg)	746.0	662.0	168.4	42.0	17.5	90.0
Oil consumption (ton)	49.2	41.0	6.9	1.6	2.6	21.8

Source: the Energy Foundation (1999).

2.2 Land Use under TOD Pattern

Energy consumption in urban transportation system is strongly related to land use. O. Mindali et al (2004) set up a conceptual model of a set of factors influencing urban transportation energy consumption from the viewpoint of land use policy [12].

Conventional wisdom asserts a strong correlation between urban density and transportation energy consumption, which suggests that higher density generates lower VMT and therefore, exhibits lower energy consumption[13-14]. Planning for high density aims at reducing trip length and total mobility needs by concentrating residential, employment and services within a compact area[15]. Many studies also suggest that mixed land-use is likely to reduce trip length, and divert trips from the private car to public transportation and walking. As a result, the reduction in the energy consumption of the transportation system is one of the main advantages of mixed land-use planning policy.

Urban spatial structure can be defined as a combination of land use formation, its densities and the spatial design of infrastructure such as transportation and communication [16]. Through study in representative cities in America and Australia, Roy (1992) found energy consumption in urban transportation also has some relationship with subcenters of city. While subcenters increase from 6 to 12, the transportation condition improves evidently, moreover, average energy consumption per person decreases 14.1% and 16.4% respectively [17]. Atsushi Akisawa (1998) investigated an optimal land use in urban areas from the viewpoint of reducing energy consumption for transportation and analyzed the urban structure of minimal transportation energy consumption [18].

In all, TOD pattern make urban land use more efficient. It requires the mixed land use and higher densities around transit station, and facilitates subcenters of city. Therefore, TOD can improve energy efficiency and save energy.

3. A CASE STUDY IN DONGGUAN, CHINA

3.1 Background of Dongguan

Dongguan city is located in south China, near Hong Kong. It is a rapidly growing industrial city. The population of the city reached 6.49 million in 2004 and would keep growing from 2004 to 2020 according to the plan of the city. Population of the city will reach 8 million in 2010 and near 10 million in 2020.The population structure of Dongguan is remarkably different from that of other cities: migrant worker population is far larger than permanent registered resident population. In 2004, the population of migrant worker reached 4.87 million, accounting for 77.5% of the total. The particular population structure of Dongguan results in a remarkably different travel characteristic.

From 1994 to 2004, the GDP growth of Dongguan has kept a high speed with average rate up to 20%, and reached 11.55 billion RMB (1.43 billion USD) in 2004. Similarly, the number of vehicles in Dongguan has been increasing rapidly in recent years (shown in figure1). By 2004, the total number of all kinds of vehicles has reached 1.01million, among which, automobile account for 32%, motorcycle account for 69%. According to the travel survey in 2005, the proportion of motorization journey accounted for 59% in Dongguan. As the uppermost travel mode, motorcycle accounted for 44.6% of the total trips of the city, private car accounted for only 7.5%, but kept increasing rapidly. The yearly growth rate of private cars reached as high as 40%. However, the transit system was not well developed and transit ridership was very low, accounting only 2.1 % of the total trips of the city.

In China, Pearl River Delta region has been the most prominent urban sprawl region during the past two decades. In 1990, Dongguan was dominated by cultivated land, orchard, and forested land, shown in figure 2. This indicated that Dongguan was still an agricultural dominated area at that time. From 1990 to 2002, urban sprawl maintained a rapid speed and most available land has become urban built-up area. And further, the trend of urban sprawl continues today. However, urbanization of Donguan is low density, unordered and low quality. Under this pattern, people travel mainly by auto or motorcycle. Presently, motorcycle is the main travel tool. With the development of economic, auto will substitute motorcycle soon. Without control, Dongguan will become Auto-oriented development (AOD) at last.

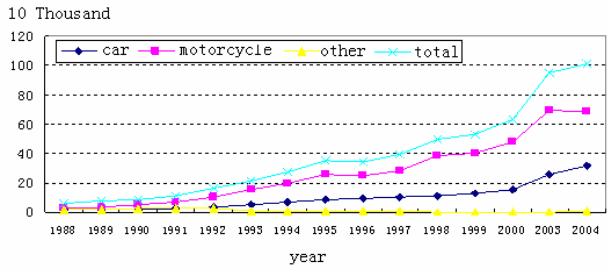

Fig.1. Development of Vehicles in Dongguan in Recent Years

From the viewpoint of Sustainable energy development, main disadvantages of transportation system of Dongguan can be concluded as following:

Firstly, rapid increase of population and vehicles will exert pressure on the limited resource and road capacity. The corresponding aftermaths such as oversized land recourse, energy shortage, traffic congestion will become serious gradually. Especially, serious traffic congestions are now common in Donguan's major traffic corridors, such as the state highway 107 and Guanchang Road. During peak hours, the average speed of motor vehicles on these roads is only 15 km/h. The impact of congestion on energy consumption and emission is obvious.

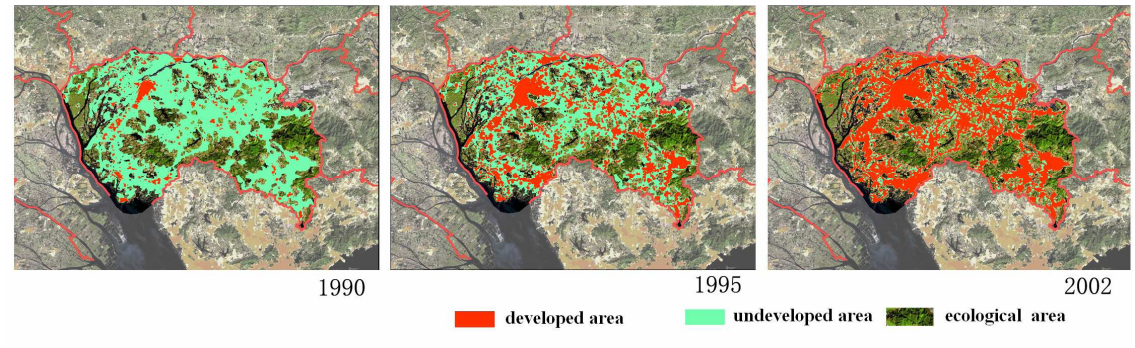

Fig. 2. The Urban Sprawl and Land Use Change of Dongguan

Source: CAUPD, The Report of LRT construction planning of Dongguan

The second, unordered and low density urban sprawl further engenders resource waste. It results in some problems such as more vehicles miles, longer trip length. It is also disadvantageous for mass-transit system development due to the low density land use. This pattern encourages the use of the private car and motorcycle, especially private car. As a result, it will increase energy consumption and decrease energy efficiency.

3.2 TOD Pattern in Dongguan

As a sustainable development strategy, TOD is adopted and carried out by Dongguan government. LRT as a mass transit system is applied in TOD design. To maximize the benefits and attract more people to use LRT as a travel mode, some effective measures are adopted in the rail transit planning projects of Dongguan, some examples are, interactive land use planning and LRT planning, carefully designed land use pattern near the LRT station, integrated LRT with bus system, financial support and so on.

The LRT network of Dongguan consists of four rail routes with the total length of 194.37 km and 49 stations. Before 2025, the whole network will be constructed. Rail transit lines are arranged alone passenger corridor in existence or potentially high density development areas which is planed to be strong development in the future. In order to improve the connection and convenience, LRT stations will integrate LRT, inter-city railway station, bus terminal as much as possible. The details can be found in the Report of Planning of Light Rail Transit by China Academy of Urban Planning and Design [19].

3.3 Evaluating the Energy Consumption Benefit of TOD in Dongguan

Two transportation scenarios for future Dongguan

Two scenarios of future Dongguan transportation system are designed to represent TOD and AOD strategies. Scenarios 1 is AOD pattern, which is the development without the LRT project, it is a do nothing scenario. Scenario 2 is TOD pattern, which is the development with the LRT project.

An improved “Four Steps” model was used in Dongguan LRT construction plan project. The detail plan of population and job opportunity within 500m from LRT station provides the model with ability to build some interactions between land use and transportation system. With the help of complicated, scientific transportation demand model, some necessary data for evaluating energy consumption are shown in table 2, table 3, and table 4.

Table2. Some General Statistics Indexes in Dongguan

Items / Years		2004	2020	2030
Population (million)	Permanent Resident	161.97	300	329
	Migrant Worker	486.95	700	871
GDP (Billion RMB)		11.55	44.2	52.6
Average Travel Frequencies	Permanent Resident	2.7	2.55	2.5
	Migrant Worker	1.0	1.5	1.6
Total Travel		924.3	2142	2353

As shown in table 3 and table 4, different development scenarios result in different traffic demand. Under AOD pattern, the proportion of car use will increase rapidly and become the uppermost traffic mode in 2020 and 2030. Accordingly, the proportion of transit use is lower than that under TOD pattern.

Under TOD pattern, more destinations can be reached by walking or by using a bicycle. Motorcycle and private car will keep a lower use proportion. Transit, including bus and LRT, will be encouraged and become the uppermost traffic mode gradually. The proportion of travel by transit will reach 22.5% in 2020, and 34.5% in 2030. At the same time, the total vehicle miles traveled reduce greatly. At the 2020 horizon, total vehicle miles traveled under scenario2 (90.97 million miles) is about 19.59 million miles lower than that under scenario1, and

it makes a 17.7% decrease compared with scenario1.

Evaluation of energy consumption benefit

Through analog computation, simulation result of energy consumption and energy-related emission per year under different scenarios are shown in table 5 and figure 3.

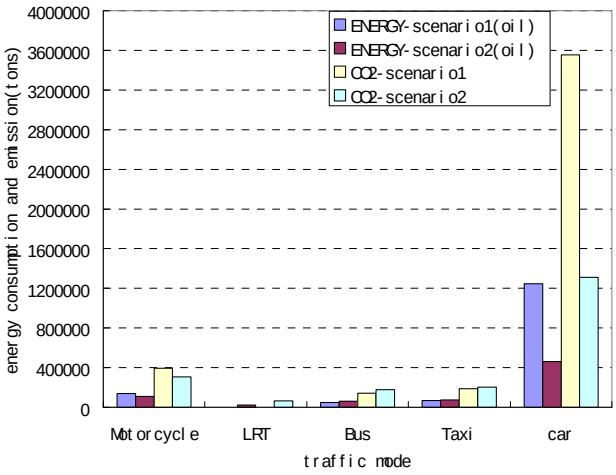

Fig. 3. Energy Consumption and CO_2 Emission of Different Transport Modes at the 2020 horizon

The simulation result indicates that both energy consumption and emission decrease evidently under TOD pattern (scenario2), compared with AOD pattern (scenario1). At the 2020 horizon, energy consumption under scenario2 (721109 tons oil) is about 779038 tons lower than what under scenario1, that is a 51.93% decrease. CO_2 emission and NOx emission under scenario2 is 51.90% and 53.05% lower respectively than that under scenario1. At the 2030 horizon, the result indicates the same rule as in 2020.

As shown in figure 4, among different travel modes, car is the uppermost sources of energy consumption and emission, whose energy consumption almost accounts for 63% and CO_2 emission account for 83% of the system. So, controlling car use and seeking its substitute is very important for sustainable energy development in urban transportation system.

3.4 Some experiences from the case study in Dongguan

As the case study shows, TOD pattern can help to build a sustainable development urban transportation system. It provides a good transport service for the residents with high mobility and few VMT and related pollution. But it is not easy to achieve. From the case study, we get some experiences:

To begin with, planning and its administration are very important for the strategy. Land is valuable and rare in urban area; it's very hard to keep the space of transportation infrastructures unchanged by interest groups. So, a strong policy and implementation is needed.

To continue, cross boundary cooperation should be strengthened. TOD is a kid of coordination between land use and transportation, so a good arrangement of business, transportation and resident is needed. It also needs a good coordination between different sectors, such as bus, LRT, private car.

Thirdly, the balance between cost and income should be kept. Massive transit system is main means for TOD, but it is often costly, both in construction and operation. So, it is every important to find a sound financial support. For many undeveloped cities, it became a key constrain of TOD strategy application.

4. CONCLUSION

From the analysis above, it can be concluded that TOD strategy can improve energy efficiency, reduce energy-related emission. Beside Benefit of energy consumption, the main benefits of TOD also include: improving accessibility and mobility, higher density to preserve more land, providing needed development, and so on. From this dimension, TOD strategy is an attractive, effective and worthwhile strategy.

In the Greater Mekong Subregion, with the rapid economic development and urbanization in recent years, more and more people swarm into cities. Urban sprawl leads to not only more vehicle miles travels, more air pollution, inefficiencies in transportation, but also more energy consumption. Some cities in GMS, such as Kunming, Bangkok, have subjected to these similar problems of Dongguan. This research is expected to provide some experience to the transportation policy maker and planner.

ACKNOWLEDGEMENT

This research is based on a cooperation planning project between the authors and the Transport Institute of China Academy of Urban Planning and Design, especially thanks to Mr. Guodong Qin and Mr. Fengjun Li.

REFENENCE

[1] Bruntland, G. (Ed.). 1987. Our common future: The World Commission on Environment and Development. Oxford: Oxford University Press.

[2] National Bureau of Statistics of China. 2006. China Statistics Yearbook 2006.Beijing: China Statistics press.

[3] Jiang Yulin, Feng Liguang. 2006. Transport-Related Resource and Environmental Issues in China. In Proceeding of EU-China Workshop on Sustainable Urban Transport. Beijing, China. 27-28 May.

[4] International Energy Agency (IEA). 2000. World Energy Outlook 2000.Paris: Louis-Jean.

[5] A. Nagurney. 2006. Transportation and Energy: Designing the Route to Prosperity and Sustainability. [On-line serial], 1.Retrieved September 10, 2005 from the World Wide Web: http://www.umassmag.com/umassmagessay.pdf

Table 3. The Data of Scenario1 (AOD)

Time (Year)	2001	2020			2030		
Traffic Mode\ Index	Proportion of Mode (%)	Average Distance Carried (km)	Proportion of Mode (%)	Total Travel Frequencies(million)	Average Distance Carried (km)	Proportion of Mode (%)	Total Travel Frequencies (million)
Motorcycle	25.2	6.3	12.9	2.76	6.1	11.5	2.71
LRT	---	----	---	---	----	---	---
Bus	5.3	8.2	11.0	2.36	8.1	12.7	2.99
Taxi	1.0	10.1	2.0	0.43	10	2.0	0.47
Car	9.8	11.8	27.5	5.89	12.6	30.4	7.15

Table 4. The Data of Scenario2 (TOD)

Time (Year)	2001	2020			2030		
Traffic Mode\Index	Proportion of Mode (%)	Average Distance Carried (km)	Proportion of Mode (%)	Total Travel Frequencies(million)	Average Distance Carried (km)	Proportion of Mode (%)	Total Travel Frequencies (million)
Motorcycle	25.2	6.3	10.0	2.14	6.1	8.5	2.00
LRT	---	16.37	6.5	1.39	15.46	10.8	2.54
Bus	5.3	7.1	16.0	3.43	7.1	23.7	5.58
Taxi	1.0	10.1	2.2	0.47	10	2.0	0.47
Car	9.8	11.6	10.3	2.21	12.3	11.4	2.68

Table 5. Simulation Results of Energy Consumption and Energy-related Emission

Years	2020			2030		
Scenario \ Index	Energy Consumption	CO_2 (ton)	NO_x (ton)	Energy Consumption	CO_2 (ton)	NO_x (ton)
Scenario1	1500146	4275125	21732	1881268	5361456	27707
Scenario2	721109	2056363	10202	897006	2558975	13206
Decrease (%)	51.93	51.90	53.05	52.32	52.27	52.34

[6] Jiang Yulin, Feng Liguang. 2006. Challenges and Policy Options for Sustainable Urban Transportation Development in China. In Proceeding of EU-China Workshop on Sustainable Urban Transport. Beijing, China. 27-28 May.

[7] Wu Hongyang, Liu Leilei. 2006. Sustainable Urban Transportation in China: Strategy and Policy Options. The Journal of World Transport Policy & Practice (submitted for publication).

[8] California department of transportation. 2002. Statewide Transit-Oriented Development Study: Factors for Success in California. (Final report). [On-line serial], 2. Retrieved September 18, 2005 from the World Wide Web: http://www.dot.ca.gov/hq/MassTrans/tod.htm.

[9] Men Lu. 2003. The impact of rail transit system on urban land use. MS Dissertation. Southwest Jiaotong University in China.

[10] Todd Litman. 2004. Evaluating Public Transit Benefits and Costs, [On-line serial], 3. Retrieved September 10, 2005 from the World Wide Web: www.vtpi.org/tranben.pdf.

[11] Todd Litman. 2005. Rail Transit Impacts on Transportation System Performance, Transportation Research Board 84th Annual Meeting. Washington, D.C. 9-13 January.

[12] Mindali,O., A.Raveh, and I.Saloman. 2004. Urban density and energy consumption: a new look at old statistics. Transportation Research Part A 38: 143–162.

[13] Newman, P., Kenworthy, J. 1990. Cities and Automobile Dependence: An International Sourcebook. Burlington□Ashgate Pub Co.

[14] Van Der Waals, F.M.J., 2000. The compact city and the environment: A review. Tijdschrift voor Economische en Sociale Geografie 91 (2): 111–121.

[15] Cervero, R. 1988. Land use mixing and suburban mobility. Transportation Quarterly 42 (3): 429–446.

[16] Anderson, P.W., Kanaroglou, P.S., Miller, E.J., 1996. Urban forms, energy and the environment: Review of issues, evidence and policy. Urban Studies 33 (1): 7–35.

[17] Roy, J.R. 1992. Transport efficiency in cities with subcentres. In Proceedings of 6th World Conference on Transport Research. Lyon, France, June 29 - July 3.

[18] Akisawa A., Kaya Y. 1998. Two model analyses of the urban structure of minimal transportation energy consumption. Applied Energy 61(15): 25-39.

[19] China Academy of Urban Planning and Design. 2006. The LRT construction planning of Dongguan Technical Report.

Design of Optimal PID Controller using Improved Genetic Algorithm for AGC including SMES Units

S. Pothiya*, C. Khamsum, W. Kongprawechnon and I. Ngamroo

Abstract*— *This paper is proposed a new optimization approach of a proportional-integral-derivative (PID) controller by the improved genetic algorithm (IGA) for automatic generation control (AGC) including superconducting magnetic energy storage (SMES) of a two-area interconnected reheat thermal system. Conventionally, the gains of PID controller are obtained by trial and error method or experiences of designers. To overcome this problem, the IGA is applied to simultaneously tune PID gains to minimize frequency deviations of the system against load disturbances. The IGA algorithm introduces additional techniques for improvement of search process such as initialization, adaptive search, multiple searches, external crossover and restarting process. Simulation results explicitly show that the performance of the proposed PID controller is superior to the conventional PID controller in terms of the overshoot, settling time and robustness.

***Keywords*— Automatic generation control, Genetic algorithm, Power system, Superconducting magnetic energy storage**

1. INTRODUCTION

Automatic generation control (AGC) is synonymous with load frequency control (LFC), it is a very important problem in power system operation and control. A power system has a dynamic characteristic meaning that it can be affected by area load change and abnormal conditions lead to unpredicted in frequency and scheduled tie-line power flows between areas. These problems are corrected by control the frequency. In the past, a governor, may no longer be able to compensate for such load changes due to its slow response [1].

To solve this problem, superconducting magnetic energy storage (SMES) [2–4], which is capable of controlling active and reactive power simultaneously [5], has been proposed as one of the most effective and significant stabilizers of power oscillation modes [6–8]. Besides oscillation control, SMES allows a power quality improvement [9], a load leveling [10] and a load frequency control [11–16], which are not possible at all with other power system controllers such as a power system stabilizer, a static-var compensator etc.

Several design methods of AGC, which is equipped with SMES, have been successfully proposed, such as a proportional control [11, 12], a digital control [13], an adaptive control [14], and a fuzzy control [16] etc. Despite the potential of modern control techniques with different structures [13–16], power system utilities still prefer the fixed structure controller.

In this paper proposes a new optimization technique, which is called improved genetic algorithm (IGA) to optimize the gains of PID controller to control frequency for a two-area interconnected reheat thermal system including SMES units. The results compare with the conventional PID controller with and without SMES in term of settling time, overshoot and robustness.

This paper is organized as follows: Section 2, a comprehensive mathematical model of AGC problem for a two-are interconnected reheat thermal system including SMES is presented. The PID controller is described in Section 3. An application of proposed IGA algorithm to optimize the gains of PID controller is presented in Section 4. The simulation results in the two-area interconnected reheat thermal system are presented in Section 5. Finally, the conclusion is provided in Section 6.

2. PROBLEM FORMULATION

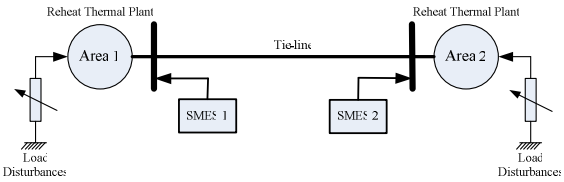

Fig. 1. A two area interconnected power system with SMES

A two area interconnected power system [12] including reheat steam turbines, governor deadbands, boiler dynamics, and SMES units shown in Fig. 1, is used to explain the motivation of the proposed method. Both areas have installed SMES1 and SMES2 in order to stabilize frequency oscillations. It is assumed that large loads with sudden changes, such as large steel mills, arc -

S. Pothiya (corresponding author) and W. Kongprawechnon are with the School of Communication, Instrumentation & Control, Sirindhorn International Institute of Technology, Thammasat University, Pathumthani 12121, Thailand. (e-mail: saravuthpothiya@yahoo.com, waree@siit.tu.ac.th)

C. Khamsum is with Electrical Engineering Department, Faculty of Engineering, North Eastern University, Thailand (e-mail: neu_ai_club@yahoo.com)

I. Ngamroo is with Electrical Engineering Department, Faculty of Engineering, King Mongkut's Institute of Technoligy Ladkrabang, Bangkok 10520, Thailand (e-mail: knissara@kmitl.ac.th)

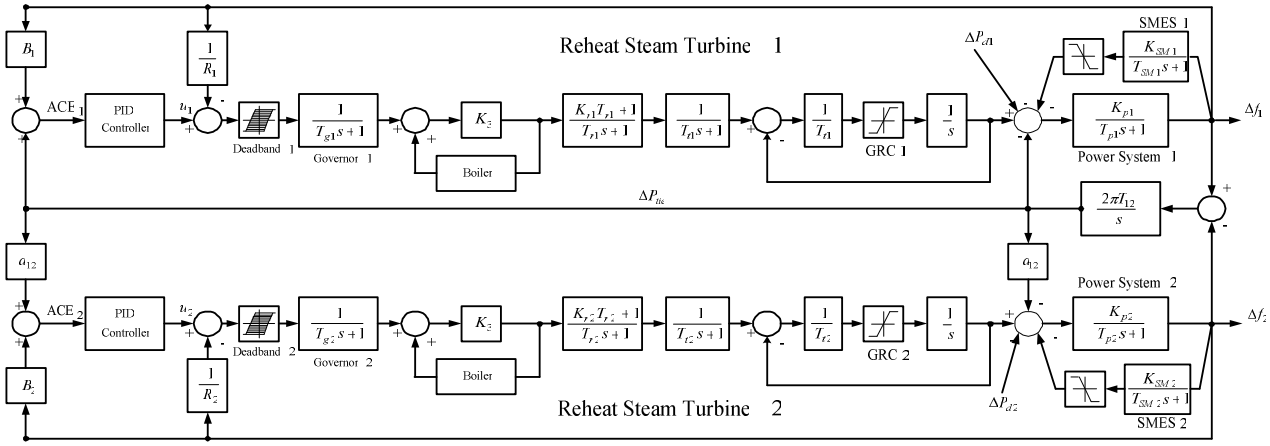

Fig. 2. Block diagram of two area interconnected power system.

furnace factories, magnetic levitation transporters and testing plants for nuclear fusions etc., have been placed in both areas. This results in a serious problem of frequency oscillations. The detailed block diagram of the interconnected power system model is depicted in Fig. 2 and the system parameters are given in Appendix.

The detailed transfer function models of the speed governors and turbines are discussed in Ref. [12]. In order to project physical constraints, a generation rate constraint (GRC) of 0.0017 [puMW/s] is considered. The transfer function of the governor, taking a deadband into account, can be expressed by

$$G_{gi}(s) = \frac{0.8 - \frac{0.2}{\pi} s}{1 + T_{gi} s} \quad , \qquad i = 1, 2 \tag{1}$$

Fig. 3 shows the model to represent the boiler dynamics [12]. This includes the long term dynamics of the fuel and steam flows on the boiler drum pressure. For a SMES unit, the limiter of $-0.01 \le \Delta P_{SMi, i=1,2} \le 0.01$ [puMW] based on a system MW base is equipped at a power output terminal. Parameters values of SMES1 and SMES2 are set at $K_{SM1} = K_{SM2} = 0.12$ and $T_{SM1} = T_{SM2} = 0.03$ sec.

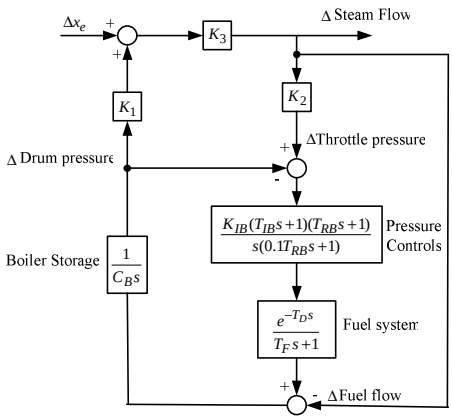

Fig. 3. Block diagram of boiler dynamics.

3. PID CONTROLLER

Designing PID controller, even for non-linear plants such as power system, can be a difficult problem. Consider the system illustrated in Fig. 4 where the PID controller obey the following control law:

$$M(s) = \left(k_p + \frac{k_i}{s} + k_d s \right) E(s) \tag{2}$$

where k_p, k_i and k_d are proportional, integral, and derivative gains, respectively.

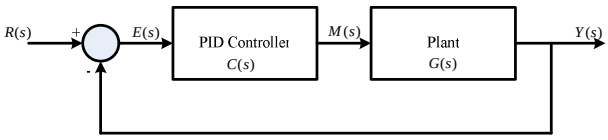

Fig. 4 A typical PID control system

The objective of PID controller design is to determine a set of gains (k_p, k_i and k_d) of the control law such that the set of roots of the characteristic equation chosen by the designer are obtained. The three gain parameters of the PID control law interact with the plant parameters $P(s)$ in a complex fashion when the designer attempts to obtain the specified roots of the characteristic equation. These roots are chosen in order to obtain the desired transient response of the closed loop, while taking the resultant zeros into account. PID controller increase the order of the characteristic equation by one. The controller introduces a new pole at original of the s-plane, and they shift the original compensated root of the closed loop system to new positions on s-plane, In addition to these effects, PID controllers introduce a pair of zeros, usually a complex conjugate pair, which will normally have a significant effect on the transient behavior of the compensated system.

The efficiency of the system can be measured by calculating the integral of time-multiplied absolute error

(ITAE) for the unit step response during [0,T]:

$$Error = \int_0^T t|e(t)|dt \quad (3)$$

The problem confronting the designer, therefore, is to calculate the three gains of the PID controller while ensuring that transient response (minimum error, overshoot, rising time, settling time and steady-state error) specification are met.

4. IMPROVED GENETIC ALGORITHM

4.1 Genetic algorithm

A genetic algorithm (GA) is a robust optimization technique based on natural selection. The basic goal of GA is to optimize functions call fitness functions. GA-based approaches differ from conventional optimization methods in several ways. First, GA search work with a coding of the parameter set rather than the parameters themselves. Second, GA search from a population of points rather than a single point. Third, GA use payoff (objective function) information, not other auxiliary knowledge. Finally, GA use probabilistic transition rules, not deterministic rules. These properties make GA robust, powerful, and data-independent.

A simple GA starts with a population of solution encoded in one of many ways. Binary encoding are common and are used in this report. The GA determines each string's strength based on an objective function and performs one or more of three genetic operators on certain strings in population.

1. Reproduction (also called selection) is simply retaining a fit string in the following generation.

2. Crossover involves swapping partial strings of random length between two parent strings.

3. Mutation involves flipping a random bit in a string.

These three operations primarily involve random number generation, copying, and partial string exchange. Thus GA is simple to implement.

4.2 Improved Genetic algorithm

A new proposed approach is called improved genetic algorithm (IGA) based on the GA algorithm as shown in Fig 5, which has several GA algorithms independently. This algorithm consists of five mechanisms; namely, *initialization*, *adaptive search*, *multiple searches*, *external crossover* and *restarting process* as follows:

i) Initialization

IGA algorithm uses the feasible solutions for random in the determination of the several groups of initial solutions, which contrast with GA algorithm. Because the probability for reaching the optimal solution is higher than single group of initial solution of the GA algorithm so that IGA can quickly be converged to the global optimum solution.

ii) Adaptive search

The step size is range of variation of current solution which is the importance factor for searching process, so that should be appropriately chosen. Low values to uses long computational time. On the other hand, high values result in may be not getting global optimum. Consequently, the adaptive search mechanism has been developed to suitably adjust the step size during the searching process. This earlier process helps to speed up the move to the vicinity of the global solution. Once the searching process approaches the near global solution, the small step size is then employed in order to move to the solution in a high resolution of solution.

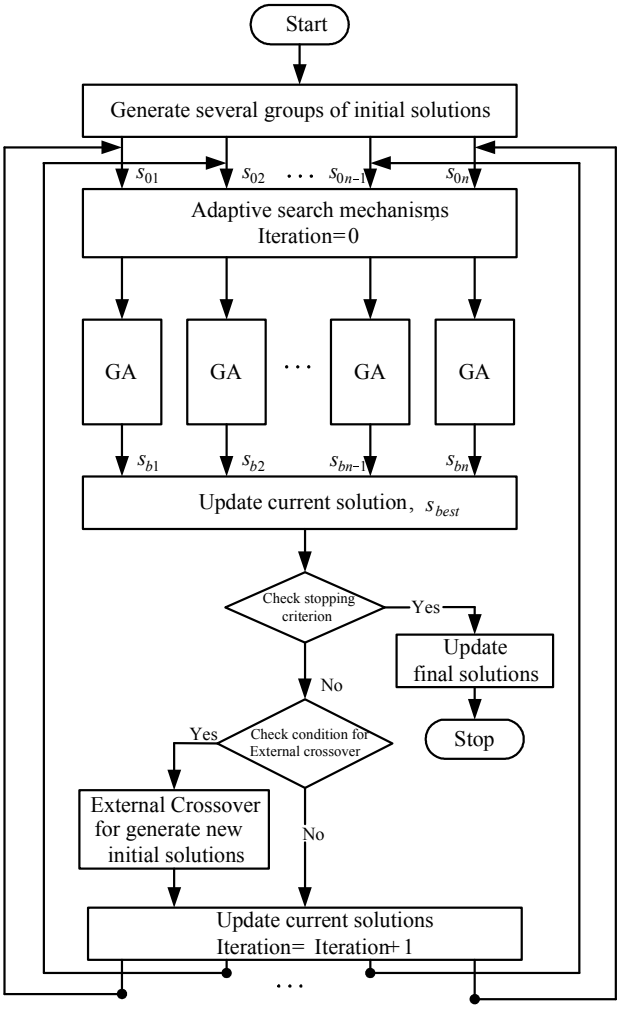

Fig. 5. Procedure of Improved Genetic Algorithm

iii) Multiple searches

In recently, the personal computer has high speed for computational. For solving the large scale problem may be uses several computers run in parallel called *parallel search*. For *multiple-search* are executed by a personal computer. This process helps the GA algorithm find the promising region of the search very quickly.

iv) External Crossover

After the iteration of the searching process satisfies, all independent GA algorithms are stopped. The external crossover process uses for compare and exchange the solutions which found by these GA, and generate the best initial solutions for next iteration.

v) Restarting process

When the searching is stroke on the local solution for a long time and procedure of GA algorithm can not escape from local solution. The restarting process is applied for help to continue searching and find a new solution.

5. NUMERICAL EXAMPLE & RESULTS

Simulations were performed using the conventional PID and the proposed optimal PID controllers applied to a two-area interconnected reheat thermal system as shown in Fig. 2, when applying 0.01 p.u.MW step load disturbances into both areas. The implementation worked with MatLab® 7.0 and Simulink. The simulation was ran on a personal computer Pentium 4, 2.66 GHz, 256 Mbytes RAM, under Window XP.

In the optimization, the integral of time-multiplied absolute error (ITAE) of the frequency deviation of the first area is selected as the performance index. Accordingly, the objective function J is set by

$$\text{Minimize } J = \int_0^\infty t\left|\Delta f_1\right| dt \qquad (4)$$

After design, the appropriate parameters value as showed in Table 1.

Table 1. Parameter value of PID controllers

Controller	k_p	k_i	k_d
Conventional PID no SMES	0.0098	0.0985	0.2075
Optimal PID no SMES	3.0008	0.5995	1.7975
Conventional PID with SMES	1.9105	0.4217	0.2089
Optimal PID with SMES	2.9910	0.5995	2.0028

The frequency deviations of first areas after a sudden load change are shown in Fig. 6. The proposed PID controller is gives the best performance than other controllers in term of settling time, overshoot and ITAE.

Next, the robustness of each controller against system parameters variations are evaluated by the settling time, overshoot, and ITAE. These values are calculated under an occurrence of load disturbances while all system parameters are varied from −30% to 30% of the nominal values. The comparison results are shown in Fig. 7, Fig. 8, and Fig. 9 show the values of settling time, overshoot, and ITAE of the first areas, respectively.

Considering Fig. 7-9, these clarifies that the robustness of the optimal PID controller against parameters variations is superior to that of the other controllers.

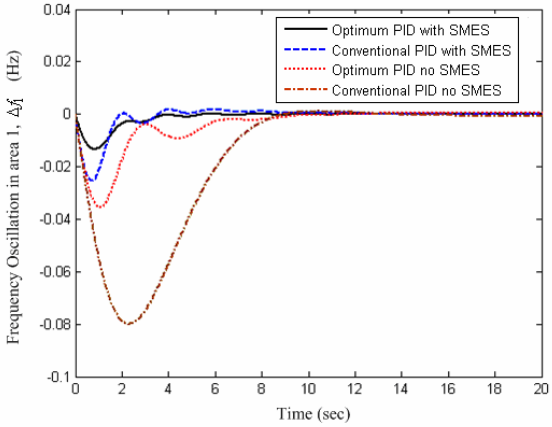

Fig. 6 The frequency deviation of first area of different controller types.

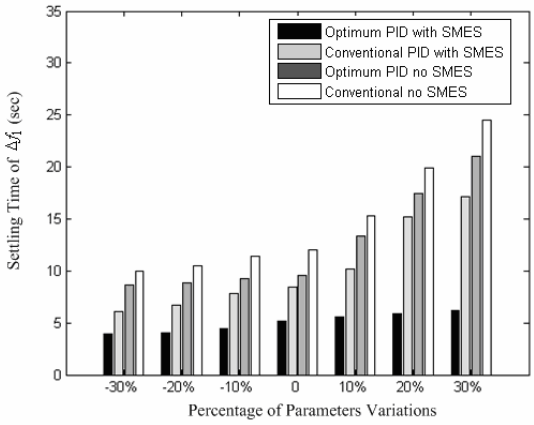

Fig. 7 Comparison results of settling time of Δf_1 under parameter variations.

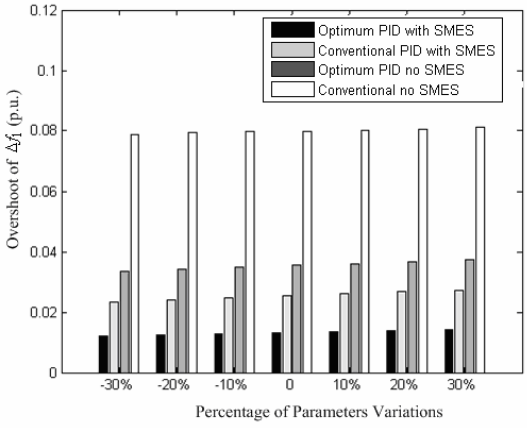

Fig. 8 Comparison results of overshoot of Δf_1 under parameter variations.

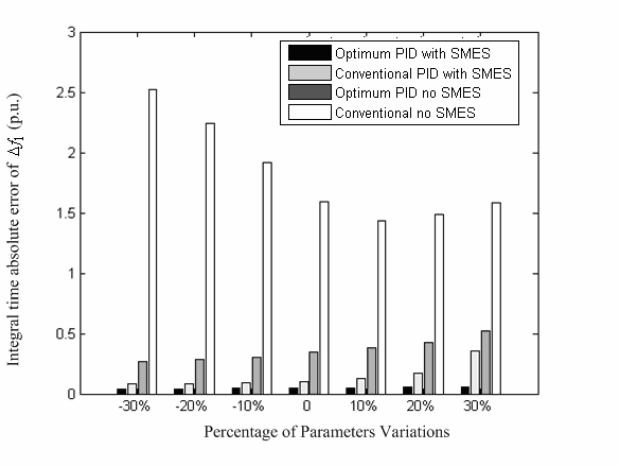

Fig. 9 Comparison results of ITAE of Δf_1 under parameter variations.

6. CONCLUSION

In this paper, a new approach, called IGA algorithm has been used for developing an optimal PID controller for AGC of a two-area interconnected reheat thermal system. The proposed technique for designing the PID controller helps us save time when compared to those from conventional trial and error design procedures. Another benefit of this approach is that it does not require experts for the design of PID controller. A number of studies have been performed with the proposed PID controller to test the effectiveness and robustness. Finally, the simulation results show that the proposed PID controller performs significantly better than other controller in the settling time, overshoot, and ITAE. Therefore, this proposed PID controller is effective, efficient and robust over a wide range of operating conditions.

REFERENCES

[1] Jaleeli, N.; VanSlyck, LS.; Ewart, DN.; Fink, LH.; and Hoffmann, AG. 1992. Understanding automatic generation control. *IEEE Trans Power Systems* 7(3): 1106-1112.

[2] Boom, RW.; Perterson, H. 1972. A superconducting energy storage for power systems. *IEEE Trans Magn* 8: 701-703.

[3] Hassenzahl, W. 1975. Superconducting magnetic energy storage be used on electric utility systems. *IEEE Trans Magn* 1: 482-488.

[4] Boenig, HJ.; Hauer, JF. 1985. Commissioning tests of the Bonneville Power Administration 30 MJ superconducting magnetic energy storage unit. *IEEE Trans Power Appl Syst* 10: 302–309.

[5] Ise, T.; Mitani, Y.; and Tsuji, K. 1986. Simultaneous active and reactive power control of superconducting magnetic energy storage to improve power system dynamic performance. *IEEE Trans Power Deliv* 1: 143-150.

[6] Mitani, Y.; Tsuji, K.; and Murakami, Y. 1988. Application of superconducting magnetic energy storage to improve power system dynamic performance. *IEEE Trans Power Syst* 3(4): 1418-1425.

[7] Rahim, A.; Mohmamad, AM.; and Khan, MR. 1996. Control of subsynchronous resonant modes in a series compensated system through superconducting magnetic energy storage units. *IEEE Trans Energy Conv* 11(1): 175-170.

[8] Pal, BC.; Coonick, AH; and Cory, BJ. 1999. Robust damping of inter-area oscillations in power systems with superconducting magnetic energy storage devices. *IEE Proc Gener Trans Distrib* 146(6): 633-639.

[9] Abdelsalam, MK.; Boom, RW.; and Perterson, HA. 1987. Operation aspects of superconducting magnetic energy (SEMS). *IEEE Trans Magn* 23: 3275-3277.

[10] Chu, X.; Jiang, X; Lai, Y.; Wu, X.; and Liu, W. 2001. SMES control algorithms for improving customer power quality. *IEEE Trans Appl Supercond* 11(1): 1769-1772.

[11] Banerjee, S.; Chatterjee, JK.; and Tripathy, SC. 1990. Application of magnetic energy storage unit as load frequency stabilizer. *IEEE Trans Energy Conv* 5(1): 46-51.

[12] Tripathy, SC.; Balasubramanian, R.; and Chandramohanan, PS. 1992. Effect of superconducting magnetic energy storage on automatic generation control considering governor deadband and boiler dynamics. *IEEE Trans Power Syst* 7(3): 1266-1273.

[13] Tripathy, SC.; and Juengst, KP. 1997. Sampled data automatic generation control with superconducting magnetic energy storage in power systems. *IEEE Trans Energy Conv* , 12(2): 187-191.

[14] Tripathy, SC; Balasubramanian, R.; Chandramohanan, PS. 1997. Adaptive automatic generation control with superconducting magnetic energy storage in power systems. *IEEE Trans Energy Conv* 7(3): 434-441.

[15] Demiroren, A.; Zeynelgil, HL.; and Sengor, NS. 2003. Automatic generation control for power system with SMES by using neural network controller. *Electr Power Comp Syst*, 31(1): 1-25.

[16] Demiroren, A.; and Yesil, E. 2004. Automatic generation control with fuzzy logic controllers in the power system including SMES units. *Int J Electr Power Energy Syst* 26: 291-305.

[17] Wu, ZQ.; and Mizumoto, M. 1996. PID type fuzzy controller and parameter adaptive method. *Fuzzy Sets and Systems* 78(1): 23-36.

APPENDIX

The system parameters are following:

$K_{p1} = K_{p2} = 120$, $T_{p1} = T_{p2} = 20$, $K_{r1} = K_{r2} = 0.333$

$T_{r1} = T_{r2} = 20$

$T_{g1} = T_{g2} = 0.2$, $R_1 = R_2 = 2.4$

$B_1 = B_2 = 0.425$, $T_{t1} = T_{t2} = 0.3$

$T_{12} = 0.0707$, $a_{12} = -1$

Boiler system (gas fired type)

$K_1 = 0.85$, $K_2 = 0.095$ $K_3 = 0.92$, $CB = 200$

$T_D = 0$, $T_F = 10$, $K_{IB} = 0.03$, $T_{IB} = 26$

$T_{RB} = 69$

Performance and Emission Characteristics of Straight Vegetable Oil (Svo) as Alternate Transport Fuel for Sustainable Development

Dilip R. Pangavhane*, Sachin S. Harak, and Prashant B. Nehe

Abstract— *The technological development has resulted in unlimited exploitation of natural resources resulting in diminishing stocks of fossil fuels alongwith increase in number of transport vehicles, there is steep rise in energy demand. Alternative transport fuels have gained more importance in past few decades. Bio-diesel is better option for conventional fuels to protect environment for sustainable development. Though the various straight vegetable oils (SVO), edible and non-edible oils can be used for manufacturing biodiesel, out of which karanja oil is best suitable for biodiesel production. Multiple engine performance tests were conducted from obtained biodiesel on a four-stroke diesel engine. The blends upto 20% biodiesel can be used in all diesel engines and are compatible with most conventional storage and distribution equipments without any engine modifications resulting same payload capacity as that of petroleum diesel. The tests results have shown that the biodiesel is no different from petroleum diesel in terms of engine performance.*

Keywords— **Alternate Transport Fuels, Bio-diesel, CI Engines, Karanja, Sustainable Development, Transesterification.**

1. INTRODUCTION

Environmental pollution is an emerging threat and of great concern in present context pertaining to its effect on ecosystem. The technological development in industrial and automobile sector has resulted in unlimited exploitation of natural resources disturbing the delicate ecological balance between living and non-living components of the biosphere. The final destination of imbalance in environment will affect the human being, because of air, water and soil pollution.

For the fast technological developed world transport becomes the important part for its existence. Because of diminishing stocks of fossil fuels and increase in number of vehicles in transport sector there is steep rise in energy demand.

To maintain the tempo of high growth rate of world economy, it is necessary to maintain these inputs of energy resources. With the fast rate of depletion of crude oil deposits, alcohol blends on conventional fuels, LPG, CNG have come to the forefront and have been extensively studied and being implemented but are non renewable. These blended fuels are not the final solution to fuel crisis, as are only a compromise for marginal increase in fuel supply. These conventional fuels available in market are made environmental friendly by technical up gradation but still there are limitations in their sustainability. Alternate fuels are only promising hope of future, which has tremendous potential to energize fuel revolution in transport sector [1].

The dependence on fossil energy is unwise because of its cost, dwindling reserves and environment pollution. Therefore many countries have already initiated programmes to increase the use of alternative source of energy. The alternate fuels have large benefits beyond air quality and have gained more importance in past few decades owing to need for stronger energy security as well as to reduce green house gas emission. New fuels give new choices for consumers, which bring down our dependency on imported oil and will save millions of rupees on import bills. When the demand for imported oil peaks up, the production and use of alternate fuels like hydrogen, biodiesel etc. will definitely become more competitive in the market thus enabling use of such cleaner fuels for sustainable development which protects the environment [2]. In the world most of the countries has accorded priority to biodiesel technology for the protection of environment for sustainable development.

Biodiesel refers to any fuel substitute derived from renewable biomass. Vegetable oils or animal fats on treatment with alcohol (mostly methanol or ethanol) give alkyl esters or fatty acids. The alkyl esters of fatty acids are consigned with a general term, biodiesel when used as fuel. The name biodiesel was introduced by National Soydiesel Development board, US (now National Board of Biodiesel), which has pioneered the commercialization of biodiesel in the US. Likewise the petroleum diesel, the biodiesel operates the combustion ignition engines.

Biodiesel has some clear advantages over the straight vegetable oil (SVO).

*Dilip R. Pangavhane (corresponding author) is Principal, Nashik District Maratha Vidya Prasarak samaj College of Engineering, Udhoji Maratha Boarding Campus, Near Pumping station, Gangapur Road, Nashik-422013, Maharashtra, India. E-mail: drpangavhane@yahoo.co.in, ndmvpcoe_nsk@sancharnet.in. Phone: 91-0253-2571439, 2317016, (M) 9422769103.

Sachin S. Harak is Lecturer, Mechanical Engineering Depart., Nashik District Maratha Vidya Prasarak samaj College of Engineering, Gangapur Road, Nashik-422013, Maharashtra, India.

Prashant B. Nehe is Lecturer, Mechanical Engineering Depart., Nashik District Maratha Vidya Prasarak samaj College of Engineering, Gangapur Road, Nashik-422013, Maharashtra, India.

1. It works in any diesel engine without any conversion or modification to the engine.
2. Viscosity is less than that of SVO.
3. It has better cold weather properties than SVO.
4. Biodiesel is clean, safe, and ready to use alternative fuel.
5. Biodiesel can be more expensive.

Though the various edible and non-edible oils can be used for manufacturing biodiesel, out of which karanja (Pongamia pinnata) is one of the best oil suitable for production of biodiesel. The Jatropha (Pongamia pinnata) is wild oilseed plant of medium sized tree that generally attains a height of about 8 m and a trunk diameter of more than 50 cm. The trunk is generally short with thick branches spreading into a dense hemispherical crown of dark green leaves. Jatropha plantation requires minimal rainfall, and it can be plant successfully on marginal, degraded, or even in deserted land. It is shrub, which can be grown on either side of railway tracks, thus preventing displacement of fertile land, which is used for food crops. Cultivation of Jatropha consists of ideal spacing for block plantations and paired row hedges 3.0m x 3.0m single rows can be planted at 2.0m spacing. The pit size of 1.5m x 1.5m x 1.5m, filled with topsoil with farmyard manure. A fertilizer mix (NPK) Nitrogen Phosphate and Potassium [15:15:15] should be applied at the rate of 250gm per plant during rainy season every year. It can be grown either from cuttings or seeds, its plants start bearing fruits from first years onwards. Each Jatropa tree can produce an average of 3.5kg of beans each year depending upon irrigation levels. Generally 2200 numbers of Jatropha trees are planted per hectare; this gives annual harvest of approximately 7 tonnes of beans or seeds, which will yield about 2.7 tonnes of karanja oil. The non-renewability of the present conventional fuels apart from deteriorating land, water and air quality has led to the look out for better alternatives. When the demand for imported oil peaks up, the production of alternate fuels like biodiesel [3] will definitely become more competitive in the markets thus enabling the use of such cleaner fuels in mere endeavor for the environment protection for sustainable development. This paper discusses the efforts made towards the production of biodiesel by Transesterification process and to compare its fuel characteristics with the petroleum diesel. The multiple performance tests were conducted from the obtained biodiesel on a four-stroke, two-cylinder water-cooled diesel engine producing 10HP, 1500 RPM, 10KV Dynamometer under different blend ratio.

2. MATERIALS AND METHOD

A. Experimentation

Though the various bio oils are used for production of biodiesel but the biodiesel obtained from karanja oil is used either as diesel fuel substitute or extender. In India there is great potential of karanja oil as compaired to the other non-edible oils. The comparative physical and chemical Properties of Karanja oil (Pongamia Pinnata) and Jatropha curcus oil is given in Table-1.

Table 1. Comparison of Physical and Chemical Properties of Karanja oil with Jatropha oil

Sr. No.	Properties	Karanja oil	jatropha oil
1	Viscosity (cSt)	15.10	52.76
2	Specific gravity	0.87	0.93
3	Flash point	197	240
4	Sulfur	13-16%	17%
5	Refractive Index	1.47	1.89

These oils cannot be directly used as fuels in the engines because of its high viscosity which may create problems in the engines. The advantage of using karanja oil is that the physical and chemical properties are far better than those Jatropha oil, hence processing becomes more simplified and economical. Apart from this Karanja tree can be grown on waste land and need not require more care for grow than that of Jatropha tree. Wood quality of karanja tree is also far better than jatropha tree which gives additional income. To reduce the viscosity of this oil, a chemical process called “transesterification” [4] is carried out for removing the triglycerides from this karanja oil. Generally four methods are adopted for converting the vegetable oil into biodiesel.

(i) Dilution (ii) Micro emulsion

(iii) Pyrolysis (iv) Transesterification

The transesterification process is best method of approach for converting vegetable oil into biodiesel. The processed oil obtained is “methyl esters” called as biodiesel, which was tested and the properties were compared with standards for diesel. As the fatty esters obtained by transesterification are very less viscous as due to less viscosity deposition of carbon gets reduced. The biodiesel obtained by transesterification has performed well in the long-term diesel engine test.

Karanja oil + Methanol = Biodiesel + Glycerol

B. Methodology

The experimental set up is prepared for biodiesel production; the brief methodology is given as below. By using constant temperature heating bath the reaction were carried out between the temperature range of 40^0C to 70^0C

C. Procedure

The karanja oil is purchased from the market and one kg karanja oil is taken as sample through filtering process and then it was heated up to 100^0C for removing any

volatile matter and water, which may present in the karanja oil sample. Then the sodium methoxide is prepared for one kg karanja oil, by mixing Thirty-five gms of MeOH and six gms of NaOH in a separate container. Then the oil temperature is set at 65^0 for two hours, with carefully and slowly the sodium methoxide is added in the reactor then the colour was changed to dark brown [5].

After two hours of completion the reaction mixture was placed in separating funnel and the system was kept in 40^0C for at least 5 Hours. During this two layers were observed out of which upper one is of Bio diesel and the bottom contains Glycerin and unreacted reactants, this process is known as settling and separation process. Then by draining out the bottom and giving out water wash to upper layer for removing any soap present in the product. Then heating the sample up to 100^0C, for removing the unreacted methanol and water remained during water wash. The obtained product is pure Bio diesel ready to use as a fuel.

Table 2. Comparative properties of Bio diesel obtained from karanja oil and Jatropha oil.

Sr No	Properties	Biodiesel from	
		Karanja oil	jatropha oil
1	Density, (40^OC) g/cm^3	0.88	0.918
2	Viscosity, (40^OC) cSt	4.84	5.51
3	Calorific Value, Kcal/kg	9792	9470
4	Flash Point, ^OC	109	240-110
5	Pour Point, ^OC	-14.00	8
6	Sulpher contents (%)	0.1	0.13
7	Carbon Residue (%)	0.24	0.64

The bio diesel obtained from karanja oil is tested for checking its physical and chemical properties i.e. the fuel properties as a fuel and compared with bio diesel obtained from Jatropha oil, are shown in the Table-2. From this table it is observed that the Properties of obtained biodiesel form Karanja oil is far better than that of Jatropha oil. The Comparison of biodiesel sample obtained from karanja oil was made with B.U. standards and is given in Table-3. From this table, it is observed that the obtained biodiesel has almost the similar values as that of B.U. standards.

Similarly the Comparison of biodiesel sample obtained from the karanja oil was made with petroleum Diesel and given in Table-4. From this table it is observed that the pollution content parameters affecting on environment are very low as compared to that of the petroleum diesel.

Table 3. Comparison of bio-diesel sample obtained from karanja oil with B.U. standards.

Sr No	Specification	Unit	(Obtained Sample) biodiesel	B.U. Standards for biodiesel
1	Density at 30^0C	G/ml	0.88	>0.8
2	Combustion point	^{0}C	192	>55
3	Kinetic viscosity	Cst	4.84	5
4	Calorific potential	MJ/Kg	41	Undefined
5	Cetane number	----	48	>48
6	Ester content	%	>99	>99
7	Sulfur content	%	0	<0.55
8	Carbon residues	%	0.024	<0.1
9	Specific gravity	^{0}C	0.895	0.87 to 0.89
10	Cloud point	^{0}C	-11	-11 to 16
11	Pour point	^{0}C	-14	-15 to 13

D. Testing as a Fuel

The multiple performance tests were conducted from the obtained biodiesel on a four-stroke, two-cylinder water-cooled diesel engine producing 10 HP at 1500 RPM with 10 KV, Dynamometer. The experimental set up is as shown in Figure: 1 with all necessary instrumentation and engine without making any modification of the present system [6-7].

The various engine performance tests were conducted with obtained biodiesel from karanja oil, as 50%, 100% and with diesel as a complete fuel.

The results obtained during the various engine trials are given in Tables 5, 6 and 7, for different combinations of biodiesel with petroleum diesel. From the obtained results it is concluded that the biodiesel also gives the more comparable engine performance as a complete fuel or its blend with diesel as that of the petroleum diesel.

Table 4. Comparison of biodiesel sample obtained from karanja oil with petroleum Diesel

Sr No	Specification	Units	(Obtained sample) Biodiesel	Diesel
1	Density at 30^0C	G/ml	0.88	0.85
2	Combustion point	^{0}C	192	55
3	Kinetic viscosity	Cst	4.84	2-8
4	Calorific potential	MJ/Kg	41	45
5	Cetane number		48	47.5
6	Ester content	%	>99	0
7	Sulfur content	%	0	<0.5
8	Carbon residues	%	0.024	<0.35
9	Cloud point	^{0}C	-11	--
10	Pour point	^{0}C	-14	--
11	Boiling point range	^{0}C	--	188-333

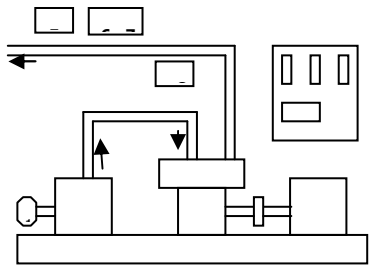

Fig. 1. Experimental Setup

1. Air flow meter
2. Air vessel
3. C.I. Engine
4. Dynamometer
5. Smoke meter
6. CO, HC analyzers
7. NO analyzer
8. Thermocouple

Table 5. Test on diesel engine with Diesel fuel

Sr. No	Break Power (KW)	Fuel Consumption (Kg/hr)	Mechanical efficiency (%)	Indicated thermal efficiency (%)
1	2.62	4.05	64.88	24.94
2	3.42	4.85	70.64	28.46
3	4.81	6.2	77.18	29.3
4.	6.28	7.1	81.52	28.93
5.	6.75	8.92	84.03	31.87

Table 6. Test on diesel engine with 50% biodiesel and 50% Diesel as a fuel

Sr No	Break Power (KW)	Fuel Consumption (Kg/hr)	Mechanical efficiency (%)	Indicated Thermal efficiency (%)
1	1.62	4.12	39.8	13.0
2	3.71	5.61	55.0	16.3
3	4.62	7.12	64.2	18.29
4	6.0	8.5	70.58	20.29
5	6.78	9.28	73	21.58

Table 7 Test on diesel engine with 100% Biodiesel as a fuel

SrNo	Break Power (KW)	Fuel Consumption (Kg/hr)	Mechanical efficiency (%)	Indicated Thermal efficiency (%)
1	1.62	4.12	46.2	12
2	3.21	5.11	55.0	14.32
3	4.67	6.57	64.2	16.50
4	6.0	7.90	70.58	18.56
5	6.96	8.86	73.00	21.58

3. RESULTS AND DISCUSSION

A. Emissions reductions with biodiesel

As the Biodiesel is made entirely from vegetable oil, it does not contain any sulfur, aromatic hydrocarbons, metals or crude oil residues. The absence of sulfur means a reduction in the formation of SO_2. Figure-2 shows the biodiesel percentage reduction of emissions as compared with the petrodiesel. The various parameters related to emission are as given below.

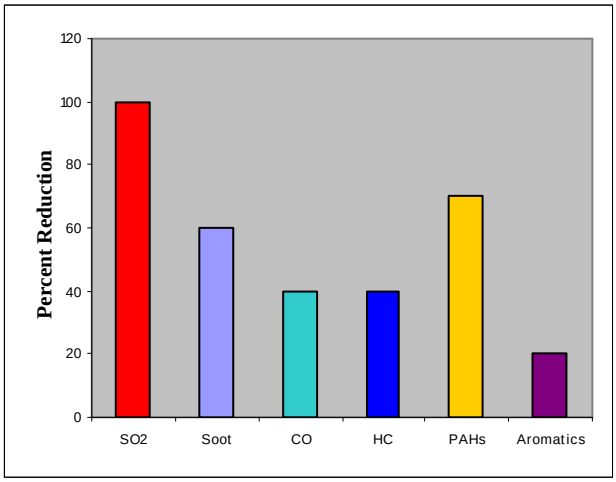

Fig. 2. The Biodiesel emissions compared with Petrodiesel

B. Lower Hydrocarbon Emissions

The Biodiesel itself burns cleanly, but it also improves the efficiency of combustion in blends with petroleum fuel. As a result of cleaner emission though our engine was older one still we notice less soot under load and less carbon during startup compared to diesel.

C. Smoke and Soot Reductions

The smoke (particulate material) and soot (unburned fuel and carbon residues) are of increasing concern to urban air quality problems that are causing a wide range of adverse health effect for the citizens, especially in terms of respiratory impairment and related illness. With necked eyes we easily noticed that there was considerable reduction in black smoke from exhaust.

D. Carbon Monoxide Emissions

Carbon monoxide gas is a toxic byproduct of all hydrocarbon combustion that is also reduced by increasing the oxygen content of the fuel. More complete oxidation of the fuel results in more complete combustion to carbon dioxide rather to leading to the formation of carbon monoxide. When the fuel was switched from lower sulfur petroleum diesel to clean biodiesel, there was a 28-37% drop in carbon monoxide emissions. During third test (i.e.100% biodiesel) CO% shown by gas analyzer was 30% less than that of Government guidelines which is advantageous for the biodiesel.

E. Nitrogen Oxides

The gas analyzer monitor report shows that there is slight increase (several percent) in NOx emissions with Biodiesel that are attributable, in part to the higher oxygen content of fuel mixture. More oxygen and better combustion of the fuel is the indication of more formation of NOx emission with Biodiesel as a fuel.

F. Noise Reductions

During the experimental trials it is observed that there is considerable reduction in engine noise and vibration as engine was working very smoothly. This will give the added life to the engine and security to its parts.

G. Energy Security Benefits

With agricultural commodity prices approaching record lows and petroleum prices approaching record high, it is clear that more can be done to utilize domestic surpluses of vegetable oils while enhancing our energy security. Biodiesel can be manufactured as per existing industrial production capacity, and used with conventional equipments; it provides substantial opportunity for immediately addressing our energy security issues.

H. Biodiesel helps to reduce greenhouse gases

Unlike other “clean fuels” such as compressed natural gas (CNG), Biodiesel and other biofuels are produced from renewable agricultural crops that assimilate carbon dioxide from the atmosphere. The carbon dioxide released during the year from burning vegetable oil, biodiesel in effect, it will be recaptured next year by growing crops in the fields to produce more vegetable oil from the biomass.

I. Social Aspects

India ranks sixth in world for energy demand accounting 3.5% of world commercial energy demand in 2003. The energy demand is expected to grow at 4.8%. The demand of diesel component is estimated around 40 million tones. The current annual import bill of crude oil in terms of foreign exchange is around Rs. 6,04,000 Crores. Diesel is mainly consumed by Industrial and transport sector, as road transport consumes almost 75%, while the railways accounts for the rest. Biodiesel can replace diesel and other fuels. It is produced from renewable materials, biodiesel considerably reduce soot emission, and it has zero sulfur content. The CO_2 emitted is also gets absorbed by trees under growth (CO_2 recycle) and similarly biodiesel is easily decomposes biologically and so there is no harm to the human being and environment which will be more helpful for sustainable development.

The main advantages of using biodiesel are:

(i) This project will develop and utilizes wastelands by growing kranja trees and will protect the environment.

(ii) Along the rail tracks and national highways karanja trees can be planted, which will protect the environment by producing the karanja oil.

(iii) There will be creations of employment opportunities in rural areas, especially to the

women, which will helps to improve the economical status of rural peoples.

(iv) This biodiesel project will indirectly promotes the organic farming by marketing the de-oiled cake, which will be available to the farmers as a fertilizer for different cropping patterns.

(v) It will restore the degraded lands and generate income opportunity for rural public.

There will be reduction in import quantity of petroleum oil because of production of biodiesel, ultimately the foreign exchange will be saved.

4. CONCLUSION

From the experimental results obtained it is concluded that the karanja oil (SVO) cannot be used directly as a fuel in the CI engine because of higher specific gravity, higher viscosity and low volatility as compared to petrodiesel. Similarly the biodiesel is more compitable with diesel and more suitable as fuel for the CI engines without any modification. There is also reduction in % of CO and HC in the exhaust gases. The non-renewability of conventional fuels apart from deteriorating land, water and air quality has led to the look out for better alternatives and the biodiesel is a substitute for the above problem. When the demand for imported oil peaks up the production of alternate fuels, like biodiesel will definitely become more competitive in the market thus enabling the use of such cleaner fuels in mere endeavor.

ACKNOWLEDGMENT

Authors acknowledge to the Managements and Directors of NDMVPS College of Engineering, Nashik, for providing the basic facilities required for conducting this experimentations.

REFERENCES

[1] Mashelkar, R.A. 2002. Report of expert committee on Auto fuel policy.

[2] Bhagavath, R. 2004. Fueling the future- The changing scenario, March-May 2004. Environment Science and Engineering 2(1): 1-8.

[3] Bio-Fuel, Report of the committee on development of bio-fuel, Planning Commission, Govt. of India, 2003.

[4] Green, D.W. and Moloney, J.O. 1998. Perry's Chemical Engg. Handbook, 7th Edition, McGraw Hill publication Co.

[5] Smith, J.M.; Van Ness, H.C. and Abott, M.C. 1999. "Introduction to chemical Engineering Thermodynamics", 5th Edition, McGraw Hill Publication Co.

[6] Senthil Kumar, M.; Ramesh, A. and Nagalingam, B. 2003. An experimental comparison of methods to use methanol and Jatropha curcus oil in a compression ignition engine. International Journal of Biomass and energy 25: 309-318.

[7] Green rating project, Environmental rating of Indian Automobile Sector. 2003. Centre for Science and Environment, New Delhi.

GMSARN International Journal
NOTES FOR AUTHORS

Editorial Policy

In the Greater Mekong Subregion, home to about 250 million people, environmental degradation - including the decline of natural resources and ecosystems will definitely impact on the marginalized groups in society - the poor, the border communities especially women and children and indigenous peoples. The complexity of the challenges are revealed in the current trends in land and forest degradation and desertification, the numerous demands made on the Mekong river - to provide water for industrial and agricultural development, to sustain subsistence fishing, for transport, to maintain delicate ecological and hydrological balance, etc., the widespread loss of biological diversity due to economic activities, climate change and its impacts on the agricultural and river basin systems, and other forms of crises owning to conflicts over access to shared resources. The *GMSARN International Journal* is dedicated to advance knowledge in energy, environment, natural resource management and economical development by the vigorous examination and analysis of theories and good practices, and to encourage innovations needed to establish a successful approach to solve an identified problem.

The *GMSARN International Journal* is a biannual journal published by GMSARN in June and December of each year. Papers related to energy, environment, natural resource management, and economical development are published. The papers are reviewed by world renowned referees.

Preparation Guidelines

1. The manuscript should be written in English and the desired of contents is: Title, Author's name, affiliation, and address; Abstract, complete in itself and not exceeding 200 words; Text, divided into sections, each with a separate heading; Acknowledgments; References; and Appendices. The standard International System of Units (SI) should be used.

2. Illustrations (i.e., graphs, charts, drawings, sketches, and diagrams) should be submitted on separate sheets ready for direct reproduction. All illustrations should be numbered consecutively and given proper legends. A list of illustrations should be included in the manuscript. The font of the captions, legends, and other text in the illustrations should be Times New Roman. Legends should use capital letters for the first letter of the first word only and use lower case for the rest of the words. All symbols must be italicized, e.g., α, θ, Q_{wt}. Photographs should be black and white glossy prints; but good color photographs are acceptable.

3. Each reference should be numbered sequentially as they appear in the text and these numbers should appear in brackets in the text, e.g., [1], [2-4]. Typical examples of references:
   - **Journal references** should contains: name of author(s); year of publication; article title; journal name; volume; issue number; and page numbers.
     Mayer, B.A.; Mitchell, J.W.; and El-Wakil, M.M. 1982. Convective heat transfer in veetrough liner concentrators. Solar Energy 28 (1): 33-40.
   - **Book references** should contain: name of author(s); year of publication; title; edition; place of publication (city) and name of publisher.
     Baker, P.R. 1978. Biogas for cooking stoves. London: Chapman & Hall.
   - **Proceedings references** example:
     Mayer, A. and Biscaglia, S. 1989. Modeling and analysis of lead acid battery operation. In *Proceedings of the 9th ECPV Solar Conference*. Reiburg, Germany, 25-29 September. London: Kluwer Academic Publishers. pp. 45-67.

4. Manuscript can be uploaded to the website or sent by email. In case of hard copy, three copies of the manuscript should be initially submitted for review. The results of the review along with the referees' comments will be sent to the corresponding author in due course. At the time of final submission, one copy of the manuscript and illustrations (original) should be submitted with the diskette. Please look at the author guide for detail.

GMSARN Members

Asian Institute of Technology

Hanoi University of Technology

Ho Chi Minh City University of Technology

Institute of Technology of Cambodia

Khon Kaen University

Kunming University of Science and Technology

National University of Laos

Royal University of Phnom Penh

Thammasat University

Yangon Technological University

Yunnan University

Published by the **Greater Mekong Subregion Academic and Research Network (GMSARN)**
c/o Asian Institute of Technology (AIT)
P.O. Box 4, Klong Luang
Pathumthani 12120, Thailand
Tel: (66-2) 524-5437; Fax: (66-2) 524-6589
E-mail: gmsarn@ait.ac.th
Website: http://www.gmsarn.org